A METHOD FOR GENERATING SIMPLIFIED FINITE ELEMENT MODELS FOR ELECTRICAL CABINETS

A Dissertation
Presented to
The Academic Faculty

by

Edwin Lim

In Partial Fulfillment
of the Requirements for the Degree
Doctor of Philosophy in Civil Engineering

Georgia Institute of Technology

December, 2016

A METHOD FOR GENERATING SIMPLIFIED FINITE ELEMENT MODELS FOR ELECTRICAL CABINETS

Approved by:

Dr. Barry J. Goodno, Co-Advisor
School of Civil and Environmental Engineering
Georgia Institute of Technology

Dr. James I. Craig, Co-Advisor
School of Aerospace Engineering
Georgia Institute of Technology

Dr. Reginald DesRoches
School of Civil and Environmental Engineering
Georgia Institute of Technology

Dr. Donald White
School of Civil and Environmental Engineering
Georgia Institute of Technology

Mr. Philip Caldwell
Schneider Electric

Date Approved: October 17, 2016

ACKNOWLEDGEMENTS

I would like to express my sincere appreciation for Dr. Barry J. Goodno and Dr. James I. Craig for their consistent support and guidance that have kept me on the track of my research. They will always be my role models to become a better researcher. I also would like to extend my appreciation to the members of the thesis committee, Dr. Reginald DesRoches, Dr. Donald White, and Mr. Philip Caldwell for all their constructive advice and valuable recommendations.

I would like to thank the CEE Department especially Dr. Donald Webster, Dr. Lawrence Kahn, and Dr. Donald White that have given me the opportunity to teach Statics course at Georgia Tech. This opportunity has given me not only partial financial support for my study but also invaluable teaching experience. In addition, I would like to thank to Dr. Barry J. Goodno for his endless effort to mentor me to become a better educator.

I would like to thank all my friends in Mason 4132 for their friendships, discussions, and laughter that I will remember forever. I also would like thank to my girlfriend, Liu Xi, for her endless support and encouragement that have made everything much easier.

Most of all, I would like to thank my parents and family for their constant support and prayers that have given me the strength to carry this cross with a smile.

TABLE OF CONTENTS

LIST OF TABLES

LIST OF FIGURES

GLOSSARY

Bare-frame cabinet model	See *Bare-frame model*
Bare-frame model	A configuration of electrical cabinet in which the enclosure panels are excluded
Benchmark beam model	A shell element model of a beam member that is developed for validation purposes
Benchmark cabinet model	A shell element model of a cabinet that is developed for validation purposes
Busbar assembly	The assembly of busbars consists of top, midtop, midbottom, bottom busbars, and the insulation bars
Cabinet assembly	The assembly of two electrical switchboard cabinets. The dimensions of each cabinet are 30 in. (width), 36 in. (depth), and 90 in. (height).
Case 1 cabinet assembly	A *properly anchored cabinet assembly* which is subjected to time history analysis by excluding the geometric nonlinear effect and with 1.0 g PGA for the ground motions.
Case 2 cabinet assembly	A *properly anchored cabinet assembly* which is subjected to time history analysis by including the geometric nonlinear effect
Case 3 cabinet assembly	A *properly anchored cabinet assembly* which is subjected to time history analysis with 2.5 g PGA for the ground motions
Case 4 cabinet assembly	The *Case 1 cabinet assembly* in which its inner supports are removed
Case 5 cabinet assembly	The *Case 1 cabinet assembly* in which its outer corner supports are removed
Class I configuration	A simple configuration of electrical switchboard cabinet in which the framing members are constructed

	using plain angle and plain channel section, and the enclosure panels are constructed using plain steel plate
Class II configuration	A complex configuration of electrical switchboard cabinet in which the framing members are constructed using folded angle sections and plain channel section, and the enclosure panels are constructed using folded steel plate
Damping model	• Rate-independent damping or Structural damping in the context of Chapter 5. • Rayleigh damping in the context of Chapter 6
Direct analysis method	An analysis and design method formulated in AISC code for calculating the demand and capacity of a member.
Direct strength method	A method to predict the localized buckling strength of a member
Effective-width method	A method to predict the localized buckling strength of a member based on effective-width equations
Effective-width prediction	Prediction of the in-plane moment and rotation of a beam member with a plain channel or plain angle section subjected to double curvature bending
Effective-width prediction method	A low fidelity method in identifying the properties of springs in the hybrid Timoshenko beam model of a member based on the effective-width prediction of that member.
Empirical effective width equation	An effective width equation derived from experimental tests of plates. This equation is obtained from AISI code.
Full-cabinet model	A configuration of electrical cabinet in which the enclosure panels are included
Hybrid beam model	See *Hybrid Timoshenko beam model*
Hybrid Timoshenko beam	A finite element model of a beam member generated

model	using Timoshenko beam elements and a rotational spring in each end of the member
Imperfect Hybrid Timoshenko beam Model	A *hybrid Timoshenko beam model* of a plain channel section member with spring properties generated using the empirical effective width equation in AISI code
Inadequately anchored cabinet	An electrical cabinet that is anchored at all intended locations, but the anchors are inadequate to carry lateral load imposed on the cabinet
Imperfect Model	A shell element of an imperfect plain channel beam member subjected to double curvature bending under geometric nonlinear analysis
Mass model	Representative models for the mass of electrical cabinets and electrical devices as the consequences of the selected finite element models (e.g. consistent mass model for framing members and busbar, and a tributary mass model for main circuit breaker, panels, meter device)
Modified effective-width prediction	Prediction of the in-plane moment and rotation of a beam member with a plain channel section subjected to double curvature bending using an *empirical effective equation* adopted in AISI code.
Partially anchored cabinet assembly	An electrical cabinet that is not anchored at all intended locations.
Perfect Model	A shell element of a perfect plain channel beam member subjected to double curvature bending under geometric nonlinear analysis
Properly anchored cabinet assembly	Electrical *cabinet assembly* that is anchored at all intended locations, and the supports can resist lateral force without damage.
Scaled Imperfect Hybrid Timoshenko Beam	An *imperfect hybrid Timoshenko beam model* in which its stiffness is scaled to 90% of its original stiffness

Shell element method	A high fidelity method in identifying the properties of springs in the *hybrid Timoshenko beam model* of a member based on a shell element model of that member.
Simplified cabinet assembly model	The simplified finite element model of the cabinet assembly. The simplified model is generated using the proposed method described in this study
Simplified cabinet model	A finite element model of an electrical cabinet constructed using beam elements, shell elements, springs and constraints.
Structural model	A finite element model for the structural components of electrical cabinets (e.g. framing members, panels, and connection)
Timoshenko beam model	A finite element model of a beam member developed using Timoshenko beam elements

SUMMARY

An electrical switchboard cabinet is one of the essential pieces of equipment in an electrical distribution system running from a power plant to important facilities such as hospitals. The cabinet houses electrical devices, such as circuit breakers, busbars, and meters that are critical to continued operation of a variety of essential facilities. The cabinet is usually constructed using cold-formed steel members, steel panels, and screw and bolt connections. Methods typically used to assess the dynamic behavior of a properly anchored cabinet are experimental tests and high fidelity finite element models in which all structural elements (i.e., members and panels) are modeled using shell elements. However, these methods are time consuming and expensive, and interpretation of the results may be difficult especially for multiple cabinet arrangements. Therefore, a method to generate a simplified finite element model for the cabinet is proposed in this study. The simplified model consists of Timoshenko beam elements, shell elements, and springs and constraint equations. This model has the capability to capture the possible nonlinear behavior of the cabinet such as buckling of steel panels, failure of screw connections, and possible elastic local buckling near the ends of beam members. The proposed simplified cabinet model was validated using the benchmark cabinet model in both geometric linear and nonlinear pushover analyses. Further applications of the simplified cabinet model in frequency response analysis and time history analysis are also discussed.

CHAPTER 1

INTRODUCTION

1.1 Problem Description

Electrical power is transmitted from a generating station through a wide area transmission system and distribution subsystems leading eventually to end-users (consumers). At the facilities of a commercial end-user (e.g. manufacturing plant, commercial building, hospital) the electrical power is distributed to different devices (loads) through transformers and switchboards consisting of switches and monitoring, distributing, and controlling equipment housed in cabinet-like structures (see Figure 1.1 which diagrams a relatively simple configuration of power distribution and shows switchgear and switchboard installations). This electrical equipment is essential to maintaining the continuity and stability of electrical distribution within a facility and is therefore critical to the operation of most facilities.

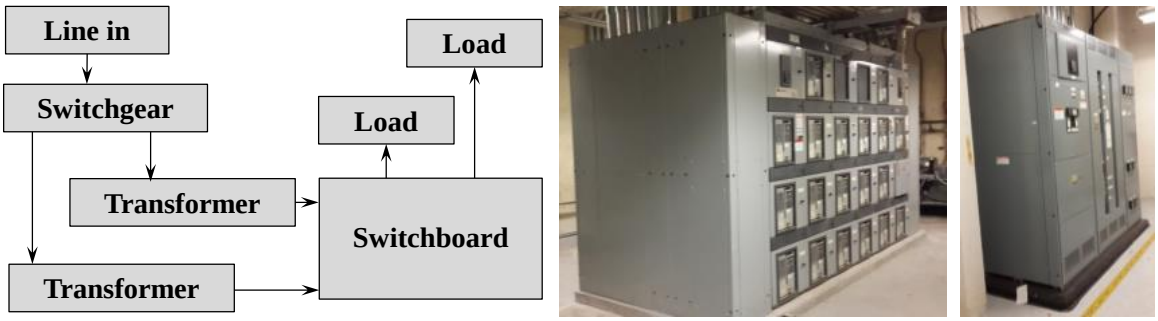

(a) Schematic diagram (b) Switchgear (c) Switchboard

Figure 1.1 A typical power distribution system within an end-user's facility

Unfortunately, the electrical equipment in such cabinets is vulnerable to damage or failure during an earthquake. In general, there are two categories of failure that can happen to the equipment during an earthquake. The first category is the failure of the equipment caused by structural damage to the cabinets during an earthquake. The structural damage to an electrical cabinet can be further categorized into one of two types

1) failure of unanchored/inadequately anchored cabinets; or 2) failure of properly anchored cabinets. The structural performance of unanchored/inadequately anchored electrical cabinets is summarized in Table 1.1. This data is based on the reconnaissance report by EQE Engineering for the Electric Power Research Institute (EQE Engineering., 1991) and Goodno et al (Goodno et al., 2011).

Table 1.1 Structural damage of unanchored/inadequately anchored electrical cabinets (Total data: 26 cabinets)

Type of structural damage	Percentage of observed damage to number of damaged cabinets (%)
Sliding	50.0
Anchorage	30.8
Overturning	11.5
Frames	11.5
Panels	7.7
Bracing	7.7
Concrete pedestal	3.8

Sliding and overturning of the electrical cabinet governs the failure shown in Figure 1.2.a and b. In addition, damage to the anchor bolt (Figure 1.2.c), damage to the base channel (Figure 1.2.d), and damage to the concrete pedestal were also observed in the surveys. This damage was mainly caused by the interaction between structural components in the cabinets (i.e., bolt and frame) and impacts between the cabinet and the adjacent structures (e.g., concrete columns, pedestal). In experimental tests, three types of failures have been observed related to properly anchored cabinets: 1) stripping or shearing of panel-frame connections (screw); 2) deformation of enclosure panels; and 3) detachment of electrical components inside the cabinet.

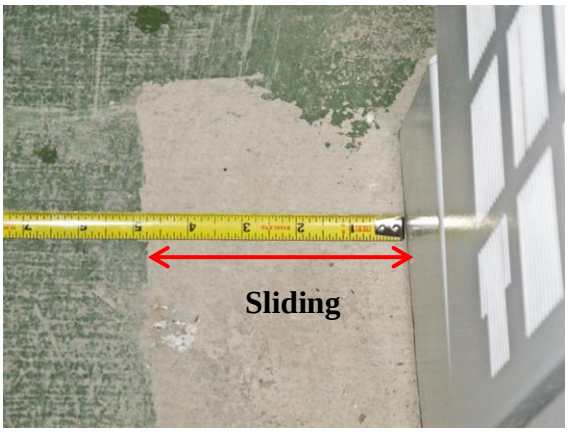

(a) Sliding (courtesy: Goodno et al.),

(b) Overturning (FEMA E74, courtesy: Degenkolb Engineers

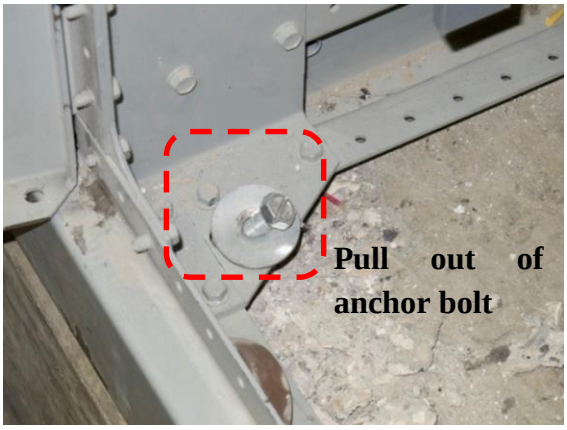

(c) Pull-out of anchor bolt (courtesy: Goodno et al. (2011))

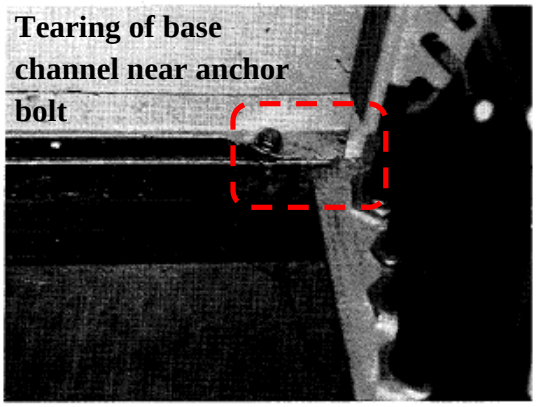

(d) Tearing of base channel near anchor bolt (courtesy: EQE Engineering. (1991))

Figure 1.2 Typical structural failures of unanchored/inadequately anchored electrical cabinets.

The second category is the failure of electrical equipment due to seismic vibration. This failure is related to the sensitivity of the internal equipment to vibration intensity inside the cabinet and to the relative displacement of the cabinet and its internal components induced by the vibration. There may be no damage to the cabinet itself in this type of failure, or even if there is, the damage is not severe enough to cause equipment failure. The proposed research focuses on the second category, specifically the performance of the cabinet structural system caused by seismic loading of properly anchored electrical cabinets.

In general, there are three methods that can be used to assess the performance of electrical cabinets. The first method is experimental test (e.g., shake table test). This method is endorsed in ASCE 7-10 (Section 13.2) for seismic qualification of any electrical cabinet that hosts active equipment because results of the test reveal how the particular cabinet has performed under input ground motion that matches required response spectra specified in the guidelines (e.g. IEEE 693, AC 156). The second assessment method is referred to as the analytical method. Here, a high fidelity finite element model of the cabinet is developed in which all structural components of the cabinet are modeled explicitly using shell elements. The third method is based on expert opinion. This method is tied to the reconnaissance surveys from the past earthquakes and observations from the past experimental tests of the cabinets.

For groups of cabinets, implementation of the first two methods (i.e., shake table testing and high fidelity finite element modeling) becomes expensive, and interpretation of the results may be difficult. Figure 1.3 shows the work content and person-hours estimation for nonstructural experimental qualification based on the complexity of the equipment. In this figure, the qualification work is divided into three categories: 1) preparation, 2) analysis, 3) experimental test. As the complexity of the equipment increases, the total hours needed to perform the qualification work increases. In all cases, the experimental test approach is the most time consuming and the analysis approach is the least time consuming. This large portion of experimental work increases the cost of equipment qualification. However, for some cases (e.g. large equipment), the portion of experimental work can be reduced by performing the qualification of the structural system of the equipment using the analytical method, and only perform the experimental test on the electrical devices based on the results of the analytical method. Although using the analytical method is relatively simpler than the experimental method, the complexity of the numerical model can be high for large equipment. This complexity may make the analytical method become inefficient. Therefore, there is a need to develop

a simplified analytical method (i.e., finite element model) to reduce the analyses time and complexity specifically for complex equipment.

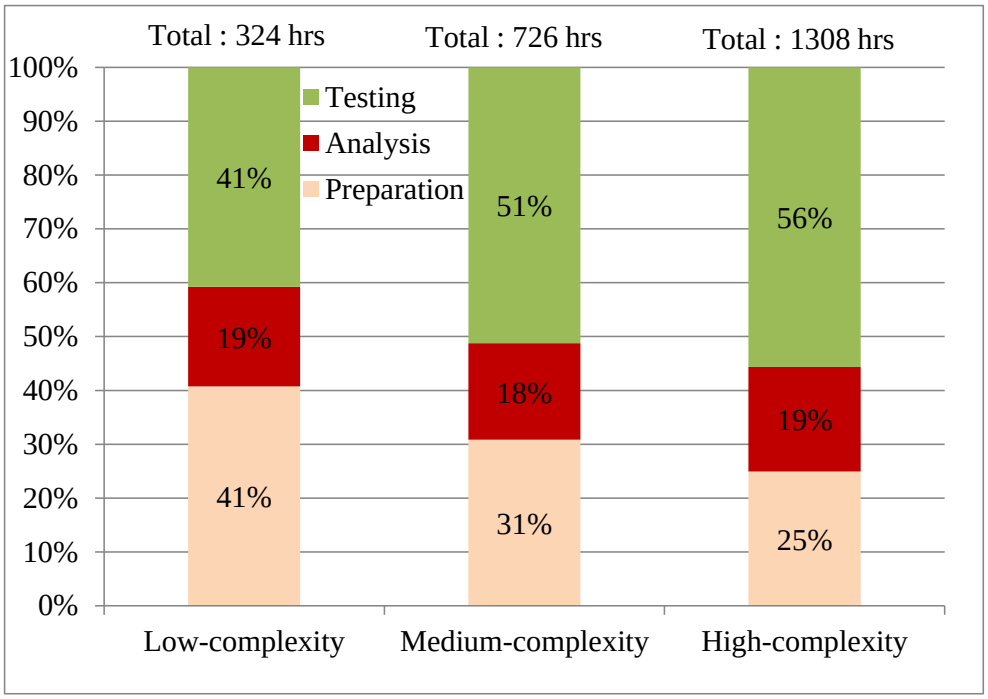

Figure 1.3 Work content and hours estimation for nonstructural qualification based on the complexity of the electrical equipment (data source: Gatscher et al. (2012))

This study proposes a generic method that can be applied to generate a simplified finite element model of the cabinet. In Chapter 2, a detailed description of the cabinet and literature reviews of the previous proposed simplified modelling of the cabinet are presented. Chapter 3 discusses the proposed method that is applied to a cabinet with a relatively simple configuration. Chapter 4 extends the application of the proposed method to a cabinet with a complex configuration and describes some additional modeling features that need to be included to improve the results. Chapter 5 describes the application of the proposed method in frequency response analyses and proposes methods to incorporate masses into the simplified cabinet model. Lastly, chapter 6 shows how the simplified cabinet model can be used to assess the performance of a group of cabinets in a time history dynamic analysis.

1.2 Objectives

The objectives of this research are to:

1) Develop a methodology for generating a simplified numerical model of an electrical switchboard cabinet that has the capability to capture the behavior of a properly anchored electrical cabinet observed during the experimental tests, including a potential elastic local buckling effect near the end of the framing members.
2) Use the simplified numerical model of the cabinet to investigate the dynamic characteristics of a single cabinet and the electrical devices installed inside the cabinet.
3) Extend the application of the proposed method to a complex configuration of electrical cabinets.
4) Extend the application of the method to study the dynamic behaviors of a group of cabinets.

CHAPTER 2

GENERAL DESCRIPTION OF AN ELECTRICAL SWITCHBOARD CABINET AND NUMERICAL METHODS USED TO ASSESS ITS PERFORMANCE

2.1 General Description of an Electrical Switchboard Cabinet

A simple way to understand the function of an electrical switchboard cabinet for a non-electrical engineer is to begin with the power distribution system in residential housing. In general, the electricity will be transmitted from the source through a meter and circuit breakers attached to a panel before it is delivered to the house appliances/loads (e.g. washing machine, refrigerator, and lights) as shown in Figure 2.1. The electrical power is distributed within the panel board into a dozen or more separate circuits, each protected by an over-current circuit breaker that can also be used to disconnect the circuit when needed.

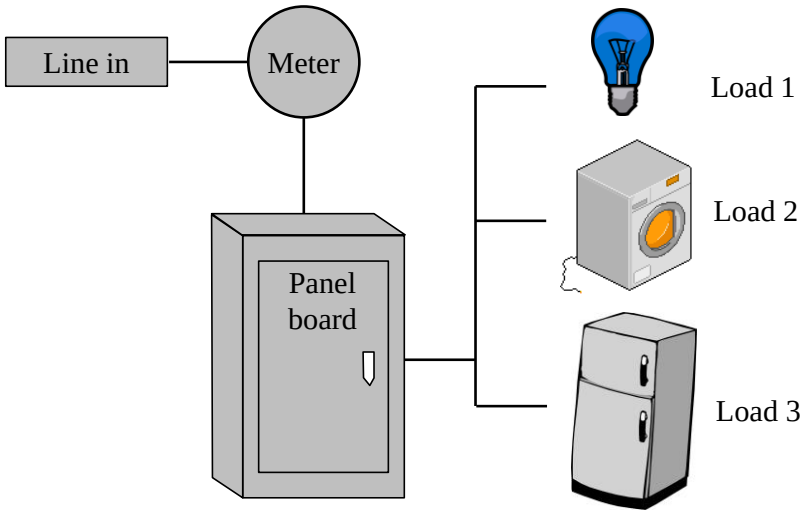

Figure 2.1 Simple electrical distribution in residential housing

For larger facilities, the electricity must go through several additional pieces of electrical equipment, such as switchgear, transformer, and switchboard, before it is

distributed to the loads. The complexity rises because there is a need to protect the operational equipment in facilities or other buildings (e.g. hospital) that often requires higher levels of current and voltage than the typical household appliances. Since electrical power is transmitted more efficiently at high voltages, transformers are used to decrease (step down) the voltage to that required by the load, and this can happen in several steps throughout the distribution system. The switchgear and switchboard have mostly the same main functions (to protect the distribution system and to distribute the electricity) as the panel board in residential housing but the size and the complexity of the switchgear and switchboard are greater than the panel board in residential housing. Switchgear may differ from a typical switchboard in terms of the following: 1) the standard used to design the equipment, and 2) the structural configurations. Switchgear typically has a larger size and often requires front and rear access. The front and rear part of a switchgear typically consist of several compartments used to house the circuit breakers and busbars, respectively (see Figure 2.2). On the other hand, a switchboard usually is smaller, and it may only require front access. Figure 2.3 shows a configuration of switchboard cabinets, and busbars and circuit breakers mounted in the cabinets. Both the switchgear and switchboard are usually constructed from cold-formed steel members with enclosing panels. In this study, only electrical switchboard cabinets are considered to limit the scope of study. However, one may find that the method used to generate the simplified model for the electrical switchboard cabinet proposed in this study can also be applied to a switchgear cabinet because of the similarities in the structural system.

(a) (b) (c)

Figure 2.2 Switchgear: (a) Complete unit, b) Busbar for distributing current and located in the rear compartment, and c) Circuit breaker located in the front compartment.

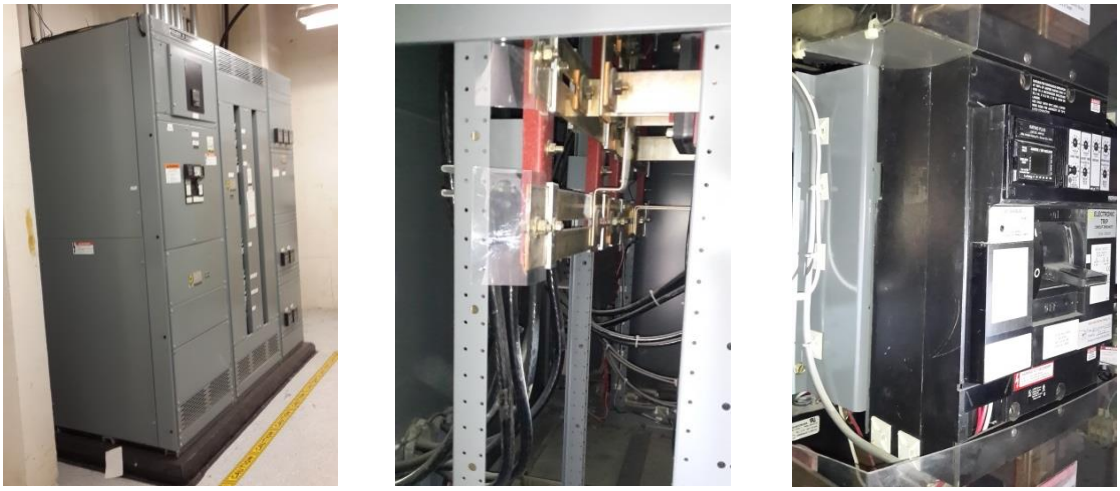

(a) (b) (c)

Figure 2.3 Switchboard: a) Complete unit, b) Busbar, and c) Circuit breaker mounted inside the switchboard cabinet

Typically, the distribution of the electrical devices inside the switchboard cabinet is scattered. However, since most of the cabinet is only required front access, many electrical devices (e.g. circuit breakers and meters) are attached on the front side of the cabinet for monitoring and maintenance purposes. These devices can be mounted on the front panels and on the vertical posts of the cabinet (see Figure 2.4.a and b). In addition, busbars are usually located on the rear or middle side of the cabinet. These busbars are

usually arranged in a group (see Figure 2.4.c) and attached to the back vertical posts or intermediate posts in the cabinets.

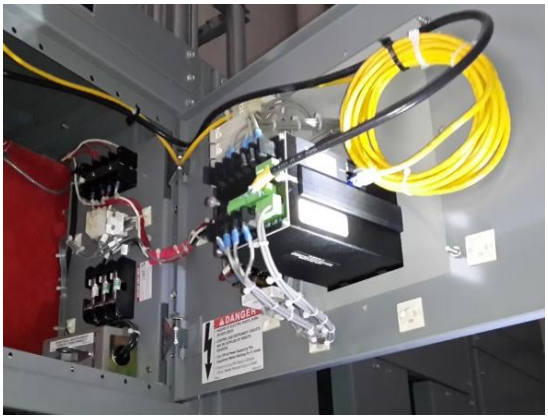

(a) Meters attached on the front panels

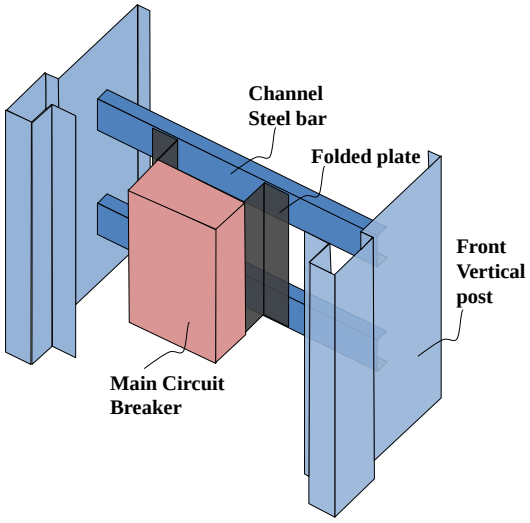

(b) Sketch of main circuit breaker attached on the vertical posts

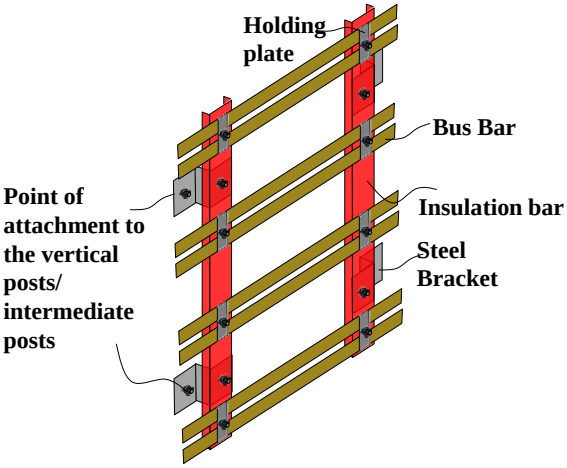

(c) Sketch of group of Busbars

Figure 2.4 Configurations of some electrical devices hosted in the switchboard cabinet

Many of electrical switchboard cabinets are custom built based on the demand and the availability of space. Hence, there is no so-called most "common" type of electrical switchboard/switchgear cabinets. AC156-"Acceptance criteria for seismic certification by shake-table testing of nonstructural components" (AC-156, 2010) requires a configuration of cabinets in the same product line that produces the highest demand and the least capacity ("the most conservative") to be certified. In selecting the "most conservative" configuration, the structural features, mounting features, mass distribution, subassemblies, and components variations of the cabinets must be considered.

2.2 Structural Features of Electrical Switchboard Cabinet

An electrical switchboard cabinet is usually constructed from thin-wall open-section cold-formed steel members enclosed by steel panels. The framing members are usually connected together with screws or bolts and the enclosure panels are usually attached to the framing member using screws. The framing system of the electrical cabinet fundamentally works in the same way as the framing system of the building. The enclosure panels are attached to the sides of the cabinet and will improve the structural integrity of the cabinet depending on the number of screws used to attach the panels to the cabinet. The framing system is then usually anchored to the ground using anchor bolts. One type of anchorage is shown in Figure 2.5. This configuration is assumed to be a fixed support in this study although one may argue that the flexibility of the anchor bolt and the channel beams cannot be ignored. Study of the flexibility of different anchor bolt configurations is beyond the scope of this research.

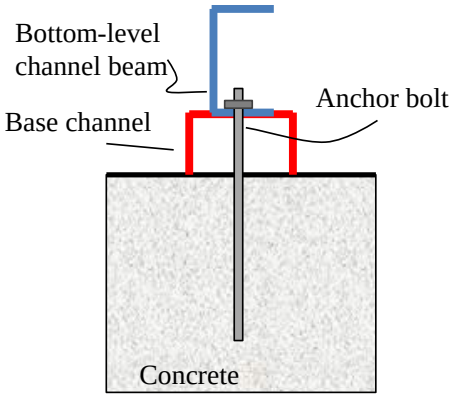

Figure 2.5 Anchor bolt configuration that is considered as a fixed support

Other components that may contribute to the functionality of the cabinets are attachments. Gatscher, et al (Gatscher et al., 2012) divides these attachments into three subcategories: 1) operational, 2) bracing, and 3) isolation. *Operational* attachments are any components attached to the cabinet in order to maintain the active operations of the cabinets. The electrical conduits shown in Figure 2.6 are an example of operational attachments, since they help to distribute the electric current. *Bracing* attachments (e.g. top bracing) can improve the structural rigidity of the cabinets and reduce relative displacement of the cabinet. Finally, *isolation* is a mechanical attachment used to change the dynamic characteristic of cabinet in favorable ways such as reducing seismic demand and dynamic amplification. An isolator is often inserted between the framing system and the anchorage. All of these attachments are outside of the scope of this research. Thus, this study focuses on the performance of the properly anchored free-standing cabinets.

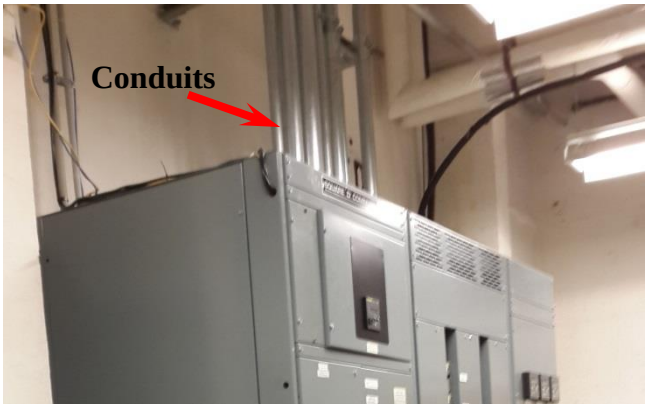

Figure 2.6 Electrical conduits on top of electrical switchboard cabinet

2.3 Literature Review on the Numerical Methods Used to Assess the Performance of an Electrical Cabinet

The benefits of a good numerical model of a switchboard cabinet and typical structural configurations for the cabinet model have been discussed in previous sections. Several methods have been developed to numerically evaluate the characteristics of electrical cabinets. Budy et al. (Notohardjono et al., 2009) developed a numerical model for a server computer structure (see Figure 2.7). Although this structure does not have the same functionality as an electrical cabinet, it has similar structural properties to an electrical cabinet in terms of the materials and the structural system used, such as the framing system and the attached panels. In their work, Budy et al. developed a high fidelity finite element model and validated the natural frequencies of the model with experimental results. This numerical model requires high computational demand because all members, panels, and connections were modeled using shell or brick elements. In addition, with such a large model, understanding the analysis and interpreting the results can be a challenging task. Therefore, this model may not be suitable for the evaluation of the wide variety of cabinets of different sizes and configurations that are in common use.

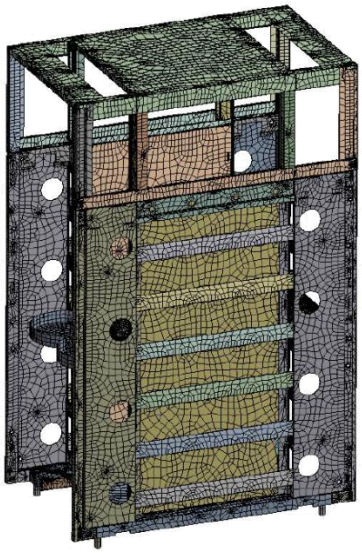

Figure 2.7 High fidelity model for a server computer cabinet (courtesy of Notohardjono et al. (2009))

In 1991, Gupta et al. (Gupta and Yang, 2002) adopted a Rayleigh-Ritz approach to develop a simplified model considering one global and one local mode to predict the performance of electrical cabinets. In their study, a high-fidelity finite element model was set as the benchmark for comparison to their simplified model. The results of this simplified model matched the performance results obtained using a detailed finite element analysis. Gupta et al. also extensively described the dynamic behavior of the electrical cabinet and the dependency of significant modes to the location of instruments inside the cabinet. However, the applicability of this method to other configurations of cabinets is unclear because the authors do not explain how the model handles the variety of partially rigid connections between framing members, and connections between panels and framing members.

Cho et al. (Cho et al., 2011) developed a simplified model which consists of nonlinear beam elements arranged vertically and five lumped masses along the height of the beam to represent the mass in each rack of the cabinet. A Duffing's type equation was adopted to define the nonlinearity in the cabinet. This model overestimated the frequencies and transfer functions of experimental tests by 12% and 10%, respectively. Despite the reasonably close prediction, there is still a need to validate this method for other configurations of cabinets. In addition, the applicability of this method in multi-cabinet configurations (assemblages of cabinets) is also unclear.

Hur (Hur, 2012) developed a method to generate a simplified electrical cabinet models that consists of frame elements for framing members, shell elements for panels, and nonlinear springs for connections between framing members and for connection between panels and framing members. This approach allows a general application of the method to different configurations of cabinets. Validation of this approach has shown that a model generated using this framework underestimated the first-mode experimental frequency by 1% and overestimated the second-mode experimental frequency by 20%. Despite its relatively accurate results and its more general applicability, some cabinet

behaviors cannot be explained thoroughly based on this work, specifically: 1) vague validations on the definition of partially rigid connections between framing members and the connections between panels and framing members that cause the contribution to the modal properties of the cabinet of the modeling features (springs) developed for each type of connections cannot be distinguished; 2) omission of the effect of warping deformations in the framing members to the behavior of cabinets; and 3) omission of the effect of elastic local buckling near the ends of a member that may exist when the cabinet is subjected to a dynamic load.

This study proposes a method to generate a simplified finite element model for electrical switchboard cabinets. This study builds upon the models developed by Hur in which the framing members and the panels are modeled with frame and shell elements, respectively. In addition, linear rotational springs and nonlinear translational springs are introduced to model the connection between framing members and the connection between panels and framing members, respectively. Additional modeling features, such as rotational springs and constraint equations, are also introduced to the simplified cabinet model to improve the capability of the model to capture: 1) possible elastic local buckling behavior near the ends of the member, and 2) the effect of warping deformation of the framing members to the behavior of cabinets. These two features are important to a good cabinet model because the framing members of the cabinet are typically constructed using thin-wall open-section cold-formed steel members that may buckle and warp due to the loadings acting on the cabinet. Chapter 3 will discuss the development of this method for a relatively simple cabinet configuration in more detail.

CHAPTER 3

DEVELOPMENT OF A SIMPLIFIED FINITE ELEMENT MODEL OF ELECTRICAL SWITCHBOARD CABINET: CLASS I CONFIGURATION

This chapter discusses a method to generate a simplified finite element model for an electrical switchboard cabinet that has a relatively simple configuration. This configuration is labeled as a class I configuration. In the next chapter, this method together with some improvements is applied to generate a simplified finite element model for an electrical switchboard cabinet that has a more complex configuration (labeled as class II configuration).

3.1 Description of the Class I Configuration

The class I configuration is a model of an electrical switchboard cabinet where all structural components are constructed from plain sections (i.e. plain angle, plain channel, and panels without folded edges). This configuration is selected because: 1) it has been found in the construction of a switchgear cabinet as shown in Figure 3.1. Since the structural system of switchgear and switchboard cabinets are typically similar, this configuration may also be relevant to electrical switchboard cabinets; 2) it provides an initial step to understand the behavior of a more complex configuration of the electrical switchboard cabinet (see Chapter 4).

(a) Front view of group of switchgear cabinets

(b) Rear view of the switchgear cabinets showing the panels without folded edges

(c) Plain channel section used as the framing members of the switchgear cabinets

Figure 3.1 Typical configuration of switchgear cabinets

Figure 3.2 shows the configuration of the basic cabinet model. The cabinet has a height of 90 in., a width of 36 in., and a depth of 24 in. Plain angle sections are used to build four vertical posts at the corners of the cabinet (see Figure 3.3.a). These vertical posts are connected with plain channel beam members (see Figure 3.3.b) attached to the posts at the top, the mid-height, and the bottom of the cabinet using bolts and screws to form the framing system of the cabinet. The configuration of the connection between the vertical posts and the beams is shown in Figure 3.4.a. This framing system is then enclosed by steel panels covering all eight openings in the sides of the frames and one panel covering the top of the cabinet. The panels are attached using roll-threaded screws

attached at the four corners of each panel. The configuration of the connection between panels and framing members is shown in Figure 3.4.b. Finally, the cabinet is assumed to have a fixed support at each of its four bottom corners.

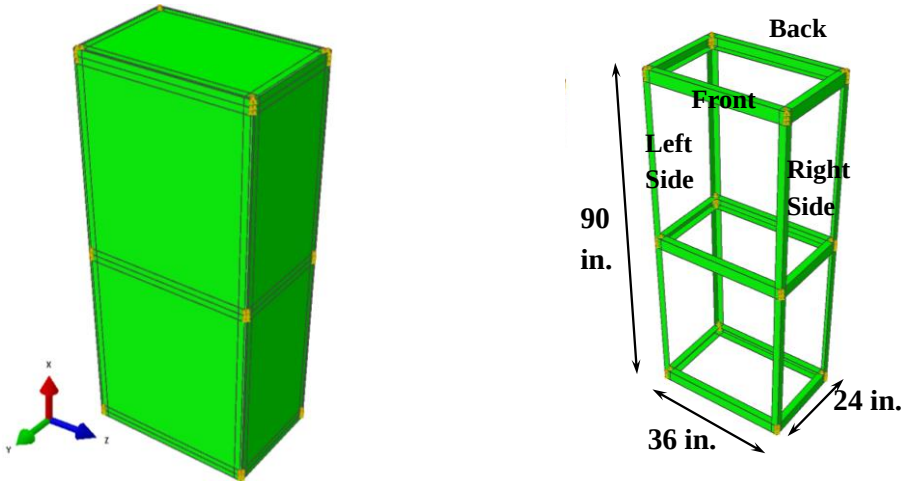

(a) Full-cabinet configuration (b) Bare-frame configuration

Figure 3.2 The class I configuration

(a) Plain angle section (b) Plain channel section

Figure 3.3 Cross sections of the framing members

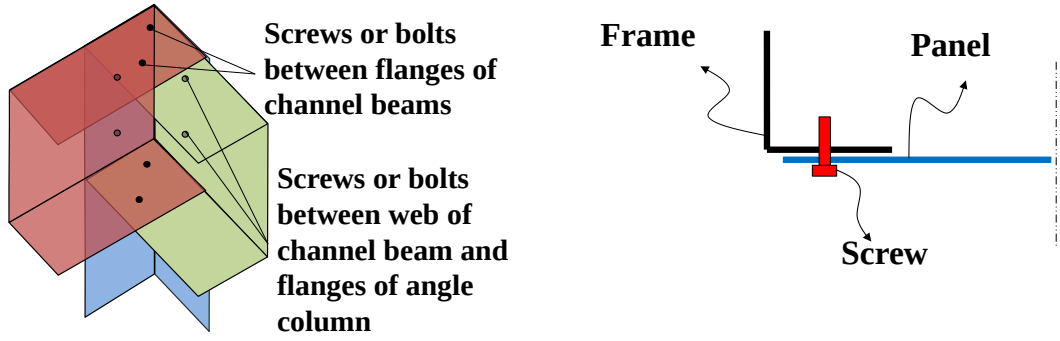

(a)Connection between framing members (b) Connection between panel and framing member

Figure 3.4 Configuration of the connections in the class I cabinet configuration

Framing members, panels and their connections to the framing members, and the connections between framing members are the main structural components of an electrical switchboard cabinet. In the simplified model, each component is represented by a finite element model or modeling features (i.e. springs, constraints). The material of the framing members and the panels is assumed to be linearly elastic, and the behavior of the connection between the framing members is assumed to be linearly elastic as well. These assumptions are taken because there is no clear evidence from earthquake reconnaissance surveys or shake-table tests that these components have yielded. The only sources of nonlinearities incorporated in the simplified cabinet model are: 1) failure of the connection between panels and framing members, 2) elastic buckling of the panels, and 3) possible elastic local buckling near the ends of the framing members due to high bending moments in thin-walled sections. The effect of dynamic load is not considered in the development of the nonlinear modeling features corresponding to the connection between panels and framing members and the elastic local buckling near the end of framing members. This dynamic effect may include the cyclic behavior on the panel-frame connection and reduction of elastic local buckling load on the framing members. Future investigations on the incorporation of this effect into the modeling features are needed. In addition, the effect of holes along the framing members and contact/friction forces between structural components are assumed to be insignificant. Small holes are usually located along the vertical posts as the places to attach electrical equipment/intermediate members in the cabinet.

3.2 Finite Element Model of the Framing Members

3.2.1 Literature Review of Numerical Models of Cold-Formed Steel Members

The frames of electrical cabinets are usually constructed from thin-walled open section cold-formed steel members. Most of these members have a shear center that does

not coincide with the sectional centroid, and as a result, any forces applied at the centroid of the cross section will not only deflect but also twist the member. This twisting in an open section will also cause axial deformation (warping) which may or may not be restrained at the ends. The complexity of this situation also increases when the limit states of the members, such as elastic local/distortional buckling, are included in an analysis. Localized buckling can develop in these sections because the flanges and the webs are thin. Figure 3.5 shows the differences between the local and distortional buckling modes for channel sections. For a plain channel section, the local and distortional buckling modes do not significantly differ. However, if additional lips at the end of the flanges are present, the two modes clearly differ.

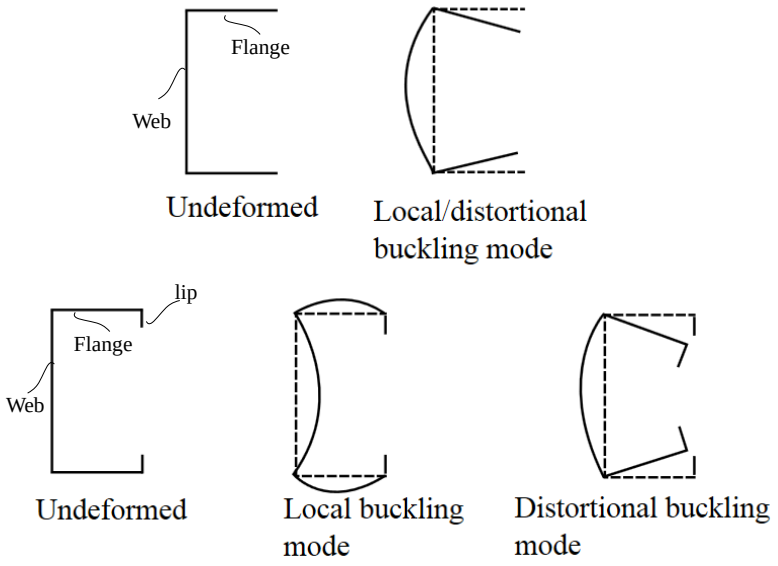

Figure 3.5 Differences between the local and distortional buckling modes in cold-formed channel section

The post-buckled strength of local and distortional buckling modes is commonly estimated in two general ways: the *effective-width method* and the *direct strength method*. The effective-width method is based on the famous effective-width equation first proposed by Von Karman (Von Karman et al., 1932). Since its first formulation, the equation has undergone several modifications so that it is applicable to the design of relevant structural members. Although the effective-width method is useful for predicting

local buckling behavior, it is deficient in predicting distortional buckling behavior. This deficiency is overcome by the application of the finite strip method, which has become the basis for the development of the direct strength method. In the finite strip method, a structural member is divided into a number of longitudinal strips along the member. The deflection of each strip is defined by a displacement function which is determined based on the boundary conditions of the member, and the strength of the member is predicted by solving the eigen-buckling equations of the system.

In contemporary structural analysis, the typical practice in modeling the localized buckling behavior of such frame members is to use shell elements in a finite element analysis. This technique may be effective for a very simple beam structure, but the computational complexity and cost increase sharply for more practical cabinet frames. Several researchers have developed a simpler model that captures local buckling behavior. Davies et al. (Davies et al., 1994) and Silvestre et al. (Silvestre and Camotim, 2003) improved a framework called generalized beam theory (GBT), which has the capability to capture the local and distortional buckling of frame members. However, because of the complexity in formulating the element, it has not been widely applied in commercial structural analysis software.

To model a single member, Wang et al. (Wang and Errera, 1971) developed another model consisting of several rigid beam elements with rotational springs at their ends. The rotational springs represented the moment-rotation relationship of the cross section and had nonlinear properties that were able to capture plasticity in the cross section and local buckling in the member. The ability to capture local buckling behavior was made possible by applying a modification of the effective-width equation proposed by Winter (Winter, 1947) to generate the moment-rotation relationship of the springs. The proposed method, validated by experimental results, exhibited close agreement with the experimental results with an error of less than 10%. Application of this method has also been recently adopted by Ayhan and Schafer (Ayhan and Schafer, 2012). The only

difference between the two methods is how the authors developed the moment-rotation relation of the springs. In their approach, Ayhan and Schafer developed an empirical method based on data fitting of the experimental and numerical tests of cold-formed steel members that fail in local and distortional buckling modes, and they linked the application of this method to ASCE 41 for earthquake analysis. Since the model considers distortional buckling behavior, their method may offer a more general application. Despite the accuracy of this approach, applying the method to a more complex structure is tedious, as the development of a particular model may require extensive effort.

This general approach can be simplified for application to a cabinet frame structure subjected to a specific type of analysis, such as a pushover analysis commonly employed in seismic design. In such an analysis, the framing members are subjected to double-curvature bending, and in this condition, high stress at the ends of the members is possible and may cause elastic local buckling of the members. In the present study, the elastic local buckling behavior is analyzed either using a shell-element or an effective-width prediction, and the resulting loss in beam rotational stiffness is modeled using a rotational spring introduced at each end of a beam member, which in turn, is modeled using simple Timoshenko beam elements commonly found in commercial software. This approach requires less modeling effort than that using the combination of rigid beams and rotational springs. This approach is proposed for application to electrical switchboard cabinets that are subjected to possible elastic local buckling of the framing members.

3.2.2 Development of the Hybrid Timoshenko Beam Model

The hybrid Timoshenko beam is a model of a framing member that is developed using Timoshenko beam elements and a nonlinear spring at each end of the framing member. The development of the hybrid model first entails the selection of either the Euler-Bernoulli or Timoshenko beam elements. The significant difference between these

elements is the ability of the Timoshenko beam element to capture the shear deformation effect in a short member (defined as a member with length-to-depth ratio < 10). Because short members may be used in the construction of electrical cabinets, the Timoshenko beam element is selected for the hybrid model.

The Timoshenko beam element does not have the capability to capture the local buckling behavior. To study the inadequacy of the Timoshenko beam element, a computational test fixture is formulated as a planar frame consisting of two rigid vertical columns pinned at their bases between which are connected a benchmark beam (modeled using shell elements) and a Timoshenko beam model, both having a channel cross section with dimensions shown in Figure 3.3.b. The arrangement is shown in Figure 3.6. The selection of shell elements enables the benchmark beam model to capture the localized buckling effect near the end of the member. The frame is restrained in translational X, Y, and Z directions and in rotational directions about the X and Y axes at the column bases. The frame is also restrained from out of plane translational movement and rotational movements about the X and Y directions at the top of the columns. During a test, incremental forces are applied at the top of the columns to impose the same rotation at each end of the beams under second order analysis. This rotation will impose double curvature bending on the beam which is a typical loading for beams subjected to lateral loads (e.g., during earthquakes).

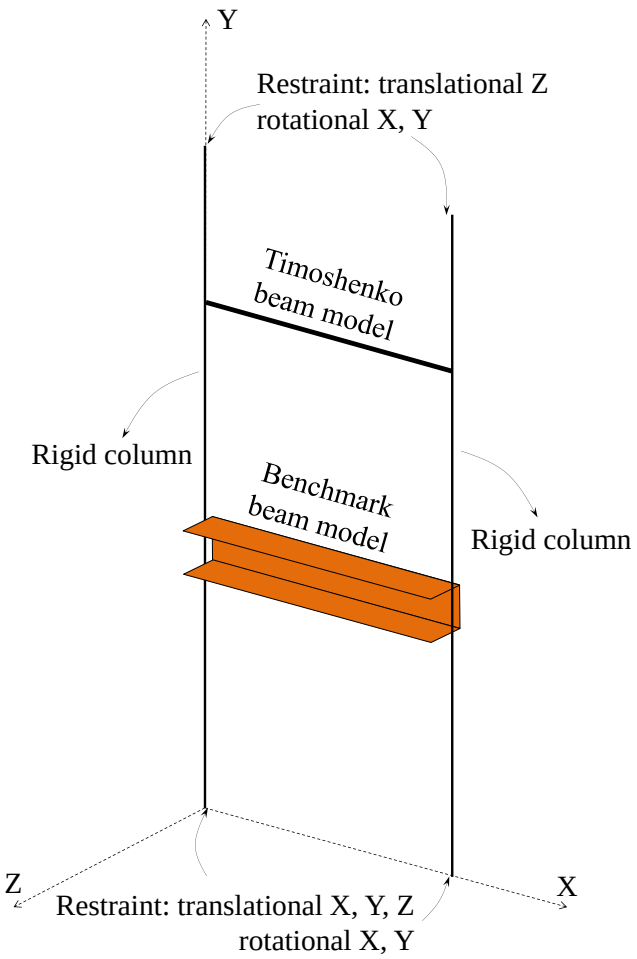

Figure 3.6 Two-rigid-column model used to study the inadequacy of the Timoshenko beam model in capturing the behavior of thin-wall open section beams

The benchmark beam model will initially behave in a linear elastic manner as shown in the sketch of the idealized end moment-rotation curve of the benchmark beam (see Figure 3.7.a). The end moments of the beam in this state induce a linear stress distribution throughout the web portion of the cross-section, as illustrated in Figure 3.7.b while the beam flange of the beam is subjected to uniform stress. The compressive stress in the members will eventually lead to localized buckling of the members as the end moments increase. The moment that causes this behavior is called the "buckling moment" (M_{cr}). After local buckling occurs, the rotational stiffness of the beam ends will decrease (see Figure 3.7.a).

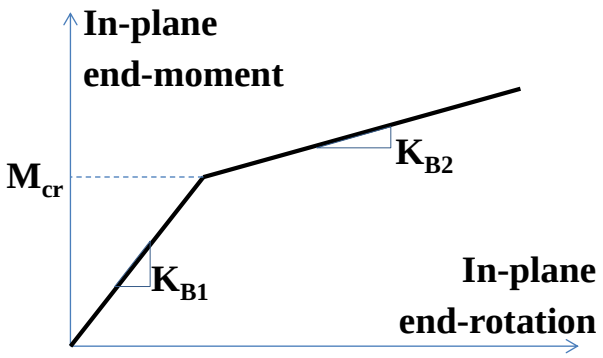

(a) Typical idealized end moment-rotation curve of the benchmark beam

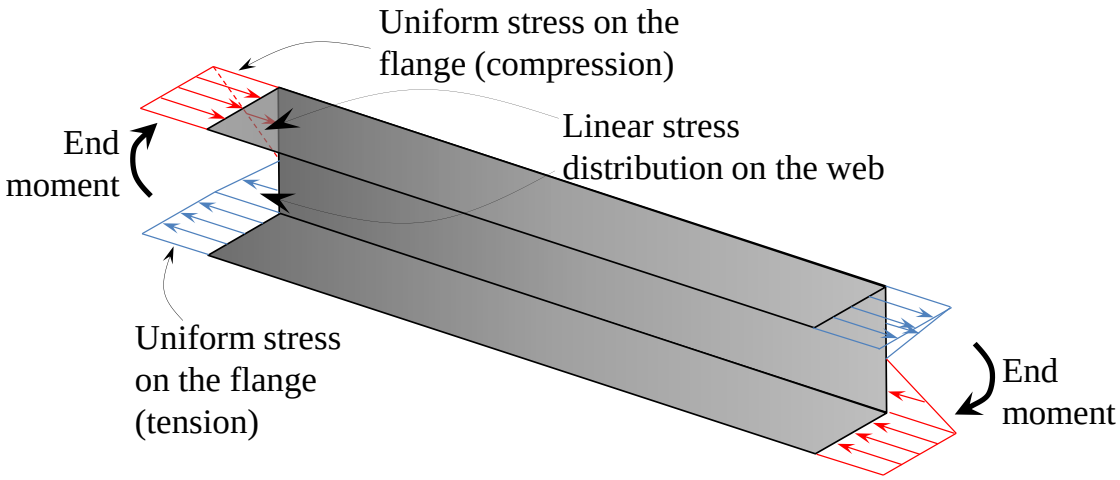

(b) Typical stress distribution of the benchmark beam in the linear elastic state

Figure 3.7 Behavior of the benchmark beam subjected to double curvature bending

A comparison of the in-plane end-moment and end-rotation of the beams for both the Timoshenko beam model (Timos. Beam) and the benchmark beam model (BM) is shown in Figure 3.8. The plot shows that the Timoshenko beam model is able to predict the initial stiffness of the benchmark beam, but as expected it does not have the capability to capture the buckling moment and the post buckling stiffness of the benchmark beam.

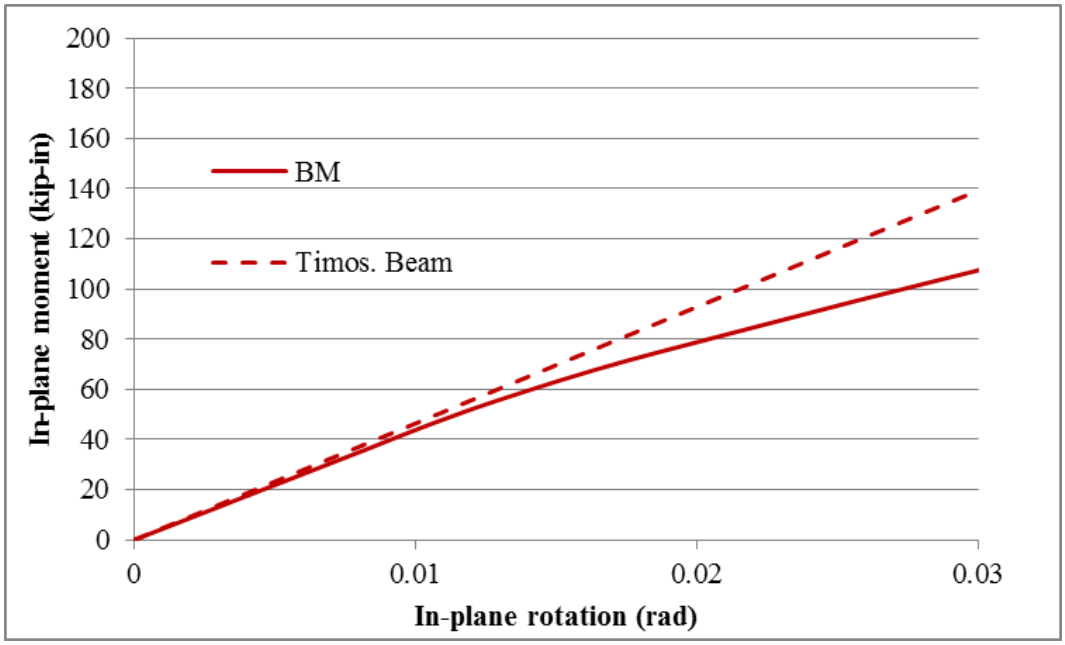

Figure 3.8 In-plane end moment-rotation plot of the Timoshenko beam model and the benchmark beam model

Therefore, a rotational spring is introduced at each end of the member to capture the stiffness-reducing effect due to elastic local buckling of the member (see Figure 3.9). The rotational springs are arranged in series in the direction 3 (in-plane direction), and the property of the springs is typically nonlinear (see Figure 3.10). The properties of the nonlinear springs are generated by excluding: 1) the coupling effect between bending and torsion, and 2) the effect of biaxial bending. Trial calculations shown that the coupling effect between bending and torsion on the members constructed using a plain channel and a plain angle section considered in this study is insignificant. In addition, only uniaxial bending is considered in this study based on the case of cabinet subjected to lateral load in the horizontal or vertical planar direction. Future investigations are needed for the application of the hybrid model on the member of electrical cabinet in which those two effects may be critical.

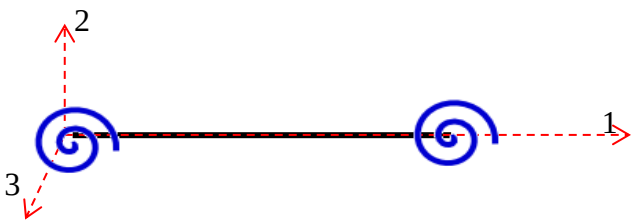

Figure 3.9 Simplified model for a steel member: frame element and nonlinear springs at both ends.

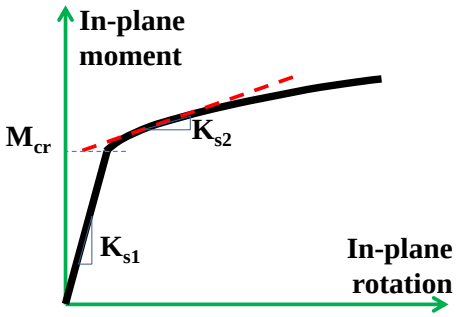

Figure 3.10 Idealized in-plane moment –rotation parameters for the rotational springs

To identify the properties of the nonlinear springs employed in the hybrid model; two approaches are used to predict the behavior of a beam member subjected to double curvature bending: 1) a high fidelity method based on a shell element model of the member (shell element method), and 2) a low fidelity method using an effective-width model of the buckled flange to describe its behavior (effective-width prediction method).

Identification of Spring Properties Based on the Shell Element Method

In this method, shell elements model of the member is analyzed by including the geometric nonlinear effect so that local buckling can be captured in the analysis. The behavior of the member is represented by an end-moment versus end-rotation curve characterized by the local buckling moment of the member (M_{cr}) and its stiffness prior to (K_{B1}) and after (K_{B2}) local buckling. Using this result, the properties of the rotational springs in the hybrid model are calculated. The local buckling moment of the member is incorporated as the break point between the initial and the post-buckled segments characterized by the initial stiffness (K_{s1}) and nonlinear post-buckled stiffness (K_{s2}),

respectively. Since the member and the rotational springs are arranged in series, the initial and post-buckling stiffness can be calculated using Eqn 3.1 and 3.2, respectively

$$K_{s1} = \frac{K_T K_{B1}}{K_T - K_{B1}} \qquad \text{Eqn 3.1}$$

$$K_{s2} = \frac{K_T K_{B2}}{K_T - K_{B2}} \qquad \text{Eqn 3.2}$$

where

K_{S1} = initial stiffness of the nonlinear spring

K_T = stiffness of the Timoshenko beam model

K_{B1} = initial stiffness of the shell element model of the beam member

K_{S2} = post-buckling stiffness of the nonlinear spring

K_{B2} = post-buckling stiffness of the shell element model of the beam member

Identification of Spring Properties Based on the Effective-width Prediction Method

In this method, an effective-width prediction of the behavior of a plain channel member subjected to double-curvature bending is the basis for generating the properties of the rotational springs used with the Timoshenko beam model of the member. Once the local buckling behavior of the beam is predicted, the spring properties are calculated using Eqn 3.1 and 3.2. In this prediction, the end-rotation of the beam is chosen as the dependent variable given the known value of the end-moment.

Figure 3.11 diagrams the general procedure used to calculate the end-rotation of the beam. The process is started by collecting the geometrical and material information of a target member. Afterward, the buckling moment and the cross-sectional moment-curvature data for the member are calculated. After the cross section moment-curvature

data is obtained, the end rotation of the beam is calculated by considering the strain energy of the member contributed by bending and shear deformations of the member. Inclusion of the torsional and warping strain energy might improve the result. However, based on trial calculations, the improvement is insignificant. More detailed descriptions of these processes are explained in the following paragraphs.

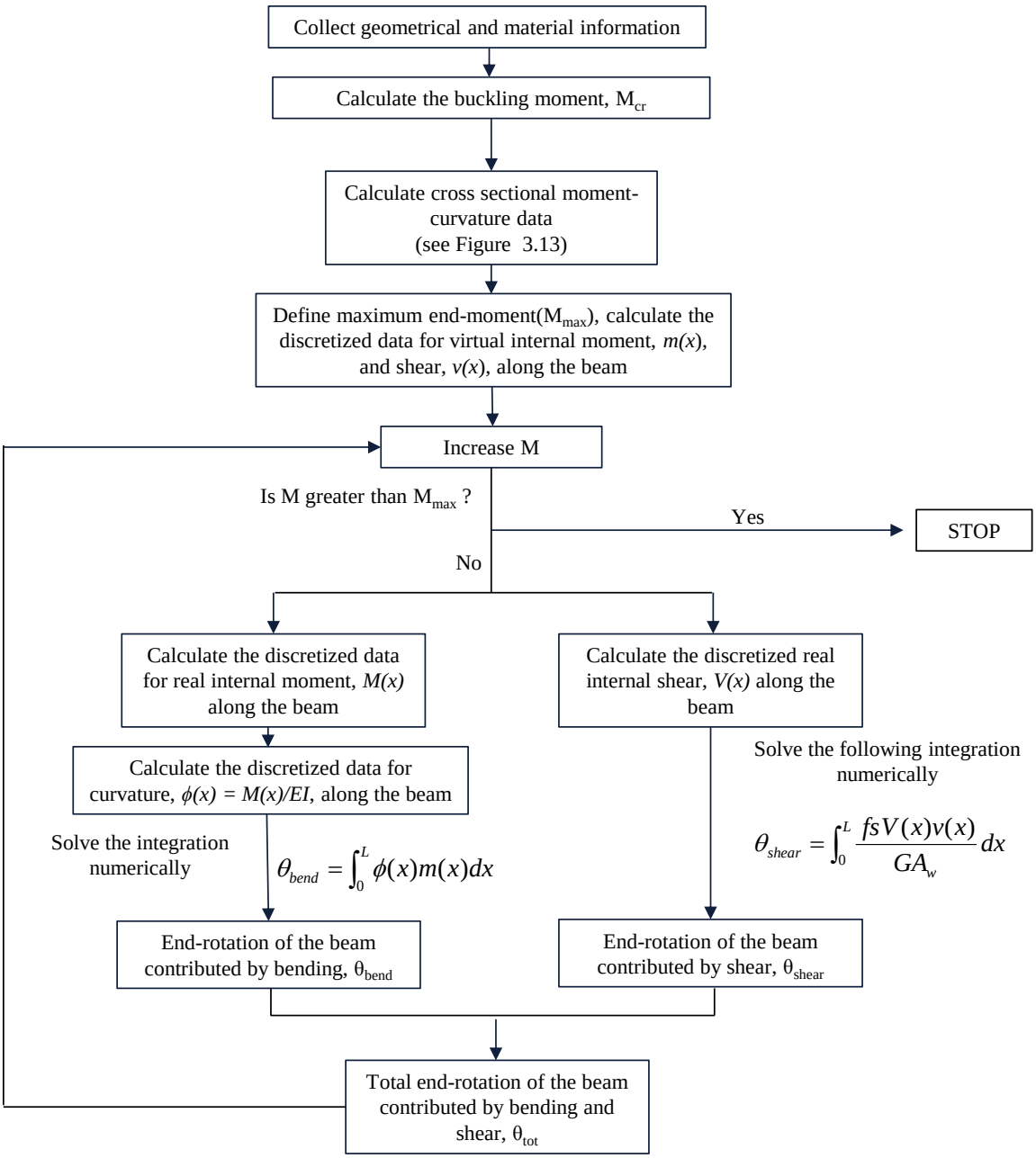

Figure 3.11 Calculation of the end-moment and end-rotation of the beam subjected to double curvature bending

As shown in Figure 3.11, the calculation of the end rotation of the member requires first the calculation of the buckling moment of the member. The buckling moment is calculated based on buckling stress obtained from a plate model (see Figure 3.12) subjected to uniformly distributed forces, N_x, across the transverse (end) edges while one longitudinal edge is free and the other which is connected to the channel web is assumed to be simply supported. These distributed forces represent the compressive stresses acting in the flanges of the member. The magnitude of the distributed forces is linearly varied between two transverse edges due to the bending moment in the beam member. The unbalanced forces are distributed along the simply supported longitudinal edge. However, the contribution of this shear force is insignificant to the buckling stress of the plate model. More detail calculations are presented in Appendix A.

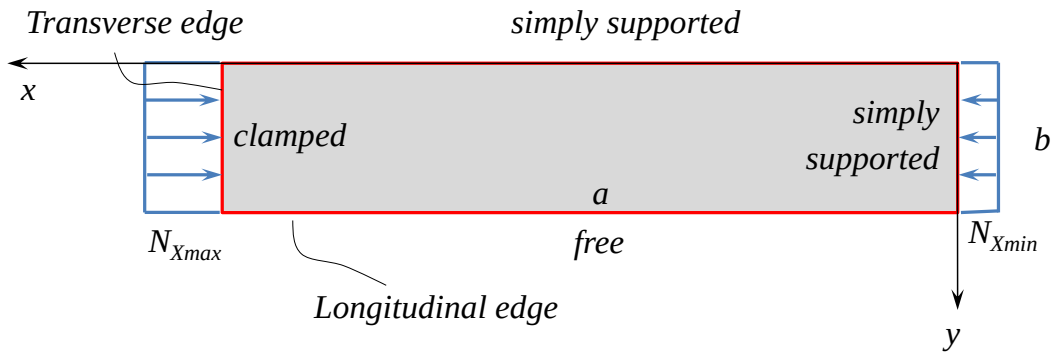

Figure 3.12 Plate model used to predict the local buckling stress of channel section member

The buckling stress for the plate is then calculated based on a Rayleigh-Ritz approach using the assumed shape function shown in Eqn 3.3.

$$u(x,y) = C_1\left(2\sin\left(\frac{\pi x}{a}\right)+\sin\left(\frac{2\pi x}{a}\right)\right)\left(\sin\left(\frac{\pi y}{2b}\right)+\sinh\left(\frac{\pi y}{2b}\right)\right) \qquad \text{Eqn 3.3}$$

where,

$u\,(x,y)$ = the shape function of the plate model

C_1 = arbitrary constant defining the magnitude of the shape function

a = length of the plate model

b = width of the plate model

Once the buckling stress equation is obtained, it can be used to calculate the buckling moment of the member by: 1) formulating a buckling moment equation of the member based on the buckling stress equation of the plate model using beam theory, and 2) finding the optimum buckling moment from the resulting buckling moment expression.

After the buckling moment and before the end-rotation of the member is obtained, the cross sectional moment-curvature curve is calculated. The slope of this curve is the beam bending rigidity, EI, which is the product of the modulus of elasticity, E, and the second area moment of the section, I (commonly called the moment of inertia). In general, the calculation of the beam rigidity can be divided into two parts: 1) calculation of beam rigidity prior to local buckling, and 2) calculation of beam rigidity after local buckling. Since the modulus of elasticity remains unchanged, the beam rigidity is sensitive to the change in the sectional second area moment. The sectional second area moment prior to local buckling is based on the original geometry of the cross section. However, the sectional second area moment after local buckling is based on the effective geometry of the cross section. The effective geometry is obtained by reducing the width, b, of the compressed flange using the modified effective width, b_e, given by:

$$b_e = \sqrt{\frac{k_c \pi^2 E t^2}{12\left(1-\mu^2\right)\sigma_{\max}}} \qquad \text{Eqn 3.4}$$

where

b_e = effective width of the element,

k_c = numerical factor obtained from the buckling stress equation of the plate model (see Appendix A for details),

E = Modulus of Elasticity,

μ = Poisson's ratio,

σ_{max} = maximum elastic stress on the element, and

t = thickness of the element.

The modified effective-width equation is formulated using the general buckling expression under the maximum elastic stress instead of the yield stress of the member as proposed in the original equation developed by Von Karman. This adjustment is based on the assumption that only elastic local buckling is possible for the framing members of the electrical cabinet due to dynamic loads. Figure 3.13 on the following page shows the flowchart used to calculate the cross sectional moment-curvature data using the modified bending stiffness.

After the cross-sectional moment-curvature data is calculated, the end rotation of the member can be computed following the general procedure shown in Figure 3.11. Once the end-moment and end-rotation of the beam are obtained, the properties of the rotational springs used in the hybrid beam model can be calculated using Eqn. 3.1 and 3.2.

All of these processes can also be applied to a member constructed with a plain angle section. However, a slight modification is needed for the plate model used to predict the buckling moment of the member. The plate model shown in Figure 3.14, which is subjected to linearly varying distributed forces on the transverse edges, is needed. This plate model represents the stress distribution on the web/flange of the member subjected to double-curvature bending.

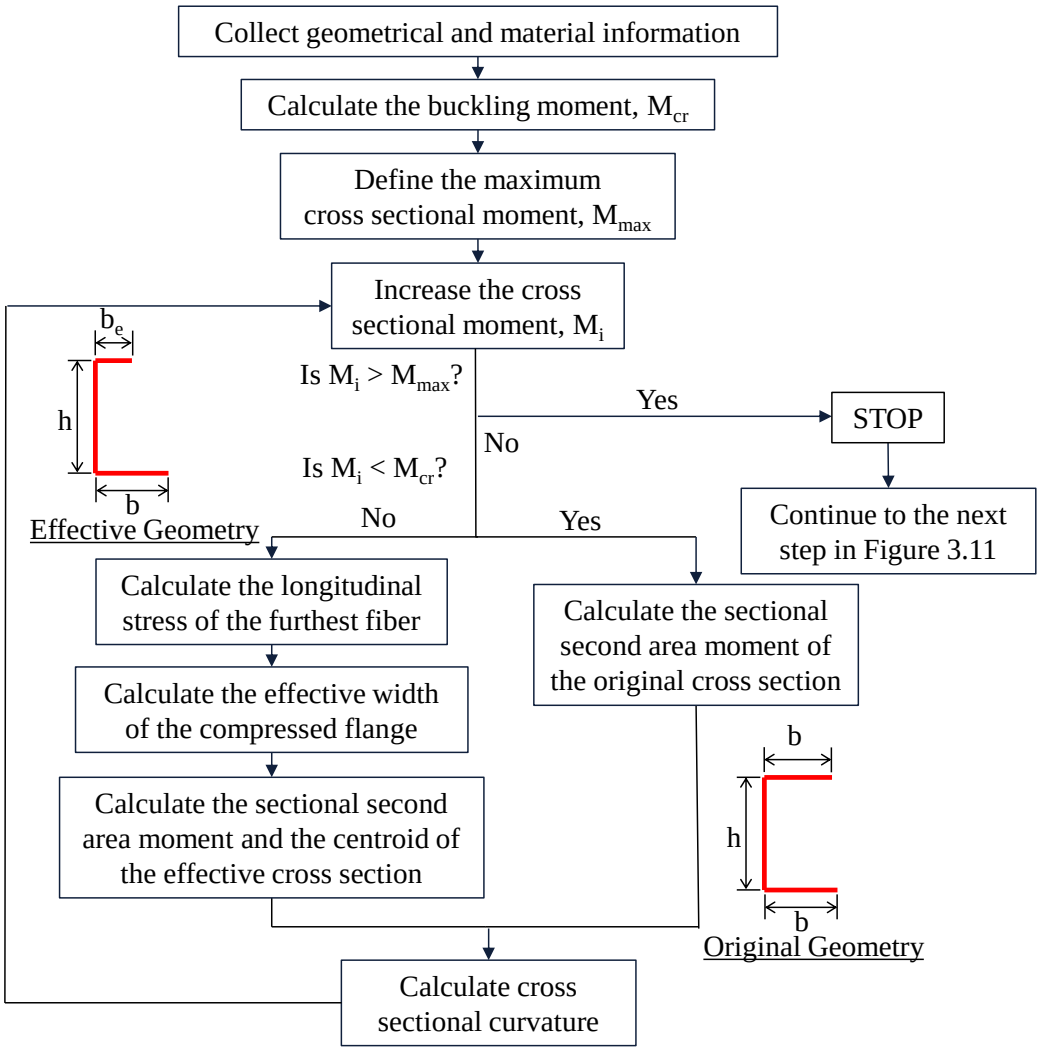

Figure 3.13 Framework to calculate the cross sectional moment-curvature data

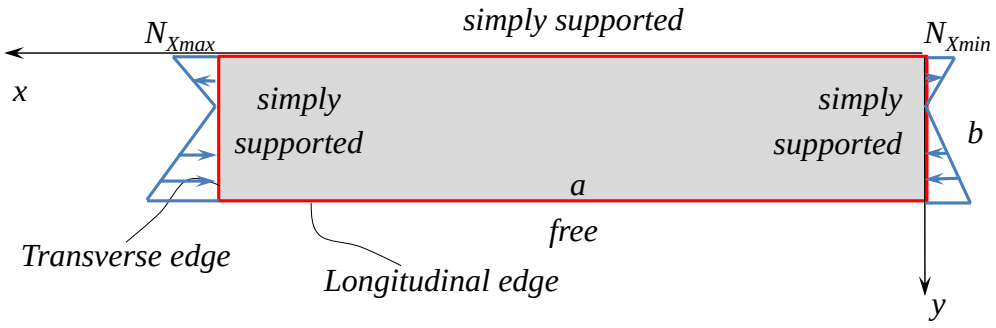

Figure 3.14 Plate model used to predict the buckling stress of angle section member

For this plate model, the shape function used to calculate the buckling stress is also modified to that shown in the following equation:

$$u(x,y) = C_1\left(\sin\left(\frac{\pi x}{a}\right)\right)\left(\sin\left(\frac{\pi y}{2b}\right) + \sinh\left(\frac{\pi y}{2b}\right)\right) \qquad \text{Eqn 3.5}$$

Note that only the *x* term of the function is changed. This change is related to the boundary conditions applied to the member to impose the unsymmetric bending condition.

3.2.3 Validation and Discussion of the Hybrid Timoshenko Beam Model

The hybrid Timoshenko beam models of two types of beams constructed using plain channel and plain angle sections are validated to shell element models of the beam members (benchmark beam model). For each cross section, two variations of length to height ratio are investigated. These investigations (see Table 3.1) involve two identification methods used to generate the spring properties in the hybrid Timoshenko beam model.

Table 3.1 Validation cases for the hybrid Timoshenko beam model

	Shell Element Method		Effective-width Prediction Method	
Plain Channel Section	Length = 14 in. (L/h = 4.67)	Length = 36 in. (L/h = 12)	Length = 14 in. (L/h = 4.67)	Length = 36 in. (L/h = 12)
Plain Angle Section	Length = 8 in. (L/h = 4.57)	Length = 45 in. (L/h = 25.7)	Length = 8 in. (L/h = 4.57)	Length = 45 in. (L/h = 25.7)

Validation of the Plain Channel Section Beam Members

Before the validation is conducted, the benchmark beam models of the beam members are developed using shell elements. All of the edge nodes at each end of the members are rigidly constrained to the centroid of the cross section. Afterward, the centroids are fixed in all DOFs except in the in-plane bending direction. Incremental in-plane rotations are then applied at the centroid of each end of the beam members under

geometric nonlinear analyses (2nd order) to imposed double curvature bending condition. Hybrid Timoshenko beam models are also constructed for the beam members. The models consist of Timoshenko beam elements and a nonlinear spring at each end of the beam members. The properties of the nonlinear springs are generated using the two identification methods discussed in the previous section: 1) shell element method, and 2) effective-width prediction method. The hybrid beam model is then fixed at both ends in all DOFs except in the in-plane bending direction, and incremental in-plane rotations are applied at the end of the beam member under geometric nonlinear analyses to impose the double curvature bending condition.

The comparisons of the end-moment and end-rotation curves of both the benchmark beam models and the hybrid Timoshenko beam models generated using the shell element method for the 14-in. (L/h = 4.67), and 36-in. (L/h = 12) beams are shown in Figure 3.15.a and b respectively. The results obtained from the hybrid beam models show a high degree of agreement with the results of the benchmark models. These results are not surprising since the properties of the rotational springs in the hybrid beam models are generated based on the same shell element models as in the benchmark beam models.

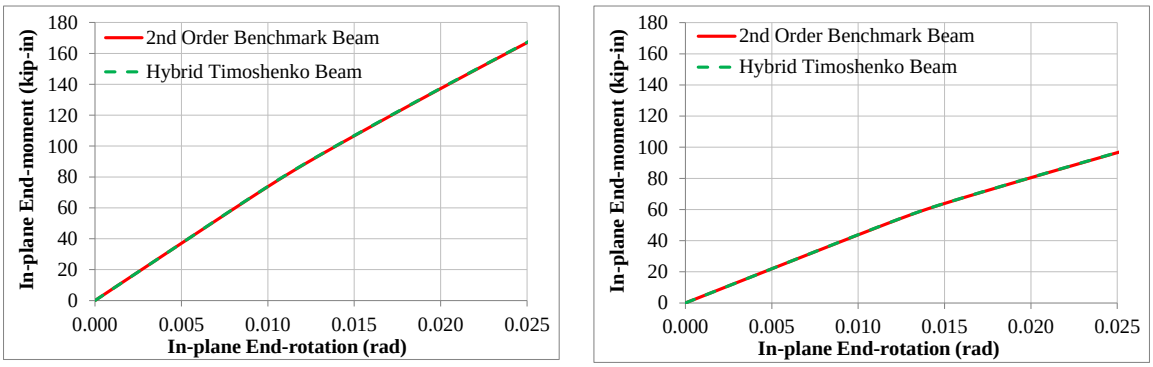

(a) L=14-in. (L/h = 4.67) (b) L=36-in. (L/h = 12)

Figure 3.15 Comparison of the end-moment versus end-rotation of the benchmark beam model and hybrid beam model (derived using shell element method) for plain channel beams.

Before the hybrid beam model generated using the effective-width prediction method is validated, the result of the effective-width prediction for each beam member subjected to double curvature bending is confirmed using the result of the benchmark beam model of the member. Two beam specimens representing short (14-in.) and long (36-in.) beams are selected to validate the effective-width prediction.

The comparisons between the end-moment and end-rotation of the benchmark beam models and the effective-width predictions for the beam specimens are presented in Figure 3.16. The results obtained from the analyses of the benchmark beam model without considering the geometric nonlinear effect (1st order) are also included in the plots to show the stiffness-reducing effect due to the elastic local buckling behavior. Based on these plots, the effective-width prediction method is able to estimate the end-moment and end-rotation of the benchmark beam models under 2nd order analyses.

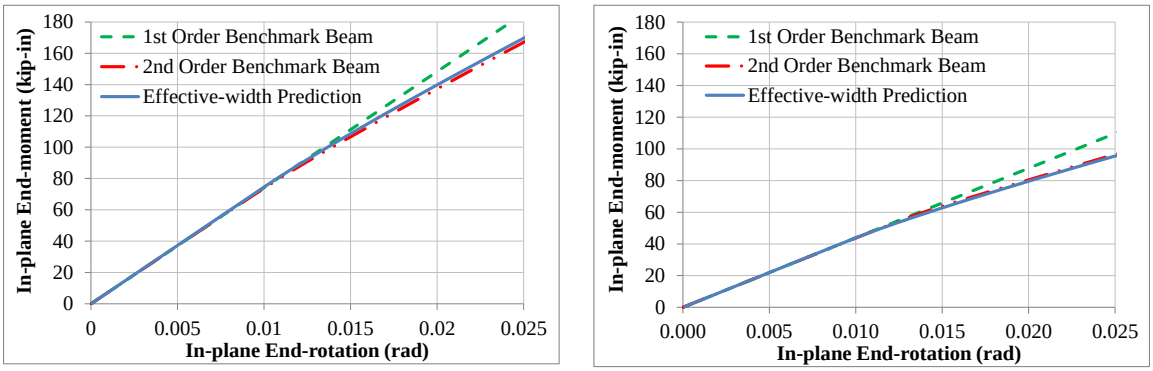

(a) L=14-in. (L/h = 4.67) (b) L=36-in. (L/h = 12)

Figure 3.16 Comparison of the end-moment versus end-rotation curve between the effective-width prediction and the benchmark beam model for plain channel beam specimens

In addition to its accuracy, this effective-width prediction method also offers a possible physical explanation to the growth of the distorted region on the beam due to local buckling as the end moments increase. The distorted region is defined as the portions of the beam over which the curvature no longer has a linear correlation with the moment distribution on the beam. Figure 3.17 shows the bending moment diagram and the distribution of curvature along the beam for a given end-moment applied to the 36-in.

beam specimen. Note that the bending moment varies linearly along the beam. However, there are some portions of the beam for which the curvature is no longer linear as the end moment is increased. This region will keep growing as the incremental end-moment is increased.

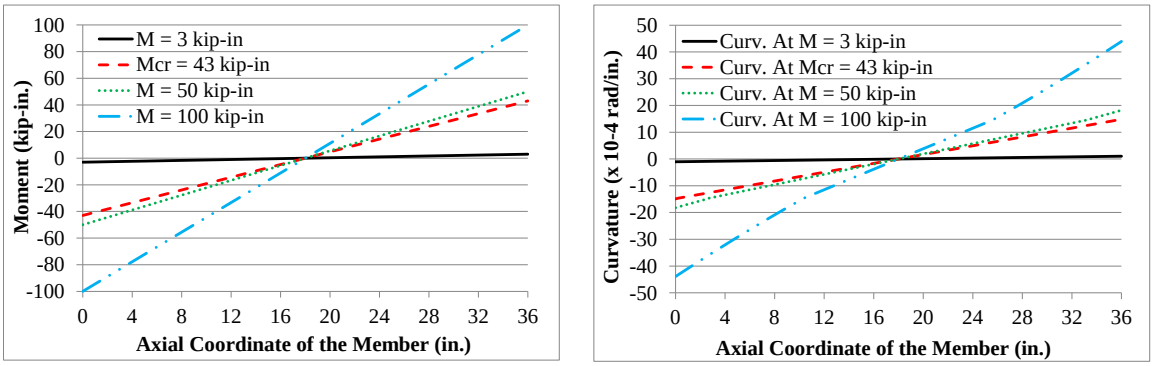

(a) Bending moment (b) Curvature

Figure 3.17 Bending moment and curvature diagrams for the 36-in. (L/h = 12) member at several values of end-moment.

Next, the effective-width prediction results are used to generate the properties of the rotational end-springs incorporated in the hybrid Timoshenko beam element model. Afterward, this hybrid beam model is analyzed in ABAQUS under double-curvature bending condition. The results of this analysis are then validated to the results of the benchmark beam models of the members. Figure 3.18 shows the comparisons of the end-moment and end-rotation between the hybrid beam models and the benchmark beam models for the 14-in. and 36-in. specimens. The hybrid beam models shows good agreement with the results obtained from the benchmark beam models. This result is expected because the properties of the springs are calculated based on an accurate prediction of the behavior of the member.

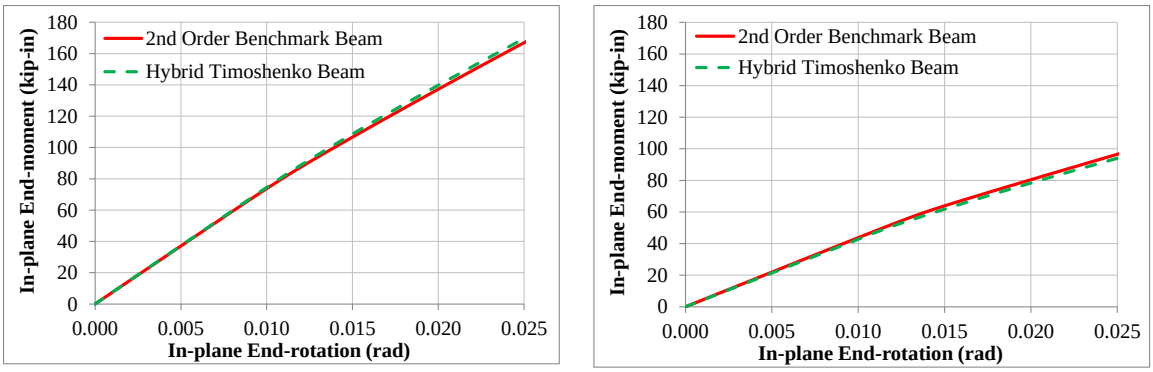

(a) L=14-in. (L/h = 4.67) (b) L=36-in. (L/h = 12)

Figure 3.18 Comparison of the end-moment versus end-rotation of the hybrid beam (derived using the effective-width prediction method) and benchmark beam models for plain channel beams.

Validation of the Plain Angle Section Beam Members

Under double curvature bending, the angle section member bends in an unsymmetric manner. This is because the moment does not act on the plane of symmetry of the cross section. The benchmark beam models for the beam members considered in these validations (L/h = 4.57 and L/h = 25.7) are developed using shell elements. All nodes at each end of the members are kinematically constrained to their centroid at that end in all translational and in-plane bending and torsional directions. Afterward, the centroid at each end is restrained in all translational and torsional directions. Incremental in-plane rotations are then applied at the centroid at each end of the members under geometric nonlinear analyses to impose double curvature bending. Figure 3.19 shows the deformation of the shell element model. Local out-of-plane deformation of the member is observed on the compressed vertical flanges at the left end while unsymmetric bending deformation is observed at the right end without any indication of local deformation on the compressed horizontal flange. The local deformation at the compressed vertical flange introduces bending stiffness reduction at the left end of the beam member. Thus, only the in-plane end-moment and in-plane end-rotation at the left end of the members is observed.

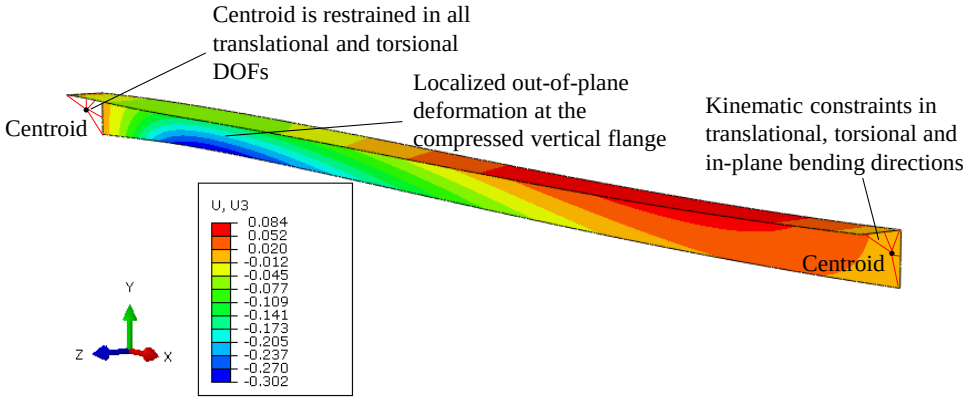

Figure 3.19 Boundary conditions imposed on the plain angle beam members and local out–of–plane deformation of the compressed vertical flange under geometric nonlinear analysis.

Hybrid Timoshenko beam models are developed for each beam member considered in these validations. As for the plain channel section members, two methods are utilized to generate the properties of the nonlinear rotational springs incorporated into the hybrid beam models: 1) shell element method and 2) effective-width prediction method. In the shell element method, the properties of the rotational springs are generated based on the in-plane moment and in-plane rotation of shell element models of the beam members. Figure 3.20 shows the in-plane bending moment and in-plane rotation of the benchmark beam models and the hybrid beam models for the members. The hybrid beam models have the capability to capture the stiffness reducing effect observed in the benchmark beam models, and these results are not surprising considering the properties of the springs are generated from the same shell element models as the benchmark beam models.

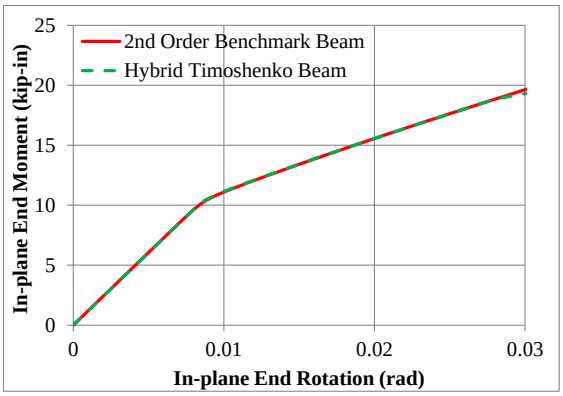

(a) L=8-in. (L/h = 4.57)

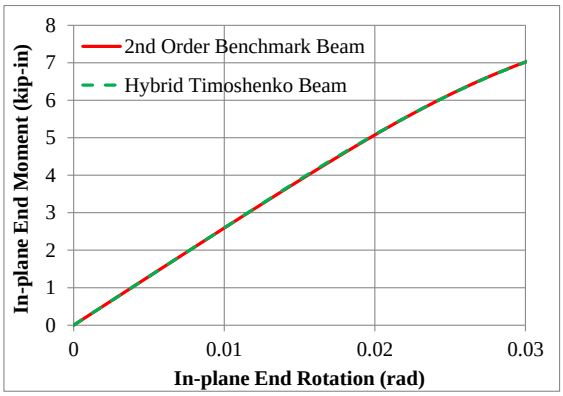

(b) L=45-in. (L/h = 25.7)

Figure 3.20 Comparison of the end-moment versus end-rotation between the hybrid beam model (derived using the shell element method) and the benchmark beam models for angle section members.

In the effective-width prediction method, the in-plane moment and in-plane rotation curves of the beam members are first obtained using the flowcharts shown in Figure 3.11 and Figure 3.13, and the plate model shown in Figure 3.14. Figure 3.21 shows the comparison of the in-plane moment and in-plane rotation obtained using the benchmark beam models and the effective-width predictions of the beam members. In these plots, the results of shell element model excluding the geometric nonlinear effect (1st order benchmark beam) are also presented to show how the elastic local buckling reduces the stiffness of the member. The effective-width prediction method is able to predict the initial stiffness, the buckling moment and the post buckling stiffness for the member with L/h ratio of 25.7 (L = 45 in.). In addition, it is also capable to predict the initial stiffness and the buckling moment of the member with L/h ratio of 4.57 (L = 8 in.) although the post buckling stiffness is over-predicted by about 50%. This over-prediction imposes a caveat on the application of this effective-width prediction method for a short plain angle member under unsymmetric bending condition. However, it should be noted that: 1) the use of this short member for the vertical post of electrical switchboard cabinet is rare, and 2) the Timoshenko beam model alone (without rotational springs) over predicts the post-buckling stiffness of the benchmark beam models by a factor of three.

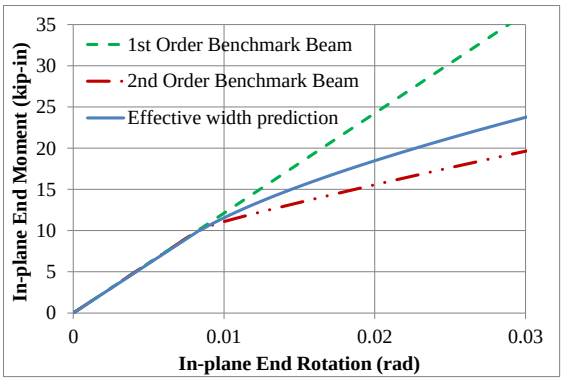

(a) L=8-in. (L/h = 4.57)

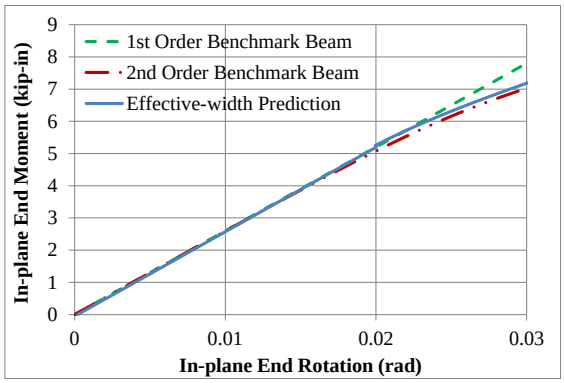

(b) L=45-in. (L/h = 25.7)

Figure 3.21 Comparison of the end-moment versus end-rotation curves between the effective-width prediction and the benchmark beam model for plain angle beam specimens

Afterward, the properties of the rotational springs incorporated in the hybrid Timoshenko beam models are calculated based on the results of the effective width prediction of the beam members. Figure 3.22 shows the comparisons of the benchmark beam models and the hybrid Timoshenko beam models generated using the effective-width prediction method. The conclusions are the same as the ones drawn for the effective-width predictions of the beam members. The hybrid Timoshenko beam model is able to predict the behavior of the beam members, except that it over predicts the post buckling stiffness of the beam member with L/h ratio of 4.57.

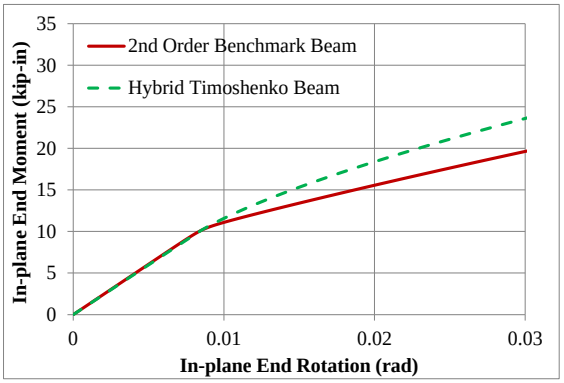

(a) L=8-in. (L/h = 4.57)

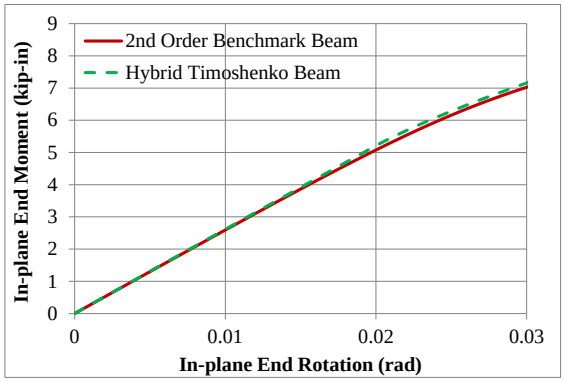

(b) L=45-in. (L/h = 25.7)

Figure 3.22 Comparison of the end-moment versus end-rotation curves between the hybrid beam model (derived using the effective-width prediction method) and the benchmark beam models for angle section members.

3.3 Modeling Features for the Connection Between Framing Members

The connections between framing members in the electrical cabinet are divided into two categories based on their locations: 1) Top or middle connection, and 2) bottom connection (see Figure 3.23). In the bottom connection, additional restraints are imposed to the bottom of the flanges of the connecting beams due to the supports of the cabinet.

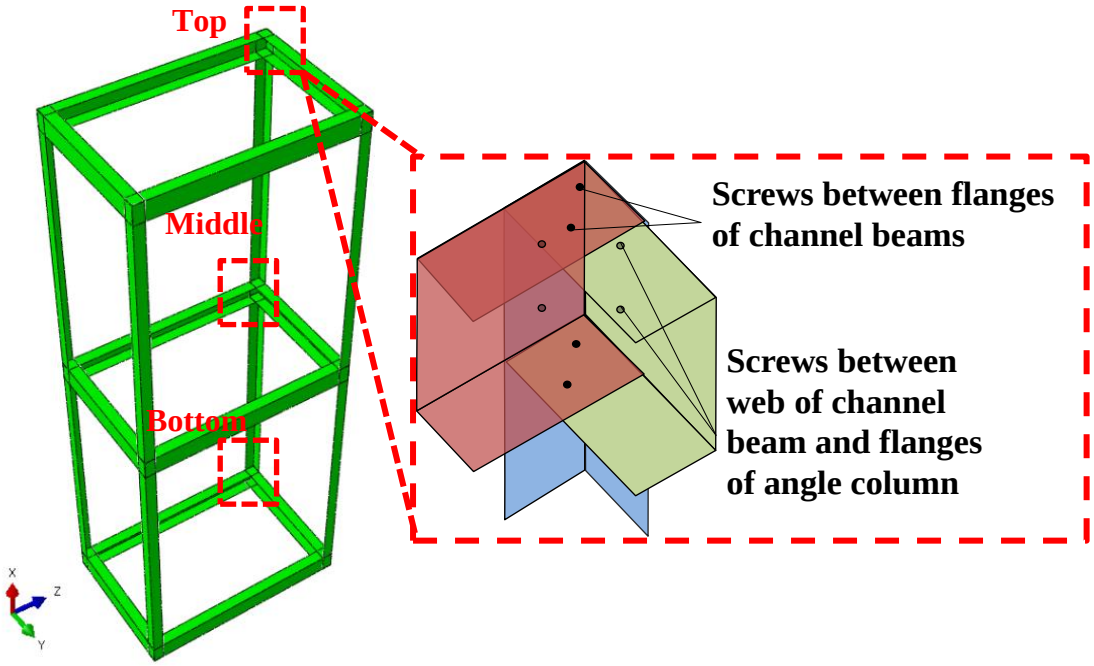

(a) Two types of joints in the electrical cabinet

(b) 3D sketch of the top corner joint

Figure 3.23 Types of connection between framing members in the class I cabinet configuration

These connections are represented as linear rotational springs in three orthogonal directions assigned to each member coincident at a joint (see the frame-frame connectors in Figure 3.24). These springs are modeled by the CONNECTOR–JOIN, ROTATION feature in ABAQUS. This feature rigidly constrains all translational DOFs (JOIN) and assigns rotational springs in three orthogonal directions (ROTATION).

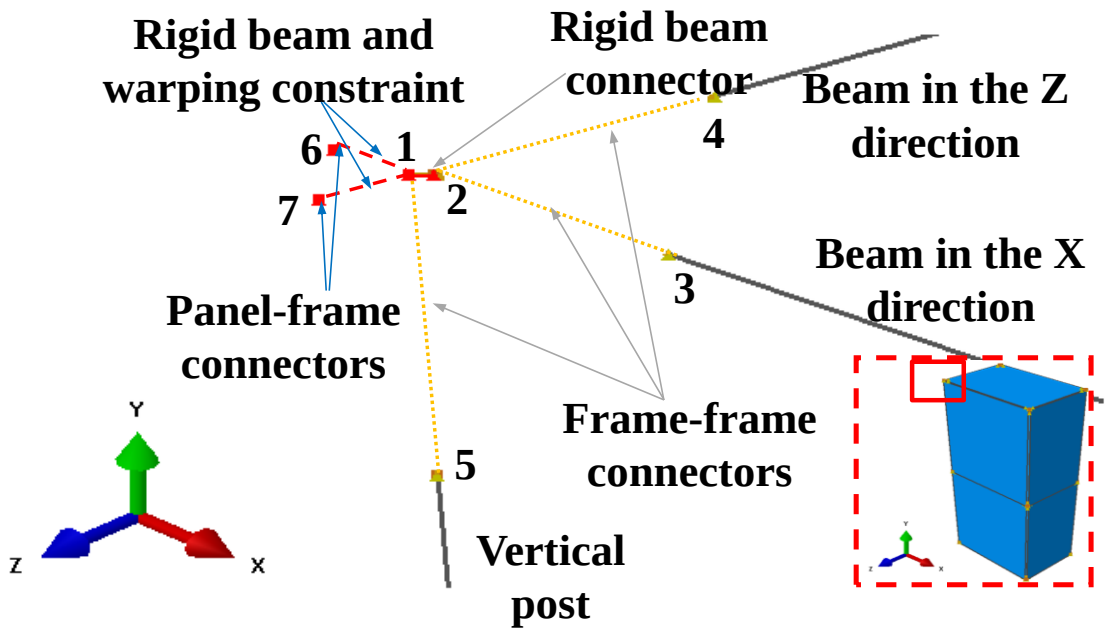

Figure 3.24 Detailed of locations of modeling features assigned to the simplified model

The stiffness of the springs for a member is obtained by imposing a unit rotation in each orthogonal direction on that member while fixing the other members coincident at the joint modeled using shell elements. The length of each member in the connection model is about 5 – 7 % of the total length of the member. These members are connected using FASTENER features in ABAQUS that assign rigid beam constraint between the connecting nodes located at the positions of the screws/bolts (see Figure 3.25). Furthermore, the edge nodes at the cut-off end of each member are rigidly constrained to its centroid at that end (see "Rigid beam or free warping constraint" in Figure 3.25), and the centroids are then fixed in all DOFs, except: 1) when a unit rotation (besides torsional rotation) is applied to a member to generate the stiffness of the springs; the centroid of that member is only fixed in the direction corresponding to the applied rotation, and 2) when a unit torsional rotation is applied to a member to generate the torsional stiffness of the springs; a free warping constraint (distributing coupling feature in ABAQUS) is assigned (instead of rigid beam) in the torsional DOF between the edge nodes at the cut-

off end of the member and its centroid at that end (see free warping constraint in Figure 3.25), and the centroid is then fixed only in the torsional direction. Unlike the rigid beam constraint, the DOFs of the slave nodes in the free warping constraint are not eliminated. The force/moment applied at the master node is distributed to the slave nodes in an average sense. In this constraint, relative displacements between slave nodes are possible. Afterward, the stiffness of the springs in each direction for each member coincident at the joint is calculated as the ratio of the reaction moment at the centroid to the corresponding applied unit rotation.

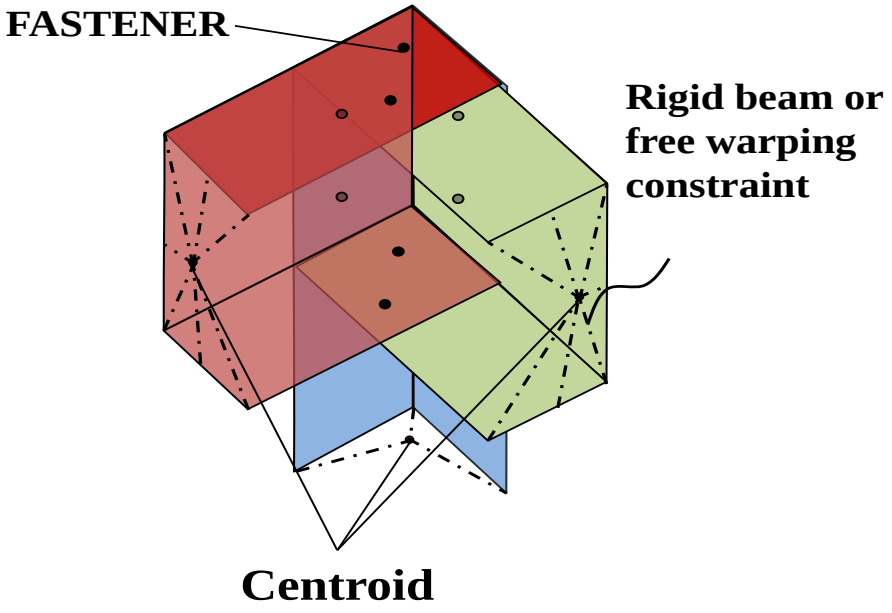

Figure 3.25 Kinematic constraints assigned to the connection model of the framing members

In addition to the rotational springs, the finite joint size of the connection between the framing members is also considered in the simplified cabinet model. The size of the joint is the same as the size of the connection models used to generate the properties of the rotational springs. Furthermore, a rigid beam constraint is also assigned between a point (point 2 in Figure 3.24) at the intersection of the beam members and a point (point 1 in Figure 3.24) at the extension of the centroidal axis of the vertical post.

3.4 Finite Element Model for the Panels and the Connection between Panels and Framing Members

3.4.1 Selection of the Finite Element Model for the Panels

The panels of the electrical cabinets are constructed from thin-steel plates (typical thickness = 3/32 in.). These panels, together with the connections between the panels and the framing members, are important to the structural rigidity of the cabinets. Furthermore, experimental tests of the electrical cabinets have shown that significant deformation of the panels can occur during an earthquake. Therefore, shell elements are selected to model the steel panels because they have the capability to capture these behaviors.

3.4.2 Development of the Modeling Features for Panel Attachment

Two modeling features are assigned for the attachment of panels to framing members: 1) Rigid beam and warping constraint, and 2) Zero-length translational springs in three orthogonal directions. The rigid beam and warping constraints are assigned to pairs of points (see points 1-6 and 1-7 in Figure 3.24) at the extension of the centroidal axis of the vertical posts and the flanges of the posts where panels are attached to them. Meanwhile, the translational springs are assigned between a corner node of the panel and a point in which the panel is attached to the framing member (see points 6 and 7 in Figure 3.24). The springs are modeled using the CONNECTOR–CARTESIAN, ALIGN feature in ABAQUS (see the Panel-frame connectors in Figure 3.24). This feature rigidly constraints the rotational DOFs of two nodes (ALIGN) and defines zero-length translational springs (CARTESIAN) in three orthogonal directions (two shearing directions and one tensile direction) between two coincident nodes.

Development of the Rigid Beam and Warping Constraint

The rigid beam constraints are applied to restrict the deformation of a point on the flanges of the vertical posts to a point at the centroid axis of the posts based on a plane-section-remain-plane kinematic assumption. Additional warping deformation constraints are imposed on those points because the vertical posts will warp when an electrical cabinet is subjected to lateral loads. The warping deformation is calculated based on an assumption that the vertical posts are subjected to a linearly varying internal torque induced by in-plane double-curvature bending of the posts. In this condition, warping is varied along the post and there is a corresponding tensile or compressive deformation on the longitudinal fibers of the member due to torsion. Afterward, this warping constraint is then defined as the amount of warping deformation per unit angle of twist.

The governing equation of the angle of twist is shown in Eqn 3.6. This equation is divided into two components: 1) pure torsion (first term in the right hand side of the equation) and 2) warping torsion (second term in the right hand side of the equation).

$$T = C\varphi' - C_1\varphi''' \qquad \text{Eqn 3.6}$$

where,

T = internal torque

C = torsional rigidity = $\frac{1}{3}\sum b.t^3$

C_1 = warping rigidity = $E\int_0^m (D-\omega_s)^2 t ds$

φ = angle of twist

t = thickness of cross section

$D = \frac{1}{m}\int_0^m ds \int_0^s r ds$, m and s are the midline distance of the cross section; r is the distance from the axis of rotation to the tangent of the middle line of the cross section

$\omega_s = \int_0^s r ds$.

Solving the second order differential equation and performing an integration over the solution will lead to the general expression of the angle of twist (see Eqn 3.15) based on linearly varying torsion, $T = T_o + t_o z$.

$$\varphi = \frac{T_o z}{k^2 C_1} + \frac{t_o z^2}{2k^2 C_1} + \frac{A_1}{k}\sinh(kz) + \frac{A_2}{k}\cosh(kz) + A_3, k = \sqrt{\frac{C}{C_1}} \quad \text{Eqn 3.7}$$

where

T_o = torsional reaction

t_o = applied torsional load.

The unknowns (T_o, A_1, A_2, and A_3) can be found by applying the boundary conditions for the post ($\varphi(0) = \varphi(L) = T_o/\beta$, $\varphi``(0) = \varphi``(L) = 0$). For this study, the boundary conditions are assumed to be free warping and partially fixed at both ends. The partial fixity is due to the out-of-plane bending stiffness (β) of the beam members connecting at the ends of the vertical post.

Once the expression for the angle of twist is obtained, the warping, w, at any longitudinal fiber of the cross section can be calculated using the following equation

$$w = \varphi'(D - \omega_s) \quad \text{Eqn 3.8}$$

The warping constraint equation is then written as the ratio of the warping deformation of a point on the flange of the member (point 6 or 7 in Figure 3.24) to the angle of twist at a point at the centroidal axis of the member (point 1 in Figure 3.24).

Properties of Screw Connections Between Panels and Framing Members

The panels and the framing members of the electrical cabinet are usually connected by thread-rolling screws. These screw connections are modeled as zero-length translational springs in three orthogonal directions (two shearing directions and one tensile direction). The shearing properties of the springs are typically defined by the uniaxial load-deformation curve obtained from lap-splice tests using two thin plates connected with one or more screws. The lap splice tests of the screw connections have been conducted by many researchers to characterize their strength. However, studies that characterize the load-deformation behavior (e.g. initial stiffness) of the screw are still limited. Pham and Moen (Pham and Moen, 2015) developed empirical approaches for predicting the load-deformation characteristic of the connection. However, validations of those approaches for other types of screws are still needed.

Due to limited information on the load-deformation behavior of screw connections, researchers typically conduct lap splice tests as part of their larger experimental test. Figure 3.26.a shows the lap splice tests on one type of screw connections conducted by Fulop and Dubina (Fulop and Dubina, 2004) as part of their experiments on a cold-formed steel shear wall. The tests were conducted with different loading rates, 0.039 in./min (1 mm/min) and 16.55 in./min (420 mm/min), to study the influence of time-dependent forcing functions on the behavior of screw connections. The results of the tests were scattered in nature and the average load displacement curves are shown in Figure 3.26.b. In a simplified sense, the curves can be described as a linearly elastic (possibly rigid), perfectly plastic curve. This type of curve is characterized by two

parameters: 1) initial stiffness, and 2) maximum load. Based on this simplification, the load-deformation curves of the springs used for the screw connection of electrical cabinet are defined.

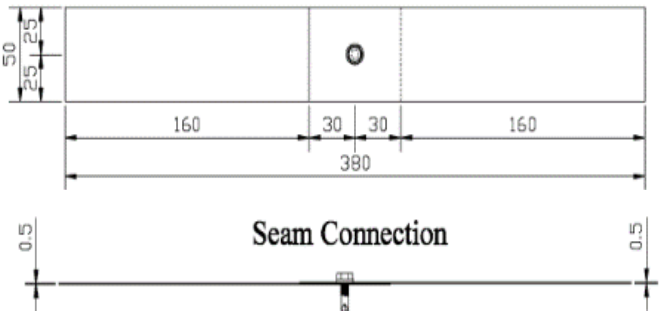

(a) specimen geometry (units in mm)

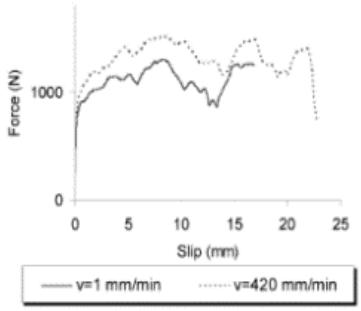

(b) average load-deformation curves

Figure 3.26 Lap splice tests conducted by Fulop and Dubina (pictures courtesy of Fulop and Dubina (2004))

One possible method to define the initial stiffness of the curve is based on an interpretation of the ECCS-TC7 guideline – "the design and testing of connection in steel sheeting and sections" (ECCS, 1984). In this guideline, it is stated that the maximum load of the connection can be defined as the load at a deformation value of 3 mm (0.118 in.). According to this information, the initial stiffness of the screw connection is assumed as the ratio between the maximum load and the deformation value of 3 mm (0.118 in.). This approach applied to calculate the initial stiffness of screw connection in shear is also adapted to define the initial stiffness in tension. Hence, the maximum shear and tensile load of the screw connection can be calculated based on Eqn. 3.12 and 3.13 as defined in AISI S100 (AISI, 2007).

$$F_{shear} = \min\left(4.2\sqrt{(t_2^3 d)}F_{u2}, 2.7\, t_1\, d\, F_{u1}, 2.7\, t_2\, d\, F_{u2}\right) \quad \text{Eqn 3.9}$$

$$F_{ten} = \min\left(0.85\, t_c\, d\, F_{u2}, 1.5\, t_1\, d_w^{'}\, F_{u1}\right) \quad \text{Eqn 3.10}$$

where

F_{shear} = shear strength of the screw connection

t_2 = thickness of member not in contact with screw head

d = diameter of the screw

F_{u2} = tensile strength of member not in contact with screw head

t_1 = thickness of member in contact with screw head

F_{u1} = tensile strength of member in contact with screw head

F_{ten} = tensile strength of the screw connection

t_c = lesser of the depth of penetration and the thickness t_2.

$d`_w$ = minimum of the diameter of the head of screw and 0.5 in. (12.7 mm).

This linear elastic perfectly plastic definition seems reasonable because it defines the 'failure' state (maximum load) of the screw connection although it may oversimplify the characteristics of the connections prior to and after the maximum load.

3.5 Validation of the Simplified Cabinet Model: Class I Configuration

3.5.1 Development of the Benchmark and Simplified Cabinet Models

In the benchmark cabinet models, all structural components of the cabinet (framing members and/or panels) are modeled explicitly using shell elements in ABAQUS. The framing members are connected together using the FASTENER–BEAM feature at the locations of the screws/bolts. This feature provides rigid beam constraints between the connecting nodes. In addition, three translational springs with properties the same as those assigned to the simplified cabinet models are used to represent the connections between the panels and the frames. These translational springs are modeled using the CONNECTOR–CARTESIAN, ALIGN feature in ABAQUS. This feature rigidly constrains all rotational DOFs and assigns translational springs in three orthogonal directions between the connecting points.

The simplified cabinet models are developed using the methods described in the previous section. Timoshenko beam elements are used to model the framing members and shell elements are used to model the panels. Next, in-plane rotational springs with properties generated based on the effective-width prediction method are attached only at each end of the vertical posts to handle the elastic local buckling behavior because, based on observation of the benchmark cabinet models, there is no indication that the beam members have buckled. The framing members are then connected using rigid beam constraints and rotational springs in three orthogonal directions (see rigid beam connector and frame-frame connectors in Figure 3.24). Furthermore, before attaching panels to the cabinet, rigid beam and warping constraints are assigned between a point at the extension of the centroidal axis of the vertical posts and a point in which the panels are attached to the flanges of the vertical posts (see "Rigid beam and warping constraint" in Figure 3.24). Lastly, the panels are connected to the framing members using the zero-length translational springs in three orthogonal directions (see panel-frame connectors in Figure 3.24). These translational springs have a linear elastic perfectly plastic behavior.

3.5.2 Validation of the Simplified Cabinet Models

Two configurations of the electrical cabinet model are considered in this study. The first configuration is the cabinet model without panel enclosures (bare-frame), and the second configuration is the cabinet model with panel enclosures (full-cabinet). The bare-frame model is needed to validate the spring properties defined for the connection between framing members. Benchmark (BM) and simplified (SM) cabinet models are then developed for each configuration of the cabinet. The models are fixed at the four corners at the bottom of the cabinet and subjected to pushover analyses in the front-back (FB) and left-right side (SS) directions (see Figure 3.2.b) by applying incremental

displacements at the top of the cabinets. The analyses are performed by including and excluding the nonlinear geometric effects (2^{nd} order and 1^{st} order, respectively). Inclusion of the geometric nonlinear effects enables the cabinet models to capture the local buckling behavior on the framing members and panels.

Validation of the Bare-frame Models

In the first order analyses, the bare-frame models behave in a linear elastic manner. Comparisons of the stiffness of the pushover curves obtained from the simplified and the benchmark cabinet models show that the simplified cabinet models underestimate the elastic stiffness by -0.3 % and -1.45 % in the SS and FB directions, respectively. If the connections between the framing members are assumed to be rigid, the simplified cabinet models overestimate the elastic stiffness by 62 % and 59% in both SS and FB directions, respectively. The results show the importance of including these features in the model and the accuracy of the spring properties developed for the connection between framing members.

In the second order analysis, elastic local buckling occurs near the ends of the vertical posts for both pushover analyses in the SS and FB directions. The local buckling reduces the rigidity of the bare-frame cabinet model as shown in the pushover curves in Figure 3.27.a and b. The simplified cabinet models are able to reproduce the initial stiffness of the benchmark cabinet models. However, they slightly overestimate the post buckling stiffness of the benchmark cabinet models. It should be noted that the vertical posts are constructed from a plain angle section and subjected to unsymmetric bending. Meanwhile, the stiffness-reducing effect incorporated into the simplified model through a rotational spring at each end of the vertical posts is only applied in the in-plane bending direction. Addition of rotational springs with coupled properties (in-plane moment and out-of-plane rotation) may improve the performance of the simplified cabinet models. However, the improvement may not be necessary for electrical switchboard cabinet

because: 1) the electrical cabinets are most likely enclosed by panels which significantly change the behavior of the framing members, and 2) the simplified cabinet models are able to predict the behavior of the benchmark cabinet models accurately up to a reasonable top displacement value of cabinet (e.g. 3 in or drift percentage of 3.33%.).

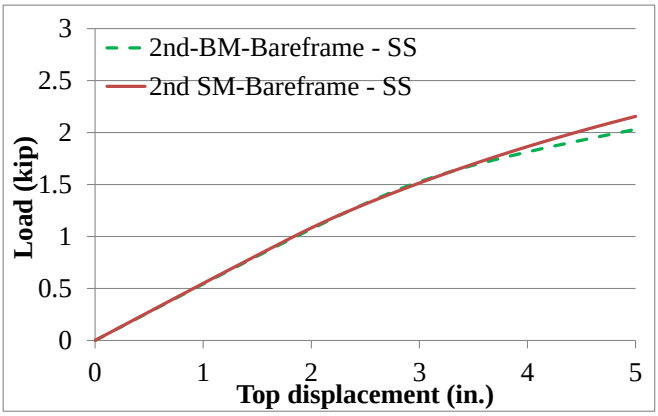

(a) 2nd order analysis in the SS (Z) direction

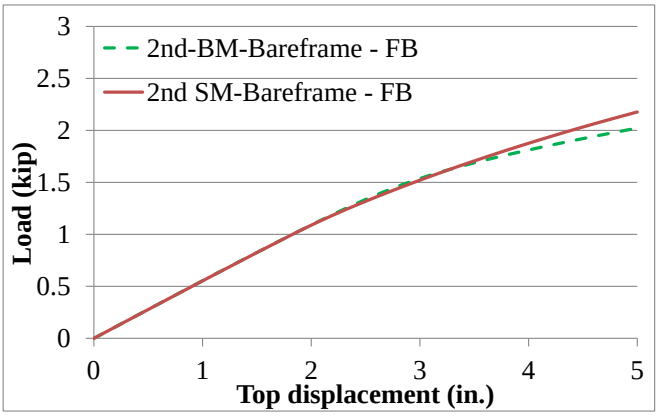

(b) 2nd order analysis in the FB (Y) direction

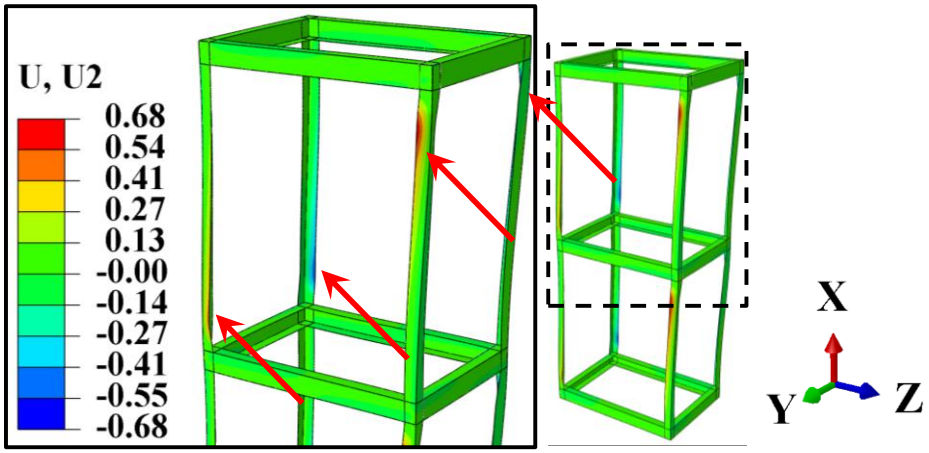

(c) Elastic local buckling near framing member ends (pushover analysis in SS direction)

Figure 3.27 Pushover curves of the bare-frame models.

Validation of the Full-cabinet Models

In the first order analyses, the behavior of cabinet models is characterized by the shear 'failure' of the connections between panels and frames. This 'failure' state is defined when the loads in the springs, used to model the connections, have reached the perfectly plastic region. Comparisons between the pushover curves obtained from the simplified and the benchmark cabinet models show that the simplified cabinet models are capable of capturing the initial stiffness, the 'failure' load, and the post-failure stiffness of the benchmark cabinet models (see Figure 3.28.a and b). Further investigations show that the simplified cabinet models excluding the warping constraint in the panel-frame connection over-predict the initial stiffness of the benchmark cabinet models by about 12% in both the SS and FB directions. This over-prediction may be still acceptable. However, it is suggested that the warping constraints are used to improve the accuracy of the simplified cabinet models.

In the second order analyses, the behaviors of the cabinet models are defined by multi-linear curves (see Figure 3.28.c and d). The main stiffness reduction is caused by two factors: 1) buckling of panels (see Figure 3.28.e), and 2) shear 'failure' of the connection between panels and frames. After the buckling of the panels, the compressed vertical posts are subjected to local deformation as shown in Figure 3.28.f. This local deformation may be caused by the axial force instead of bending moment since this deformation is spread out along the length of the posts. However, the stiffness reduction caused by this local deformation is not significant to the overall behavior of the cabinet because the stiffness of the pushover curves after the buckling of panels is almost linear. Therefore, including this behavior in the simplified cabinet model is not necessary.

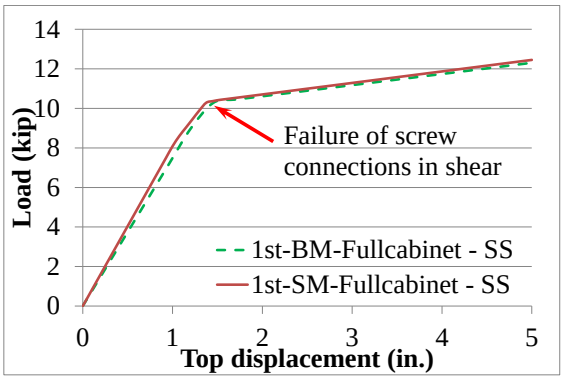

(a) 1st order analysis in SS (Z) direction

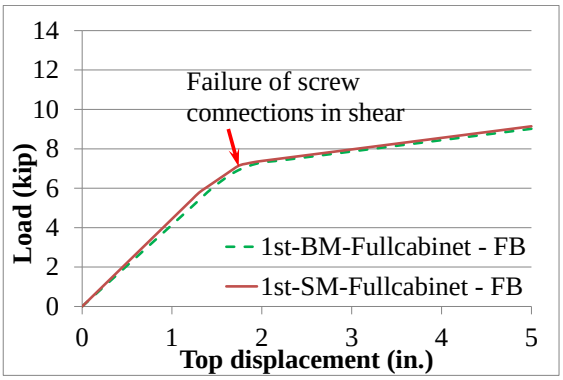

(b) 1st order analysis in FB (Y) direction

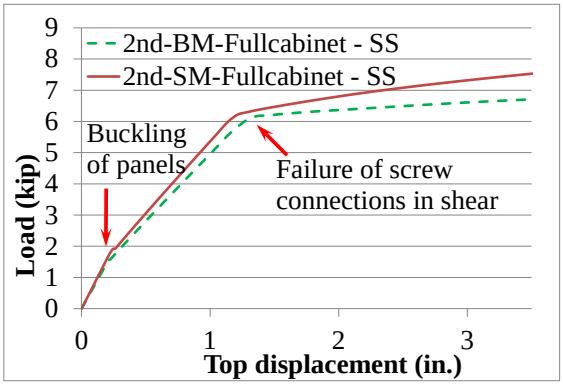

(c) 2nd order analysis in SS (Z) direction

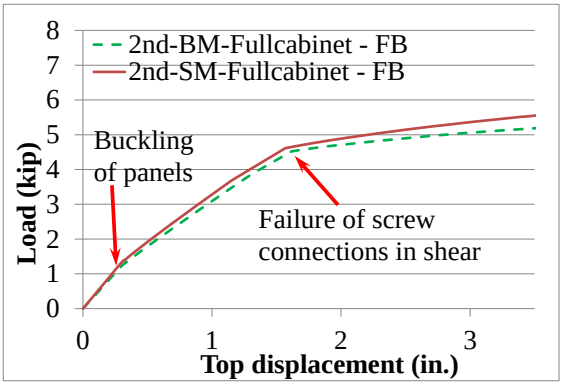

(d) 2nd order analysis in FB (Y) direction

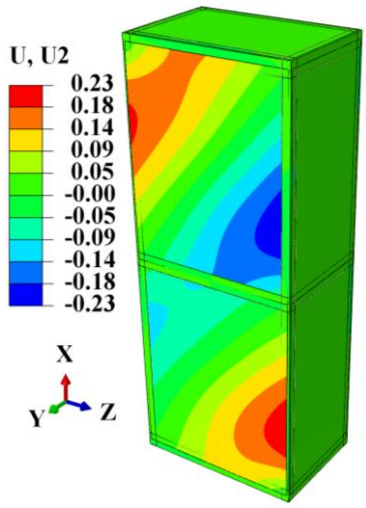

(e) Out-of-plane deformation of the panels at the buckling load (pushover analysis in the SS direction).

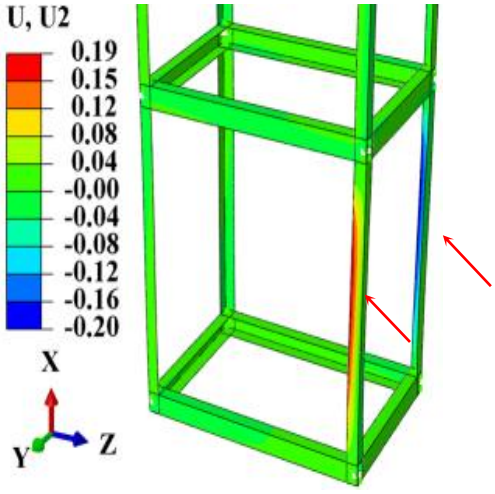

(f) Local deformation in the flanges of the compressed vertical posts (pushover analysis in the SS direction).

Figure 3.28 Pushover curves of the full-cabinet models.

In general, the load-displacement curves produced by the simplified cabinet models are in a good agreement with the curves produced by the benchmark cabinet

models. The simplified cabinet models overestimate the buckling load of the panel, the 'failure' load of the connection, and the initial and the post buckling stiffness of the cabinet by less than 10% for both the SS and FB directions. However, the post failure (screw connections) stiffness is over predicted by about +12% in the FB direction and about two times the stiffness of the benchmark cabinet model in the SS direction. Despite this over prediction, the pushover load of the cabinet is overestimated by less than 10% for a realistic maximum top displacement of the cabinet (e.g. 3 in. or drift percentage of 3.33%). This indicates that the load carrying capacity of the cabinet is significantly reduced after the 'failure' of the screw connections between the panels and the framing members.

3.6 Other Issues in Modeling of the Framing Members

3.6.1 Effect of Geometric Imperfection on a Plain Channel Beam Member.

In real life applications, geometric imperfection is often introduced as a result of manufacturing, fabrication, and construction process. In structural analysis, this imperfection is often characterized by the imperfection shapes and magnitudes . Inclusion of small imperfection magnitude reduces the buckling load of the members; and, therefore, it may be critical to their performance. In this section, the effect of geometric imperfection on a plain channel beam member (L= 36 in., L/h = 12) is investigated.

For cold-formed steel structure, there are two types of imperfection shape that are usually considered in the analysis (Schafer and Peköz, 1998): 1) global imperfection and 2) local imperfection. Two methods to incorporate the geometric imperfections have been proposed by Schafer: 1) spectra approach and 2) *brute force* approach. The spectra approach involves a tedious calculation of the imperfection modes as in generating random input ground motion in earthquake engineering. Afterward, the imperfection is scaled to a statistical magnitude obtained from the measurement of imperfections.

Meanwhile, the *brute force* approach is simpler in application and relies on buckling mode shapes or deformation of the member. The imperfection modes can be scaled to the statistical or the commonly accepted value (*rule of thumb*). Recently, the proposed method has been updated by Zeinoddini and Schafer (Zeinoddini and Schafer, 2012), and one of the updates is related to the statistical magnitudes for each type of imperfection modes as shown in Table 3.2. For plain channel section, there is no difference between the distortional and the local buckling modes. Thus, the magnitude of imperfection is selected as the largest magnitude between the statistical magnitude of distortional (larger) and local modes. In addition, there are three global modes, Bow, Camber and Twist, that need to be considered.

Table 3.2 Statistical magnitude from the measured imperfections (data source: Zeinoddini and Schafer (2012))

	Distortional, D (δ_o/t)	Bow, G1 (L/δ_o)	Camber, G2 (L/δ_o)	Twist, G3 (x 10^{-4} rad/in)
Mean	1.03	2242	3477	1.596
St. dev.	0.97	3054	5643	1.02
25^{th} -Percentile	0.43	4755	6295	0.887
50^{th} -Percentile	0.75	2909	4010	1.33
75^{th} -Percentile	1.14	1659	2887	2.172

Sensitivity analyses are conducted to study the effect of the geometric imperfection on the channel beam member (L = 36 in., L/h = 12). Shell element models of the beam members are generated and subjected to incremental in-plane rotation imposing a double curvature bending condition. The geometric nonlinear effect is included in the analyses so that the stiffness reduction due to local buckling is observable. The end-moment versus end-rotation curve of the beam is taken as the parameter in this study. In addition, three independent variables are considered in these analyses: 1)

number of local buckling modes included in the imperfection shape, 2) combination of local and global modes, and 3) magnitude of imperfections. The *brute force* approach combined with the statistical magnitudes in Table 3.2 is utilized in this study due its simplicity.

Effect of Number of Local Buckling Modes Included in the Imperfection Shape on the Behavior of a Channel Beam Member

The imperfection modes used in this study are generated from eigen-buckling analysis of the perfect beam member in a double curvature bending condition (see Figure 3.29). Three combination of local buckling modes (1 and 2; 1, 2, 5, 6, 9 and 10; 1, 2, 5, 6, 9, 10, 25, 26, 49 and 50) are considered in this study, and they are scaled to the mean statistical values in Table 3.2.

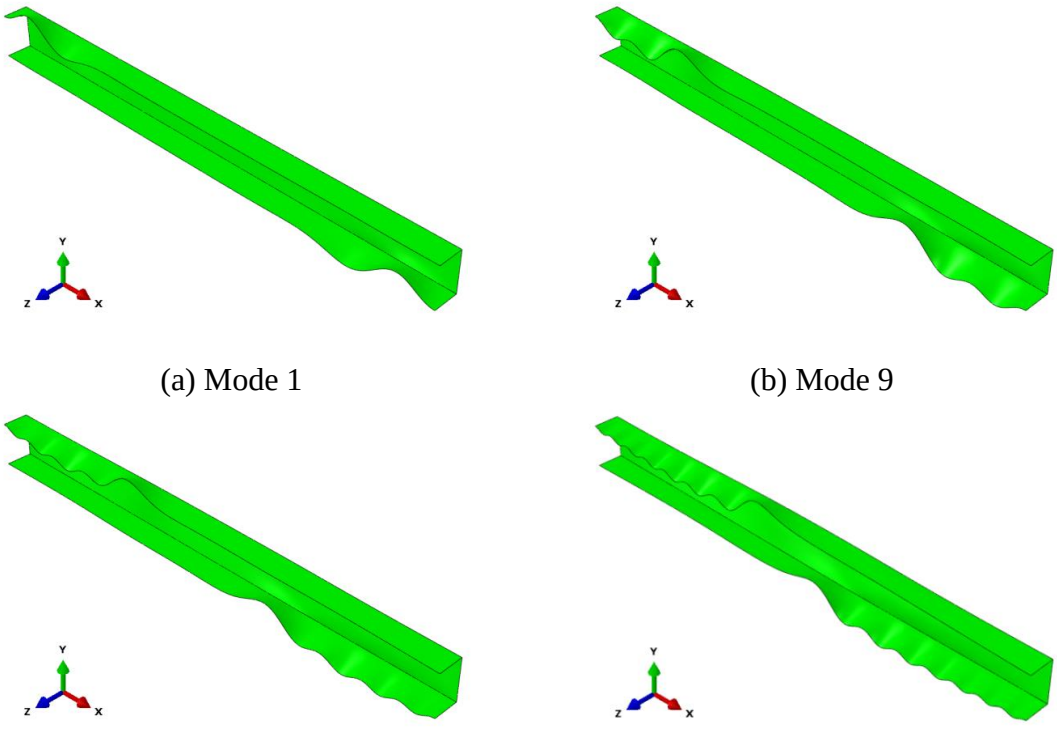

(a) Mode 1 (b) Mode 9

(c) Mode 25 (d) Mode 49

Figure 3.29 Several buckling modes of the beam member subjected to double curvature bending.

These combinations of imperfections are applied to the shell element models of the beam members subjected to the incremental in-plane rotations. Figure 3.30 shows the end-moment versus end-rotation curve of the beam models under the assigned imperfections. A plot of the end-moment and end-rotation curve obtained from a perfect shell element model (perfect model) is also presented for comparison. A convergence pattern is observed as the number of modes included in the imperfection shape increases. However, there is no significant difference between the imperfection shape that is constructed using modes 1 and 2, and the converged imperfection shape. Therefore, the inclusion of the first two local buckling modes is sufficient.

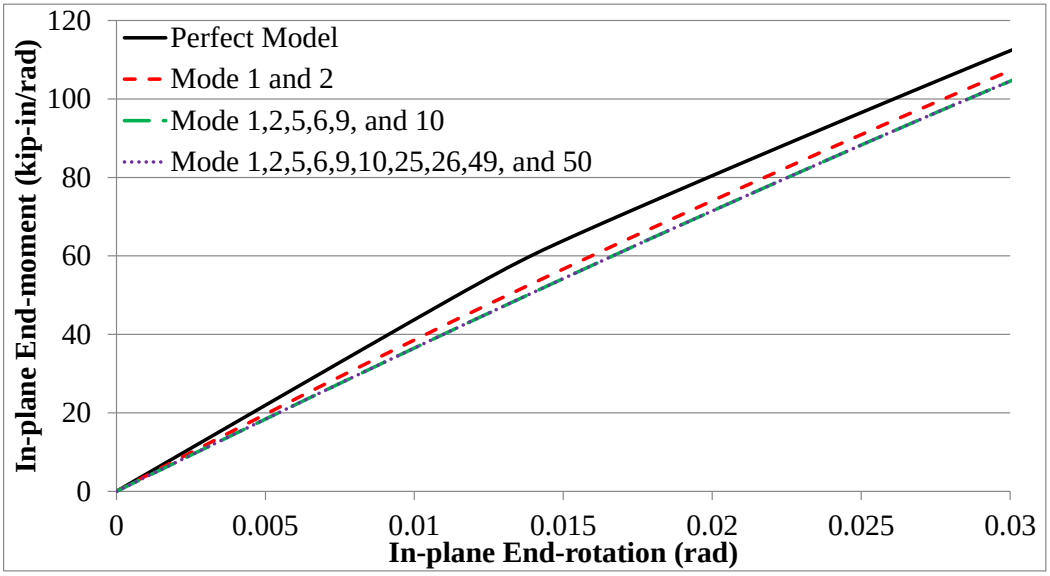

Figure 3.30 End-moment and end-rotation of a plain channel beam with local buckling modes as the imperfections

Effect of Combined Local and Global Imperfection Modes on the Behavior of a Channel Beam Member

Three global modes are considered in this study. These modes corresponds to the deflections in the weak axis, strong axis, and longitudinal axis (twist) directions as shown in Figure 3.31.These deflections are obtained based on the shell element models of the perfect beam members under geometric linear analyses. The maximum deflection of each

mode is then scaled to the mean value obtained in Table 3.2. Afterward, these shapes are combined together with the imperfection based on the local modes.

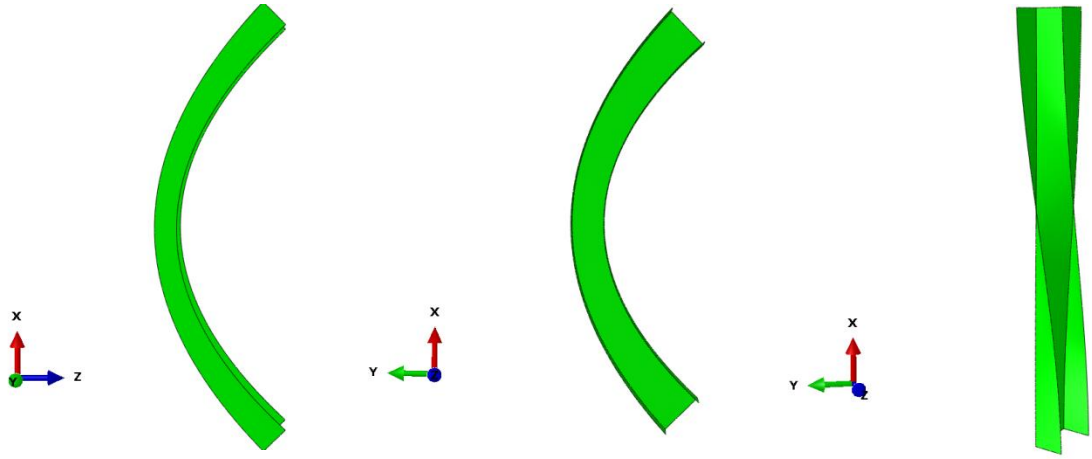

(a) Bow (b) Camber (c) Twist

Figure 3.31 Shapes of global imperfections.

Figure 3.32 shows the end-moment versus end-rotation plot of the beam models with two types of imperfections: 1) Only local modes (mode 1 and 2) scaled to the mean magnitude (see Mean Local in Figure 3.32), and 2) combination of local and global modes scaled to the mean magnitudes (see Mean Local and Global in Figure 3.32). This study shows that, for this particular case (double-curvature bending), the inclusion of global modes has no significant effect to the behavior of the beam member.

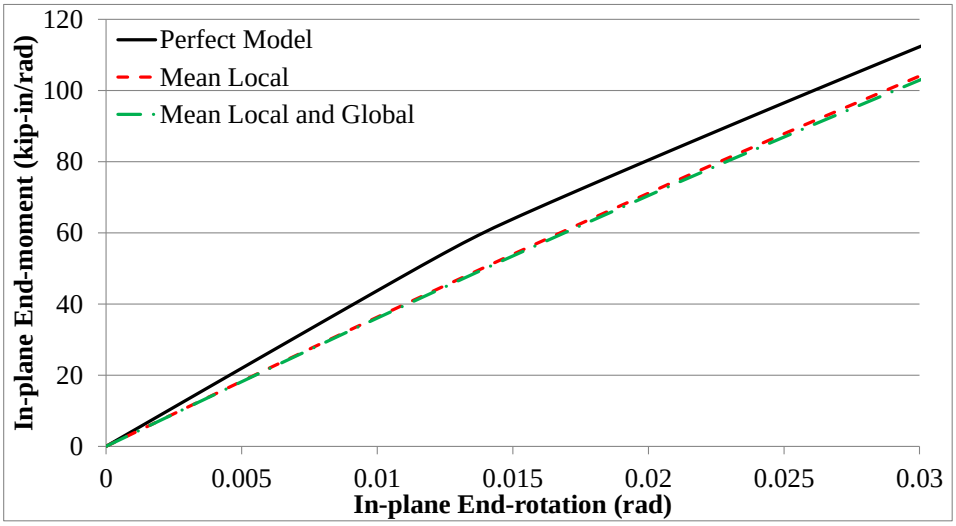

Figure 3.32 End-moment and end-rotation of a plain channel beam: combination of local and global modes as the imperfections

Effect of Imperfections Magnitudes on the Behavior of a Channel Beam Member

Four values of imperfection magnitudes are investigated in this study. These values are based on the mean, the 25th-percentile, the 50th-percentile and the 75th-percentile magnitudes shown in Table 3.2. The plot of the end-moment versus end-rotation of the beam with different magnitudes of imperfections is shown in Figure 3.33. Changing the imperfection magnitudes alters the initial stiffness of the curve. In addition, as the imperfection magnitude increases, the clear distinction between the initial stiffness and the post buckling stiffness vanishes. Schafer (1999) proposed that the use of the 25th percentile and the 75th percentile value be adopted for cold-formed steel structures. This proposal has been further verified in the experimental tests conducted by Yu and Schafer (Yu and Schafer, 2007).

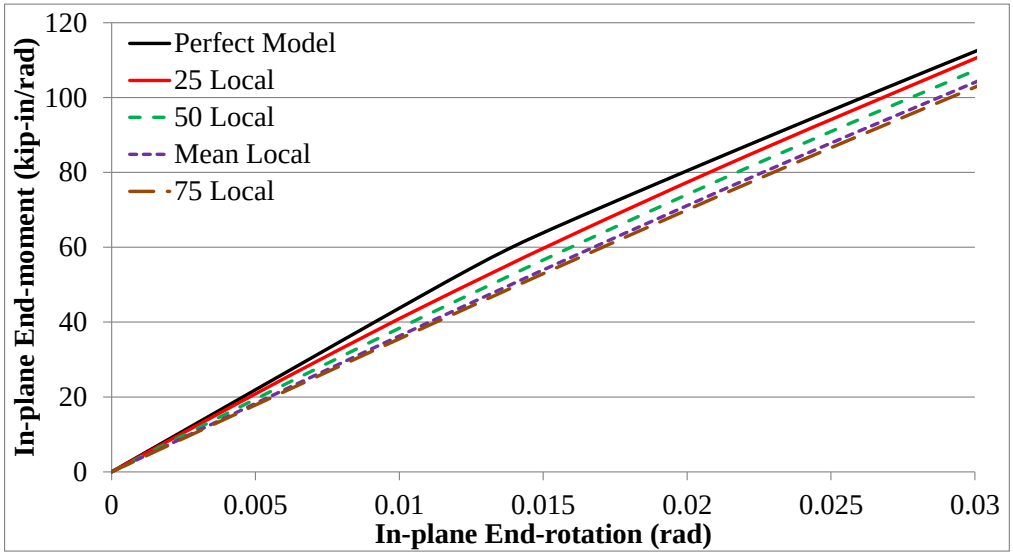

Figure 3.33 End-moment versus end-rotation of a plain channel beam for varying imperfection magnitudes.

Based on these sensitivity studies, it can be concluded that: 1) only the first two critical local modes are needed in modeling the imperfection; and 2) the shape of imperfections should be scaled to the 25th-percentile and the 75th-percentiles magnitude based on the recommendation by Schafer. Better conclusions might be drawn after

verifying the results with experimental tests of a beam subjected to double curvature bending.

Based on these conclusions, the "real" behavior of a channel section beam subjected to double curvature bending is generated using shell elements (imperfect model). In this model, the first two local buckling modes are incorporated as the geometric imperfections as shown in Figure 3.34. These imperfection modes are combined together and scaled to the imperfection magnitude of distortional mode based on the 25th-percentile, and the 75th-percentile value. The comparisons of the end-moment versus end-rotation relations of the perfect model and the imperfect models are shown in Figure 3.35. The geometric imperfection reduces the initial stiffness of the beam by 5% and 10% for the imperfect model scaled to the 25th -percentile and the 75th -percentile magnitudes, respectively.

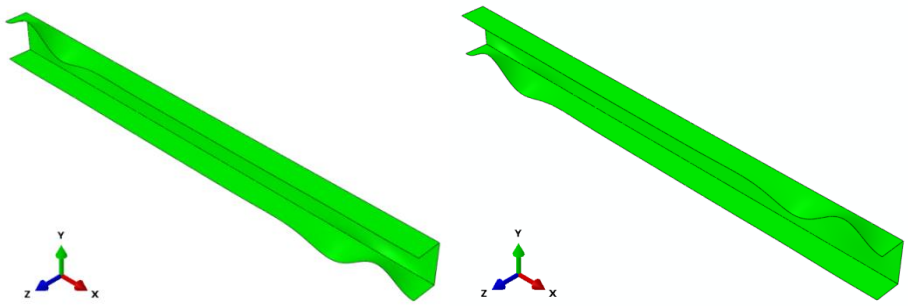

Figure 3.34 The first two buckling modes incorporated in the geometric imperfection

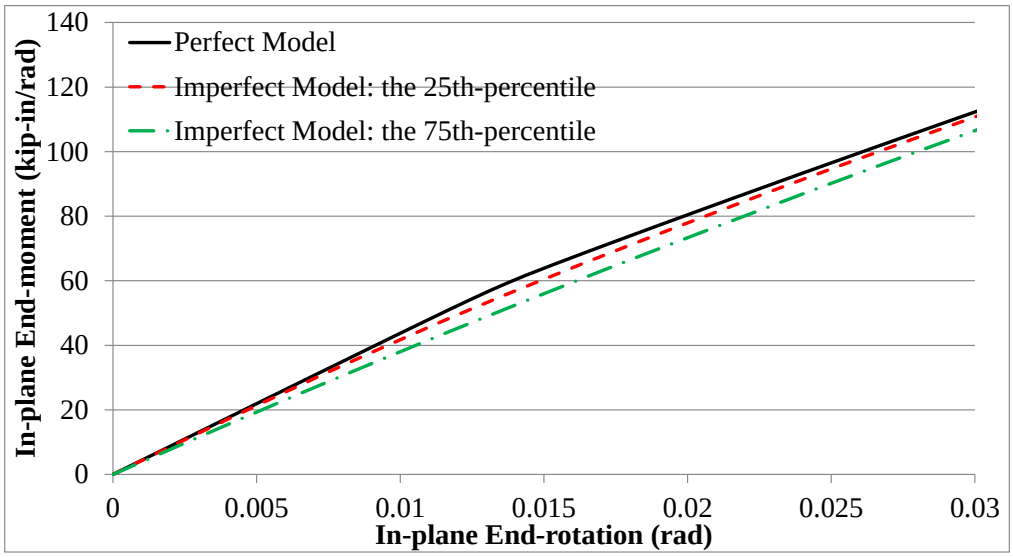

Figure 3.35 Comparison of the perfect and the imperfect models

Inclusion of the geometric imperfections in the hybrid Timoshenko beam model can only be conducted for the global modes. However, it has been shown that the beam is insensitive to the global modes. Therefore, including this global imperfection is not necessary. To approximate the effect of local imperfection modes on a beam member, an empirical effective-width equation can be used in the effective-width prediction of the behavior of a beam member subjected to double curvature bending developed in the previous sections. This empirical effective width equation is taken from the AISI code for calculating the effective width of the cross section. This empirical equation is selected because it is expected that the effect of geometric imperfection is included during the experimental tests used to derive the equation.

Figure 3.36 shows the plot of the end-moment versus end-rotation for both imperfect benchmark and hybrid Timoshenko beam models generated using the modified effective-width prediction method. The adoption of the empirical effective-width equation in generating the properties of rotational springs in the beam model is able to slightly obscure the slope change associated with local buckling of the beam. However, it

does not change the initial stiffness. This can be explained as the effective width equation has no contribution in calculating the initial stiffness of the beam. To match the initial stiffness of the beam, the hybrid Timoshenko beam model is scaled to 90% of its initial value. After applying this small adjustment factor, the results of the hybrid beam models lie between the results of the imperfect benchmark beam models scaled to 25th and 75th percentile. It must be admitted that the justification of this factor still needs deeper investigation; perhaps, this adjustment factor can be seen as similar to the factor used in the direct analysis method adopted in AISC code where an adjustment value is applied to consider the onset of yielding before reaching the maximum strength of the structure.

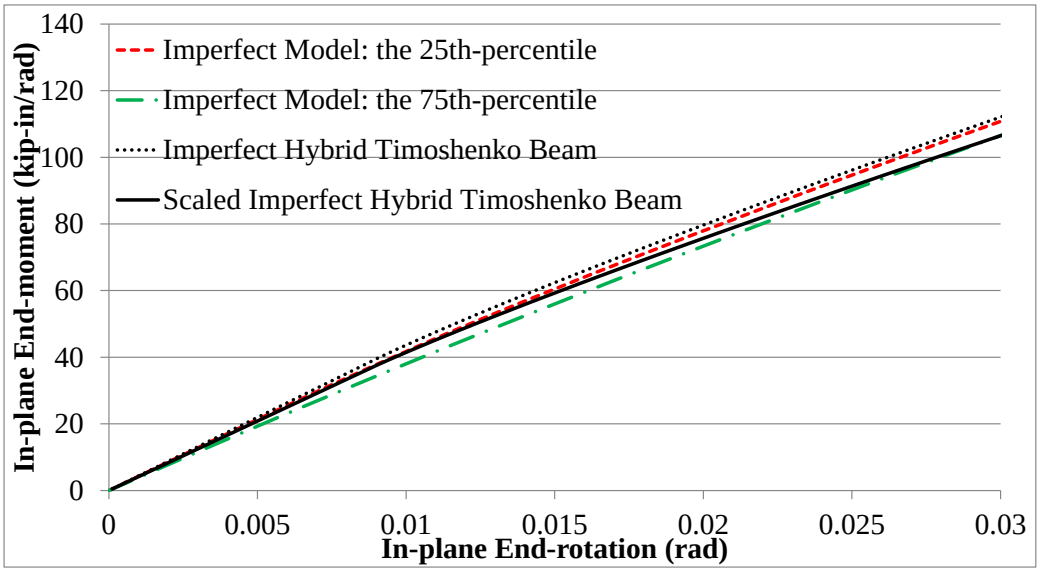

Figure 3.36 Comparison of the end-moment and end-rotation of the imperfect beams between the simplified and the benchmark models.

In further analyses conducted in this study, only perfect models are considered in order to have a fair comparison between the simplified and the benchmark cabinet models. Inclusion of geometric imperfection may alter the linear elastic stiffness of the cabinet which cannot be captured by the simplified cabinet model if the stiffness is sensitive to the local imperfection of the framing members. Therefore, further

investigations into the effect of geometric imperfections in the numerical model of electrical cabinet may be needed in the future.

3.6.2 Effect of Axial Forces on the Vertical Post

A plain angle section is used as the vertical posts in the class I cabinet. Under lateral load, this member will be subjected to combinations of axial load, bending moments and torsion. In generating the simplified cabinet model, the effects of these internal forces on the local buckling effect of the member are treated separately for simplification purposes. The interaction between the axial load and moment may be considered after more detailed observations are conducted to prove this interaction is critical.

Under the action of axial load, there are three main behaviors/limit states that need to be considered for an angle section: 1) flexural buckling in the weak axis direction, 2) flexural-torsional buckling of the member and 3) local buckling of the elements (web/flange) of the cross section. Experimental efforts to study the buckling behaviors of this member have been carried by Popovic (Popovic et al., 1999) and Young (Young, 2004). The results of the experimental tests show: 1) a short column is vulnerable to local buckling in the inelastic state, and 2) a long column is vulnerable to global buckling behavior (the flexural (Euler) buckling, flexural torsional buckling or the interaction of the flexural and flexural-torsional buckling).

Another factor that needs to be considered in investigating the global buckling behavior of the member is the compactness of the element (web/flange) that is often measured as the ratio of the width to the thickness of the element. A slender element is

vulnerable to local buckling before the member can reach its full global buckling capacity. This phenomenon was observed in the experimental test of the long column conducted by Popovic.

Theoretical prediction of the elastic flexural buckling of the member is defined by the classic Euler formula shown in Eqn 3.11

$$\sigma_{eGy} = \frac{\pi^2 E}{\left(KL / r_y \right)^2} \qquad \text{Eqn 3.11}$$

where,

σ_{eGy} = elastic global buckling stress about the weak axis of the member

E = modulus of elasticity

K = effective length factor

L = length of the member

r_y = radius of gyration about the weak axis of the member

In the inelastic range, the Structural Stability Research Council (SSRC) has proposed an empirical formula (see Eqn 3.12) that estimates the inelastic buckling behavior of the member. The result of this estimation is closed to the result of the tangent modulus method.

$$\sigma_{iGy} = F_y - \left(\frac{F_y^{\,2}}{4\pi^2 E} \right) \left(\frac{KL}{r_y} \right)^2 \qquad \text{Eqn 3.12}$$

where,

σ_{iGy} = inelastic global buckling stress about the weak axis of the member

F_y = yield stress of the member

The theoretical elastic flexural-torsional buckling equation (Yu and LaBoube, 2010) of the member is shown in Eqn 3.13.

$$\sigma_{eFT} = \frac{1}{2\beta}\left[\left(\sigma_{eGx} + \sigma_z\right) - \sqrt{\left(\sigma_{eGx} + \sigma_z\right)^2 - 4\beta\sigma_{eGx}\sigma_z}\right] \qquad \text{Eqn 3.13}$$

where,

σ_{eFT} = elastic flexural-torsional buckling stress of the member

$$\beta = 1 - \left(\frac{x_o}{r_o}\right)^2$$

$x_o y_o$ = distance of shear center from the centroid

σ_z = torsional buckling stress

σ_{eGx} = elastic global buckling stress about the strong axis of the member.

The inelastic flexural-torsional buckling equation for the member is derived by substituting the tangent modulus expression into Eqn 3.13. The inelastic flexural-torsional buckling equation of the member is shown in Eqn 3.14 (Yu and LaBoube, 2010).

$$\sigma_{iFT} = F_y\left(1 - \frac{F_y}{4\sigma_{eFT}}\right) \qquad \text{Eqn 3.14}$$

where,

σ_{iFT} = inelastic flexural-torsional buckling stress of the member.

The local buckling equation is derived for a case where the member is fixed at both ends. This equation is formulated from the buckling stress of the element

(web/flange) of the members represented as a plate under uniformly distributed force. The element is clamped at the transverse edges, simply supported at one longitudinal edge and free at the other longitudinal edge as shown in Figure 3.37.

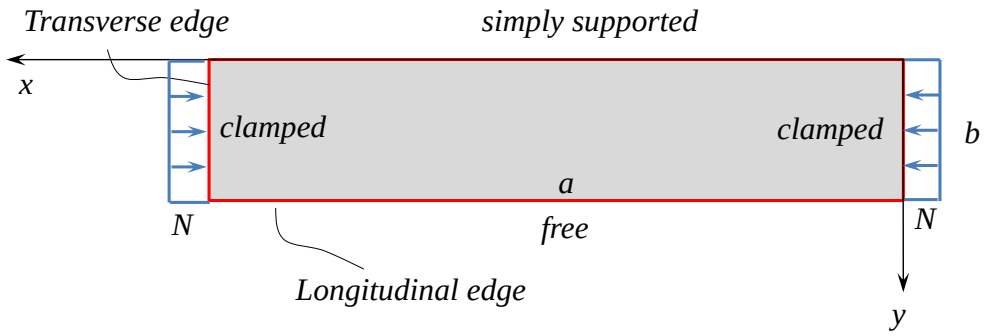

Figure 3.37 Plate model used to derive the local buckling equation of the member

The buckling equation is calculated using a Rayleigh-Ritz approach and the following shape function is assumed

$$u(x,y) = C_1 \sin\left(\frac{\pi x}{a}\right)^2 \left(\sin\left(\frac{\pi y}{2b}\right) + \sinh\left(\frac{\pi y}{2b}\right)\right) \qquad \text{Eqn 3.15}$$

where,

$u\,(x,y)$ = the shape function of the plate model

C_1 = arbitrary constant defined the magnitude of the shape function

a = length of the plate model

b = width of the plate model.

After calculating the critical distributed forces, N_{bcl} for the plate, the buckling stress can be calculated by dividing N_{bcl} by the thickness of the plate. The final buckling stress expression for a plain angle section with a width of 1.75 in. is shown in Eqn. 3.16 which is expressed in terms of the length of the plate/column (a).

$$\sigma_{eLbcl} = \frac{N_{bcl}}{t} = \frac{2.97911 + 87.8765/a^2 + 0.0076913a^2}{t}$$ Eqn 3.16

where,

σ_{eLbcl} = elastic local buckling stress of the member

N_{bcl} = distributed buckling forces on the edge of the member

t = thickness of the member.

Those five equations are plotted in Figure 3.38 together with the buckling stress equations proposed by AISI code and the buckling stress obtained from eigen-buckling analysis of the finite element models of the angle section members. Based on the plot, the AISI equation approaches the global buckling equation for the long members and approaches the flexural-torsional buckling equation for the short and intermediate members. Meanwhile, the results of the ABAQUS model approach the elastic local buckling curve for the short member and the flexural-torsional buckling mode for the intermediate member and the elastic flexural buckling mode for the long member. Moreover, there is a small transition zone between the short member and the intermediate member that cannot be predicted by any buckling curves. Perhaps, this zone is the region where the interaction of local and flexural torsional buckling mode is critical. More advanced theoretical models may be needed to predict the buckling stress in this zone.

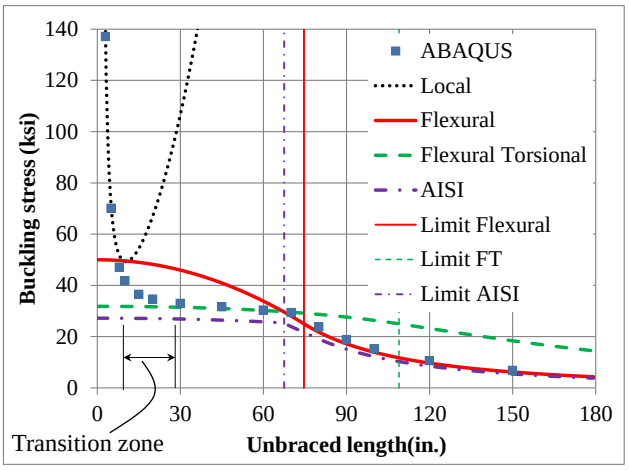

Figure 3.38 Comparison of the buckling stress obtained from ABAQUS model and theoretical prediction

To apply this plot to the vertical post of a cabinet, the possible buckling mode of a post is estimated by assuming the unbraced length of the cabinet as 45 in (mid height of cabinet) and an effective length factor of 1.0125 (sway case). According to Figure 3.39, the most probable buckling mode is the elastic flexural buckling mode in the weak axis direction.

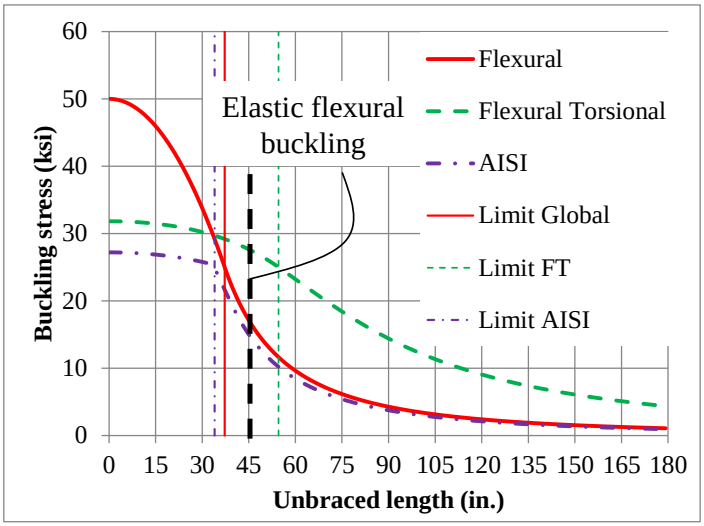

Figure 3.39 Buckling stress of the angle section member with respect to the unbraced length of the member

Although the member is vulnerable to flexural buckling, there is still a possibility that the local buckling of the elements (web/flange) in the member may occur prior to the flexural buckling and the occurance of the local buckling depends on the slenderness of the elements. The slenderness of the elements is often measured as the slenderness ratio (λ) between the width and the thickness of the elements of the member.

The interaction between the local and the flexural buckling behavior of the pin-ended angle section member in the elastic material state has been experimentally studied by Bridget, Jerome and Vosseler (Bridget et al., 1934). In their studies, it was reported that the local buckling behavior was more likely to occur if the slenderness ratio was high. On the other hand, the flexural buckling behavior was more dominant if the slenderness ratio was low. In addition, the slenderness ratio that divides these two behaviors was obtained by intersecting the flexural buckling curve with the local buckling curve (one-half-wave).

To better understand the interaction of the local and the flexural buckling, eigen-buckling analyses are performed on a set of finite element models with the boundary conditions shown in Figure 3.40. The finite element models have the same dimensional value as the typical angle section used in the electrical cabinets (1.75x1.75 plain angle, L = 45 in.), except that the thickness of the member is varied.

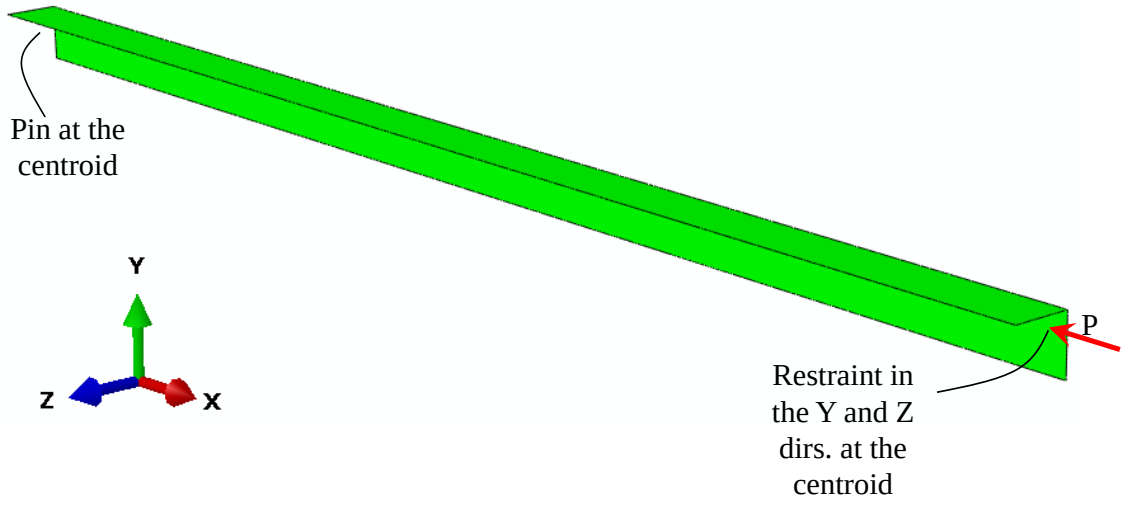

Figure 3.40 Boundary conditions and the loading condition for the eigen-buckling analysis (pin-ended)

Figure 3.41 shows the plot of the local and flexural buckling curves together with the results obtained from the finite element models of the members. The local buckling curve is generated based on a buckling equation for a plate model that is simply supported at two transverse edges and one longitudinal edge, and free at the other longitudinal edge. The plate model is then subjected to uniformly distributed force. Meanwhile, the flexural buckling curve is generated using Eqn 3.11. The results of the ABAQUS simulations confirm the plots of the local and the flexural buckling curves. In addition, the local and the flexural buckling curves are intersected at the slenderness ratio of 24.9.

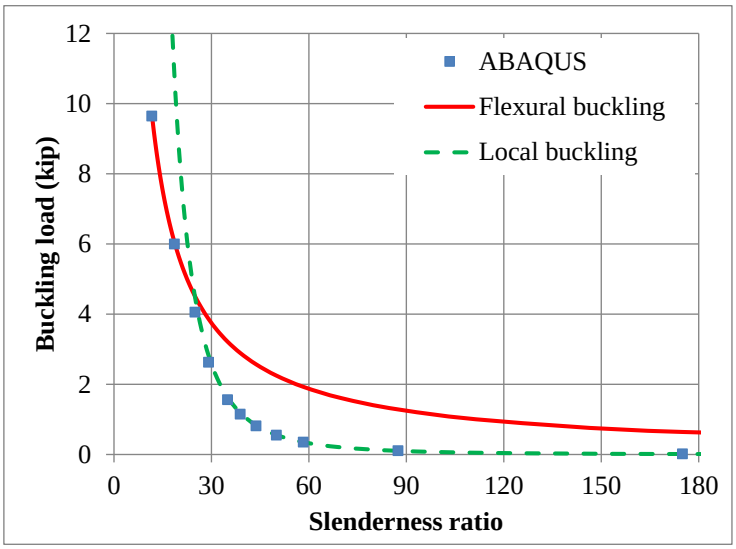

Figure 3.41 Interaction between the local and the flexural buckling behavior for a simply supported angle section column subjected to axial load (pin-ended, K = 1.0)

Next, the numerical study is extended to a more realistic case of the vertical posts in the cabinets. In the lateral load condition, sidesway is a more realistic case for the vertical posts. Hence, the effective length factor for this condition is usually larger than 1.0. The effective length factor can be obtained from the alignment chart in the steel manual based on the rotational restraints at the end of the member. However, the visual accuracy of the chart can be subjective, especially if it involves precise values. Therefore, the efffective length factor is obtained from a finite element model of the member that is partially restrained (rotational restraints, $k_r = 6\ EI_b/L_b$) at both ends and simply supported at one end. Based on the numerical model, an effective length factor of 1.0125 is obtained.

Similar eigen-buckling analyses to those discussed previously are conducted. At this time, the boundary conditions for the member are modified as shown in Figure 3.42. The results of the finite element models are plotted together with the local and flexural buckling curves in Figure 3.43. The flexural buckling curve is generated with an effective

length factor, K = 1.0125 using Eqn 3.11, and the local buckling curve is generated based on a plate model that is simply supported at two transverse edges and one longitudinal edge and free at the other longitudinal edge. The effect of the rotational restraint is excluded in the derivation of the local buckling equation, and this exclusion does not change the results significantly when they are compared to the results of ABAQUS model.

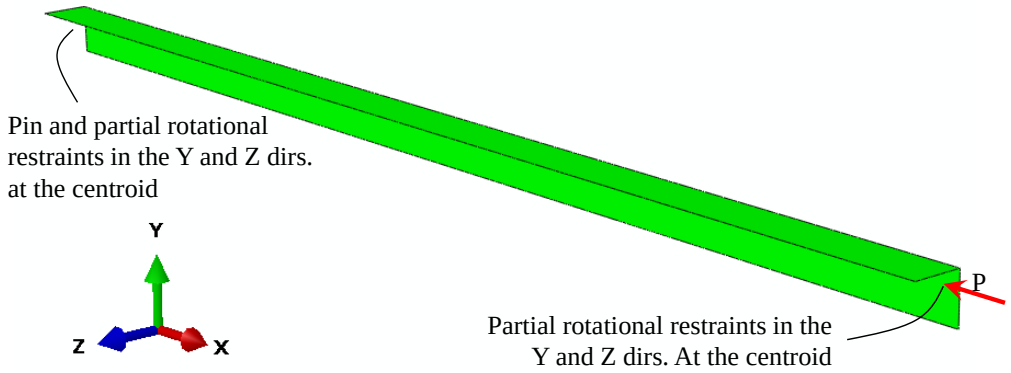

Figure 3.42 Boundary conditions and loading condition for the eigen-buckling analysis (K = 1.0125)

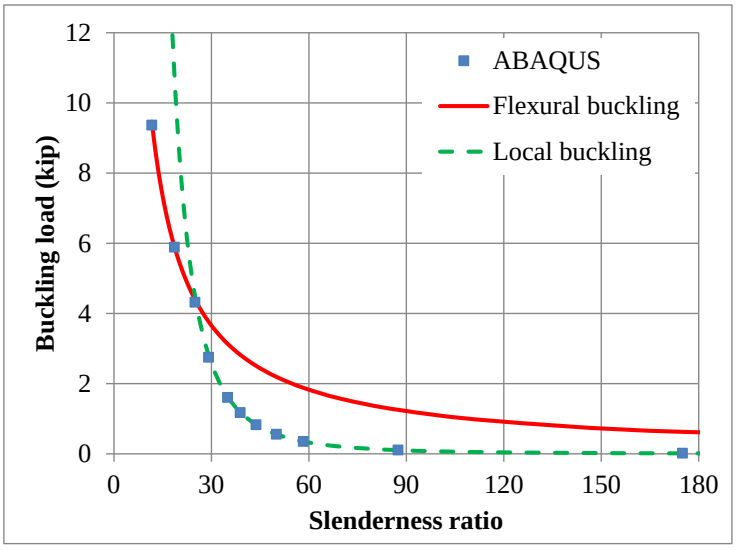

Figure 3.43 Interaction between the local and the Euler's buckling behavior for a simply supported angle section column subjected to axial load (K = 1.0125)

According to the plot, the local and the flexural buckling curves are intersected at the slenderness ratio, λ = 25.00. The slenderness ratio of the plain angle section used for the vertical post of the cabinet (λ_r = 1.75 / 0.09375 = 18.67) is below the slenderness ratio for the local buckling to occur (λ = 25.00). Hence, the plain angle section is non-slender. Therefore, the member is more vulnerable to flexural buckling which typically does not produce a softening behavior when it buckles. Hence, only a simplified beam model (e.g. the hybrid Timoshenko beam model) that can capture the elastic local buckling behavior under double curvature bending is necessary for the vertical post of the cabinet.

CHAPTER 4

DEVELOPMENT OF A SIMPLIFIED FINITE ELEMENT MODEL OF ELECTRICAL SWITCHBOARD CABINET: CLASS II CONFIGURATION

A method to generate a simplified finite element model for a simpler configuration of electrical switchboard cabinet has been proposed and validated in Chapter 3. In this chapter, application of the methodology is extended to an electrical switchboard cabinet with a more complex configuration. This complex configuration is selected because it represents a class of electrical switchboard cabinets observed during a site visit to the electrical room in the Sustainable Education Building (SEB) at Georgia Institute of Technology.

4.1 Description of the Class II Configuration

Figure 4.1 shows the bare-frame and full-cabinet models of the class II configuration. The height, width and depth of the cabinet is identical to the class I configuration. The beam of the cabinet is constructed from a plain channel section, and the front and back vertical posts of the cabinet are constructed by folded angle sections as shown in Figure 4.2.a. These framing members are connected together with screws/bolts (see Figure 4.2.b) to form the framing system of the cabinet. An unfolded panel is used to cover the top side of the cabinet and folded panels (see Figure 4.3.a) are used to enclose the cabinet on the left, right, front and back sides of the cabinet. Figure 4.3.b shows the configuration of the connection between panels and vertical posts. Due to the configuration of the folded panels, there is a significant eccentricity in this connection.

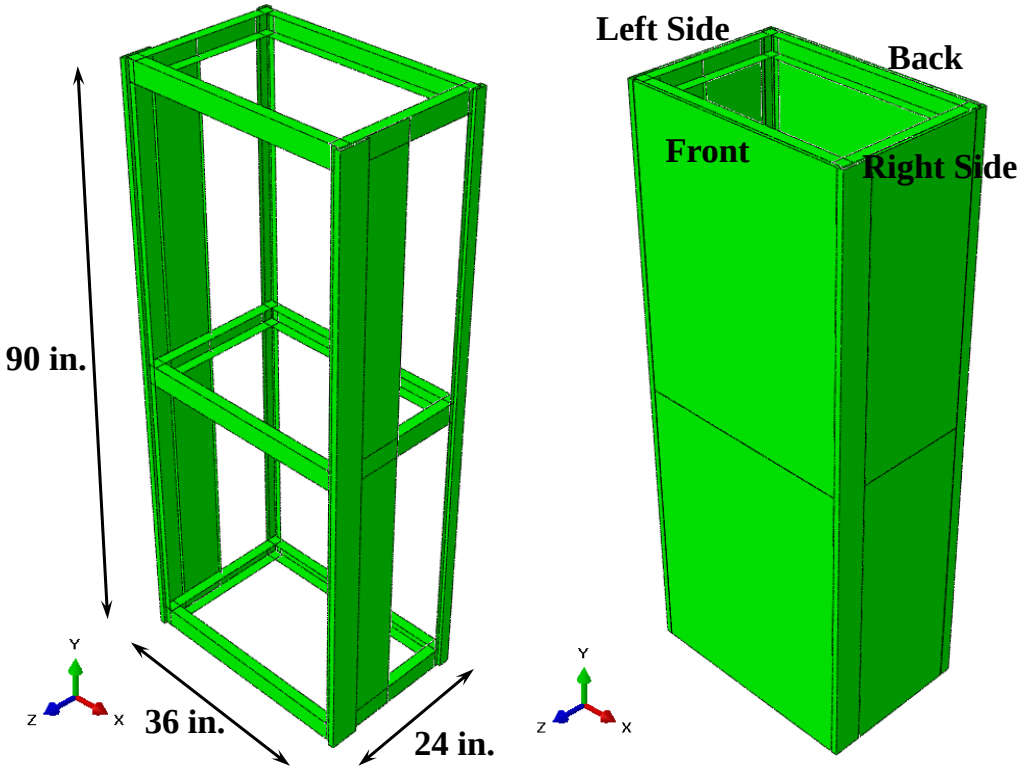

(a) Bare-frame model (b) Full-cabinet model

Figure 4.1 Class II configurations of the electrical switchboard cabinet

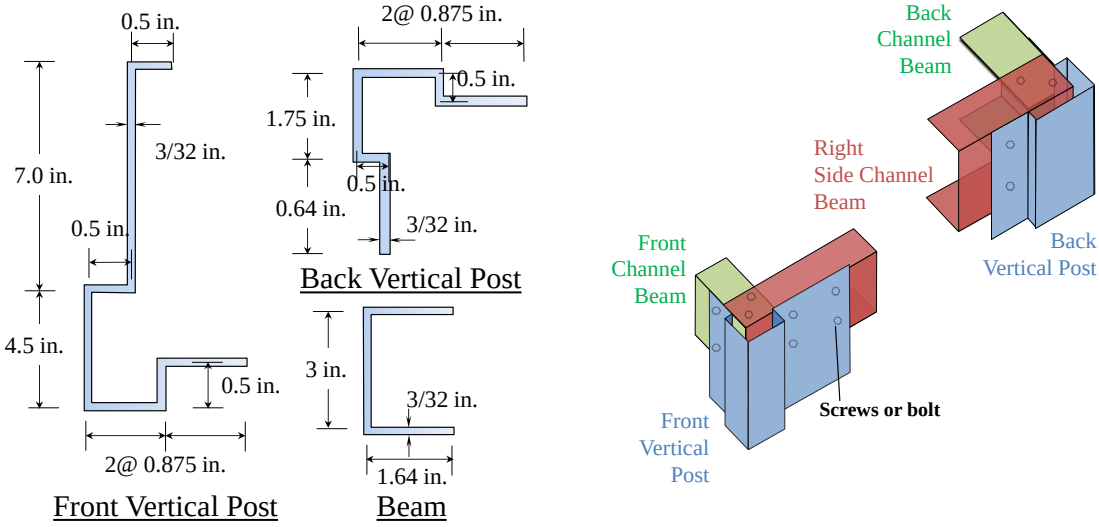

(a) Cross sections of the framing members (b) Connection between framing members

Figure 4.2 Configuration of the framing members and their connections.

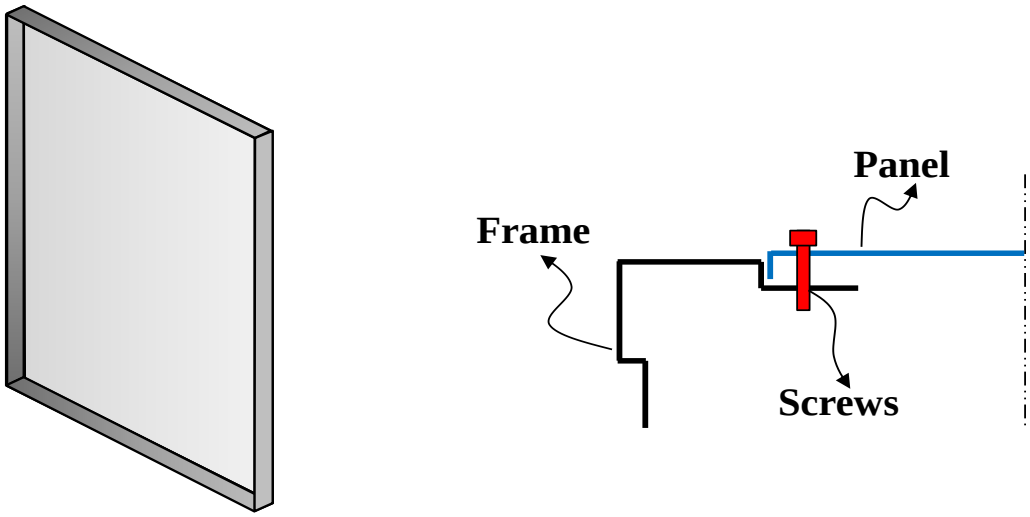

(a) Folded panel

(b) Connection between panels and framing members

Figure 4.3 Configurations of the panel and its connection to the framing member.

4.2 Development of the Simplified Finite Element Model of Electrical Switchboard Cabinet

Development of the simplified finite element model for the class II configuration follows the same general method as that discussed in Chapter III. Finite element models and modeling features (springs and constraints) are selected or developed for each structural component of the cabinet: 1) framing members, 2) panels and their connection to the framing members, and 3) connection between framing members. Due to the complexity of the framing members and the panels, slight adjustments are needed in the application of the method to generate a simplified finite element model for the cabinet. Table 4.1 compares the elements and modeling features applied to the simplified cabinet models of the electrical cabinet having the class I and the class II configurations. In the next section, the development of the simplified finite element model for the cabinet is discussed, and the adjustments needed for the model are explained in detail.

Table 4.1 Comparison of the finite elements and modeling features for the structural components of the electrical cabinets with the class I and the class II configurations

Structural Components	**Class I**	**Class II**
Framing members	Hybrid Timoshenko beam model*	Timoshenko beam model**
Connection between framing members	Rotational springs and rigid beam constraints	Rotational springs and rigid beam constraints
Panels	Shell elements	Shell elements
Screw Connection between panels and framing members	• Rigid beam and warping constraints • Translational springs	• Rigid beam and warping constraints*** • Translational Springs • Rotational Springs

Note:

* The hybrid Timoshenko beam model is only assigned to the bare-frame cabinet model. Meanwhile, only the Timoshenko beam model is used in the full-cabinet model.

** Based on the observation of the benchmark cabinet models, no rotational spring is required at the ends of framing members since local buckling of the framing members is insignificant to the overall behavior of the electrical cabinet

***Warping constraints are needed only in the left and right side of the cabinet

4.2.1 Finite Element Model for the Framing Members and Panels

The Timoshenko beam element is used to model the framing members of the cabinet. As discussed in Chapter III, this element was selected because of its ability to capture shear deformation effects in short members. For the class II configuration, the rotational springs at the end of the vertical posts are removed because further investigations of the benchmark cabinet model have shown that the local buckling near the ends of the vertical posts has a minor effect on the lateral stiffness of the cabinet (see Section 4.3.2 for further discussions). However, if local buckling is found to be critical in future investigations (e.g. for other configurations of electrical switchboard cabinets), the hybrid Timoshenko beam model can be applied with rotational spring properties

generated based on use of a high fidelity shell element model for the framing members. Application of the effective-width prediction method to generate the spring properties may lead to incorrect results due to the possibility of distortional buckling modes for complex sections that cannot be captured by use of the conventional effective width equation applied in the effective-width prediction method.

The panels of the electrical cabinet are modeled explicitly using shell elements. This finite element model was chosen because it has the capability to capture the deformation of the panels which may have an adverse impact on electrical devices (mass) attached to the panels.

4.2.2 Modeling Features for the Connection between Framing Members

The connections between framing members are divided into four types based on their position in the cabinet: 1) Front – Top or Middle, 2) Back – Top or Middle, 3) Front – Bottom, and 4) Back – Bottom (see Figure 4.4). As in the class I configuration, additional restraints are imposed to the bottom connections due to supports of the cabinet.

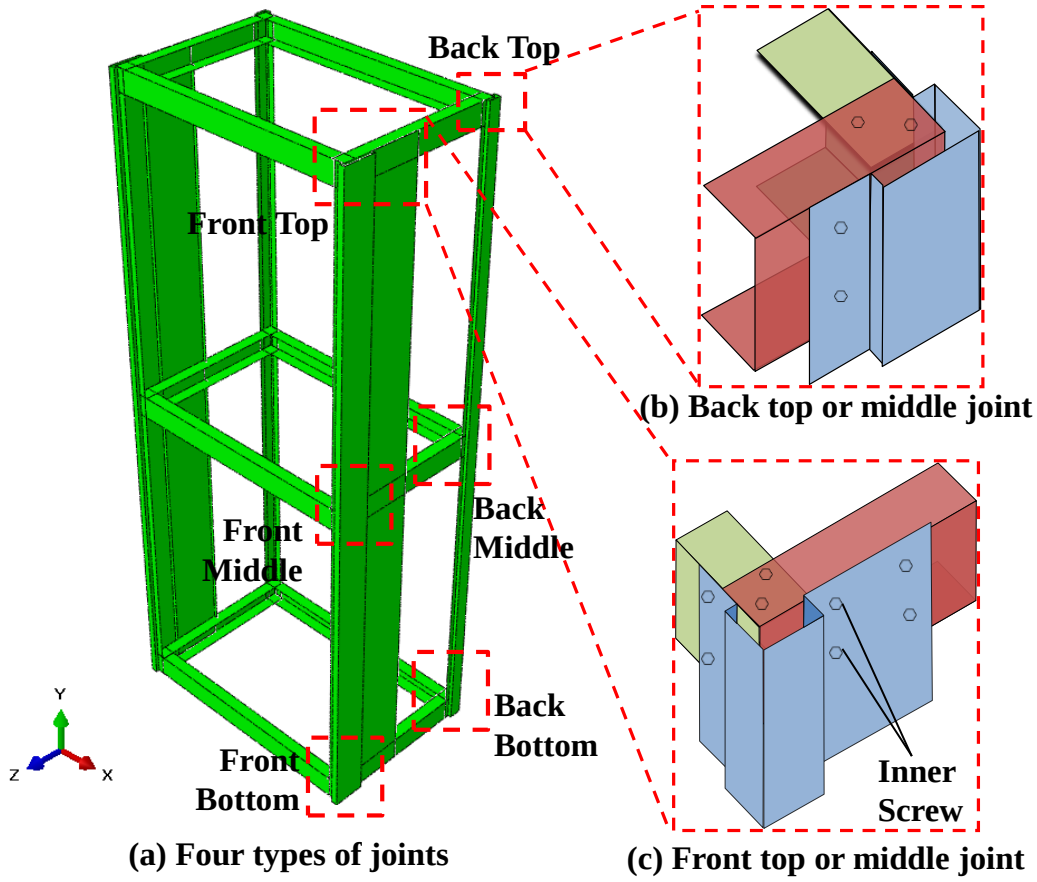

Figure 4.4 Types of joints in the class II cabinet configuration

The connections between the framing members in the simplified model of class II cabinet configuration are modeled using rigid beam constraints (see Rigid beam connector in Figure 4.5) and rotational springs (see frame-frame connectors in Figure 4.5) as in the class I configuration. The rigid beam constraints are represented using CONNECTOR-BEAM feature in ABAQUS. This feature rigidly constrains all translational and rotational DOFs between the connecting nodes (see points 1 and 2 in Figure 4.5). In addition, the rotational springs are represented using CONNECTOR – JOIN, ROTATION feature. This feature rigidly constrains all translational DOFs (JOIN) and assigns linear elastic rotational springs in three orthogonal directions (ROTATION).

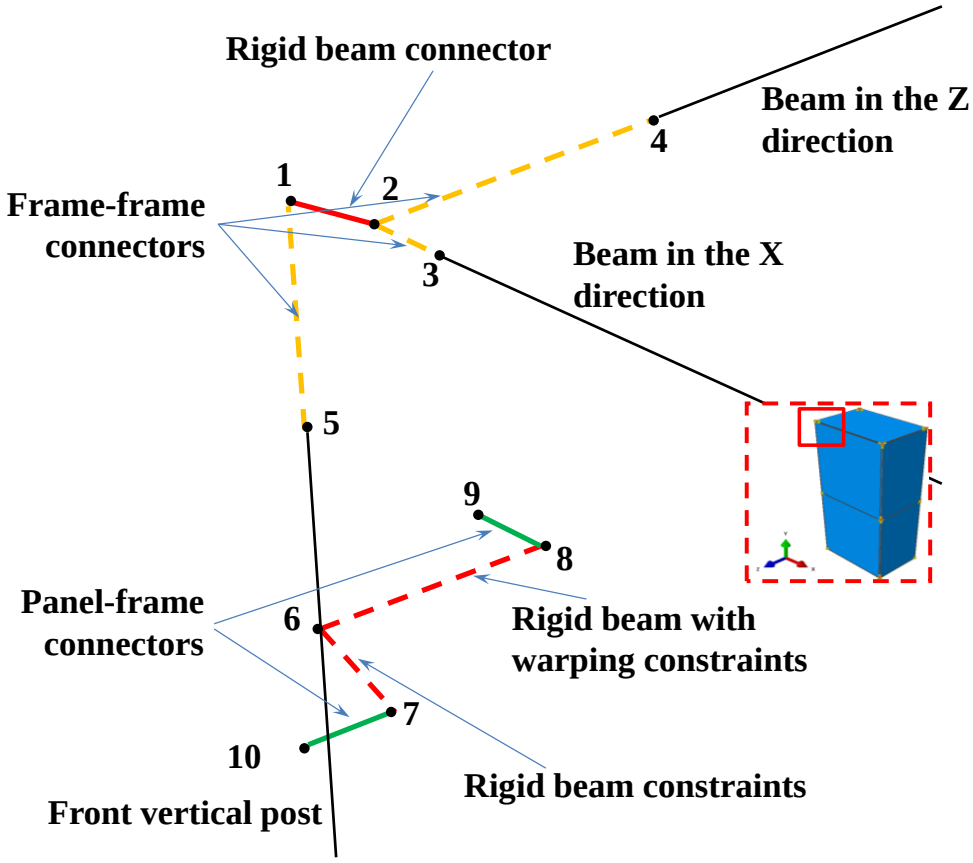

Figure 4.5 Detailed of locations of modeling features assigned to the simplified model of class II cabinet configuration

The stiffness of the rotational springs is determined using the same method as in the class I configuration based on shell element models of the joints as shown in Figure 4.6. The framing members are connected using FASTENER-BEAM feature in ABAQUS that rigidly constrains the connecting nodes between the coincidence members at the location of the screws/bolts (see FASTENER in Figure 4.6). Afterward, rigid beam or free warping constraints are assigned between the edge nodes along the cut-off end of a member and the centroid at that end based on the rules discussed in Section 3.3 for the class I cabinet configuration. The stiffness of the springs of a member is then obtained by imposing a unit rotation in each orthogonal direction at the centroid of that member while fixing the centroid of other members that are also attached at the joint.

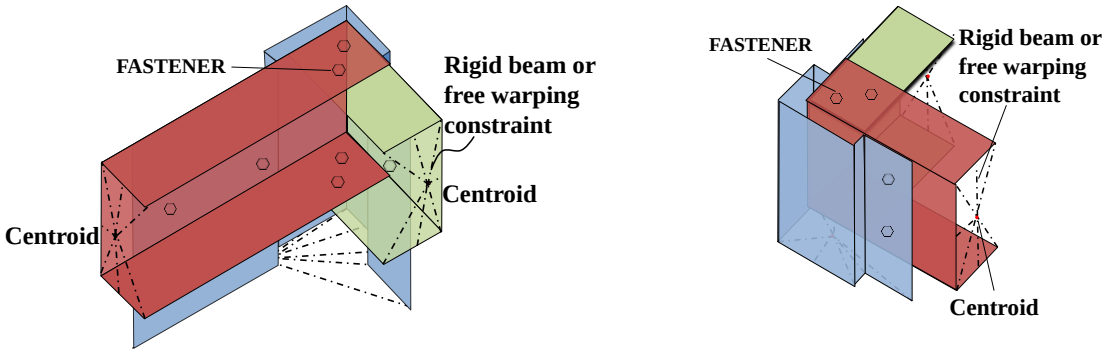

(a) Front joint (b) Back joint

Figure 4.6 Kinematic constraints assigned to the shell element models of the connections between framing members

In addition, finite-joint size is also considered in the simplified cabinet model based on the cut-off length of the members in the shell element models of the joints, except for the longer beam member (about 7 in. long) in the front joint of the cabinet. The finite-joint size corresponding to that member is taken as the distance between the inner end of that member and the inner screws (see Inner screw in Figure 4.4.c), because the displacement of the beam member at that location is considerably smaller than the displacement at its tip end.

4.2.3 Modeling Features for the Connection between Panels and Framing Members

The connection between panels and framing members are still represented by the rigid beam and warping constraint equations and the panel-frame connectors as in the class I configuration. However, the warping constraint equations are only assigned to the attachment points of the left and right side of the panels in the class II configuration (e.g. point 8 in Figure 4.5). Meanwhile, rigid beam constraints are assigned to the attachment points of the front, left, right and back sides of the panels (e.g. points 7 and 8 in Figure 4.5). This decision was made because the simplified cabinet models are already accurate compared to the corresponding benchmark cabinet models when they are pushed laterally in the side-to-side or X direction (note that front and back panels are critical to the overall

structural rigidity of the model in this case). At the same time, the results of the simplified cabinet models without warping constraints deviate significantly from the corresponding benchmark cabinet models when they are pushed in the front-back direction (Z direction). Therefore, warping constraints are introduced on the left and right sides of the panels. The warping constraints are calculated using the same equations and boundary conditions as described in Section 3.4.2.

The panel and frame connectors are assigned with CONNECTOR – CARTESIAN, ROTATION features in ABAQUS between two attachment points (e.g. 7-10 and 8-9 in Figure 4.5) on the framing members and panels. Linear elastic, perfectly plastic translational springs in three orthogonal directions as defined in Section 3.4.2 are still applicable for the class II configuration. However, the significant eccentricity in the connection causes a secondary moment that must be carried by the lip of the vertical posts that eventually makes the connection more flexible (see Figure 4.7.a). This flexibility is considered in the simplified cabinet model by adding linear elastic in-plane rotational springs in two orthogonal directions to the existing translational springs. The stiffness of the springs is assumed to be the bending stiffness of a cantilever beam subjected to tip-end moment with the effective width calculated based on the average of the diameter of the screw (b_1) and the projected width at the constraint edge (b_2) (see Figure 4.7.b) obtained by projecting an angle θ to the constraint edge. This angle is obtained by averaging the principal angles of the elements in front of the screws in plane-stress analyses of plate models having constant depth (d) but varying width (w) as shown in Figure 4.8.a. The plate models are subjected to unit shear force applied eccentrically from the center of the screw. Afterward, the nodes at the constraint edge and the edges along the depth of the plate models are fixed. Figure 4.8.b shows the results of the sensitivity study of the plate model for the connection between the front or the back panels and the cabinet. From this curve, θ for the connection is taken to be 25^o (the converged value). The analyses to determine θ are repeated for the front and back

connections between the left-side or the right-side panels and the cabinet. The analyses reveal values of θ = 30^o and 21.8^o for the left-side or right-side front and the left-side or right-side back connections, respectively.

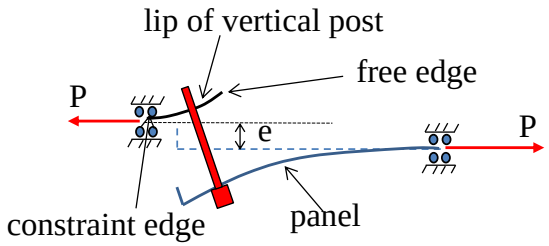

(a) Kinematics of the screw connection with excessive eccentricity

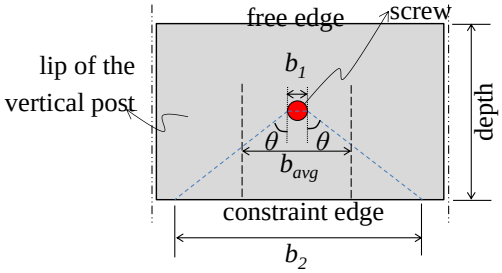

(b) Description of the nomenclature used to generate the stiffness of the additional rotational springs

Figure 4.7 The effect of excessive eccentricity to the flexibility of the screw connection

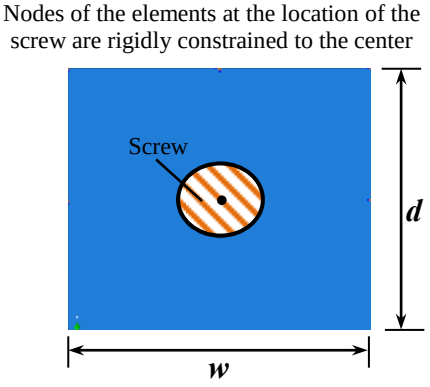

(a) Plate model used in the analyses

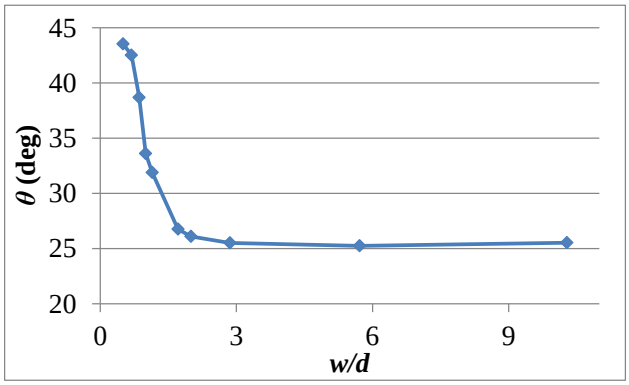

(b) Change of θ corresponding to the ratio of the varying width (w) to the constant depth (d)

Figure 4.8 Plane-stress finite element analyses to determine angle θ

4.3 Validation of the Simplified Cabinet Model: Class II Configuration

As in the class I configuration, the simplified cabinet models of the class II configuration are validated by using their benchmark cabinet models. These simplified cabinet models are subjected to pushover analysis in the front-back (FB) and the side-to-side (SS) directions by applying displacements at the top of the cabinet. The pushover analyses are performed on the bare-frame (without panels) and full-cabinet (with panels)

configurations of the cabinet by not including (1^{st}-order) and including (2^{nd}-order) the geometric nonlinear effect.

4.3.1 Development of the Benchmark (BM) and Simplified (SM) Cabinet Models

In the benchmark cabinet models, the framing members and panels of the cabinet are modeled explicitly using shell elements. The framing members are connected using the FASTENER – BEAM feature in ABAQUS that rigidly constrains all DOFs of the connecting nodes. In addition, the panels are connected to the framing members using CONNECTOR – CARTESIAN, ALIGN feature. This feature allows the assignment of translational springs in three orthogonal directions and rigidly constrains all rotational DOFs of the connecting nodes. The properties of the translational springs are the same as the properties defined in Section 3.4.2. The cabinet models are then fixed at the four bottom corners of the cabinet.

In the simplified cabinet models, the (ordinary) Timoshenko beam model is used to represent the framing members of the cabinet. Partial rigid connections between the framing members are represented using the CONNECTOR – JOIN, ROTATION feature in ABAQUS (see frame-frame connectors in Figure 4.5), and CONNECTOR – BEAM feature (see rigid beam connector in Figure 4.5). Constraint equations are then assigned between two nodes at a point on the centroidal axis of the vertical posts and a point on the flanges of the vertical posts to which the panels are attached (see joints 6-7 and 6-8 in Figure 4.5). The rigid beam and warping constraint equations are assigned to the connecting nodes of the left-side and right-side of the panels and framing member (joints 6-8) but only rigid beam constraints are assigned to the connecting nodes of the front and back panels, and framing members (joints 6-7). In addition, the panels are modeled explicitly using shell elements, and connected to the framing members using CONNECTOR – CARTESIAN, ROTATION feature (see Panel-frame connector in Figure 4.5). This feature allows the assignment of both translational and rotational

springs between the connecting nodes. The properties of the translational springs are the same as those assigned in the benchmark cabinet model and discussed in Section 3.4.2. In addition, the properties of two rotational springs in the in-plane directions follow the discussion in Section 4.2.3. In addition, the other rotational DOF (drilling DOF) of the connection model is assumed to be rigid. It should be noted that all rotational DOFs of the panel-frame connection model in the benchmark cabinet models are rigid because it is expected that the in-plane flexibility contributed from the flanges of the vertical posts is explicitly included in the model since the framing members are represented using shell elements. Finally, the simplified cabinet models are fixed at the four bottom corners of the cabinet.

4.3.2 Validation of the Simplified Models

Validation of the Bare-frame Model

In the first order analyses, the pushover curves of the benchmark cabinet models in the front-back (FB) and side-to-side (SS) directions are linear. The simplified cabinet models are able to capture this behavior and only over-predicted the stiffness by +6%. In the second order analyses, the pushover curve in the SS direction is almost linear, and the simplified cabinet model slightly over-predicts the stiffness of the curve by +9%. Further studies using the benchmark cabinet model have shown that local deformations (see Figure 4.9) occurred near the ends of the framing members. However, these local deformations are not critical to the overall behavior of the cabinet since no significant stiffness reducing effect is found in the pushover curve. As a result, only the "ordinary" Timoshenko beam model is included in the simplified cabinet models.

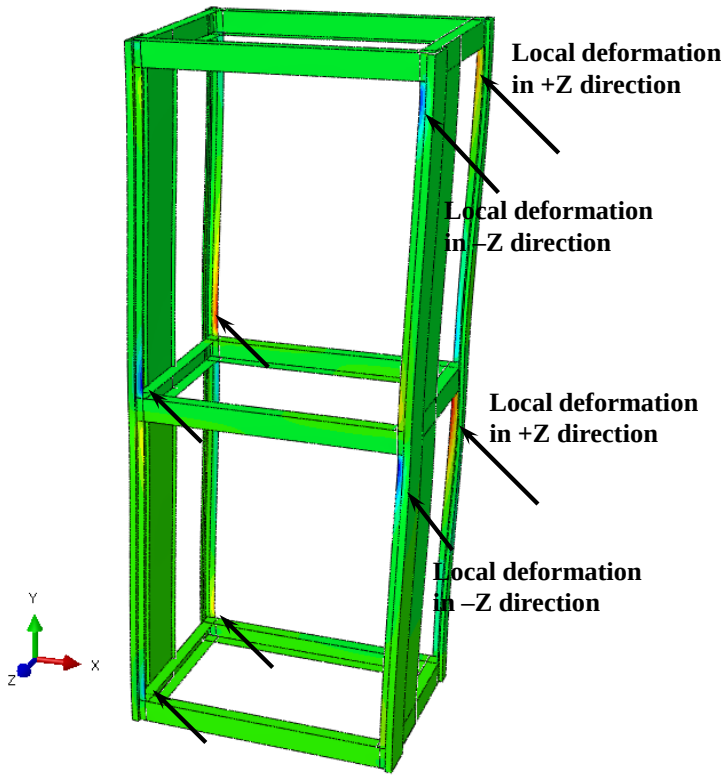

Figure 4.9 Local deformations (in Z direction) near the ends of compressed flanges of the vertical posts; no significant impact on the overall behavior of the cabinet

The vertical posts experienced global buckling indicated by out-of-plane deformation of the compressed vertical posts shown in Figure 4.10.a.and b based on the pushover analysis in the FB direction. Trial calculations of the global buckling modes on both the compressed front and back vertical posts with effective length factor K = 1.00 reveals that the flexural-torsional buckling is the critical buckling mode of the vertical posts (see Figure 4.11.a and b.).

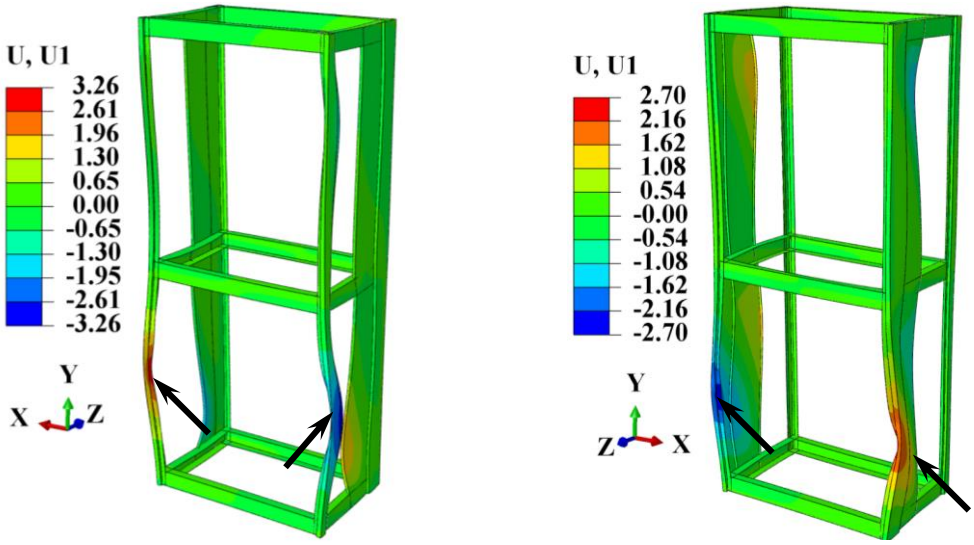

(a) Pushover analyses in the –Z direction (b) Pushover analyses in the +Z direction

Figure 4.10 Deformation of framing members in the X direction showing the global buckling of the compressed vertical posts

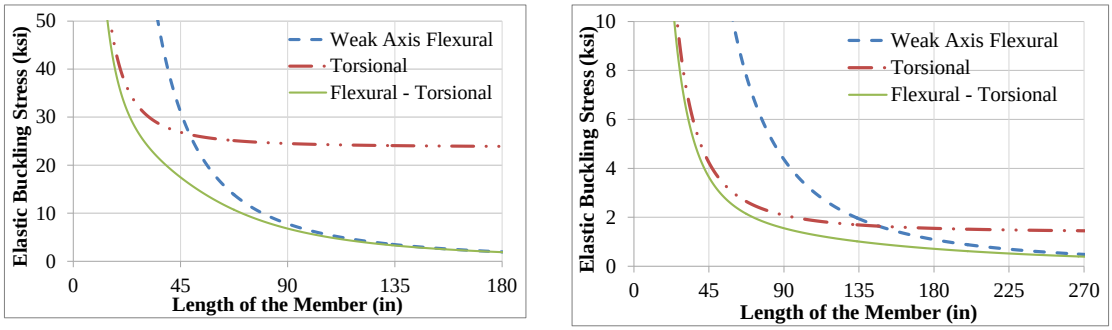

(a) Pushover analyses in the –Z direction (b) Pushover analyses in the +Z direction

Figure 4.11 Global buckling curves

The simplified cabinet model is able to capture the initial stiffness of the pushover curves but it is incapable of predicting the post-global buckling curves of the benchmark cabinet models (see Figure 4.12). The stiffness of the simplified cabinet model pushed in the FB direction is reduced significantly with a slow convergence rate after the buckling load is reached. The analysis is finally terminated after the number of increments exceeds the maximum number of increments set prior to the analysis. At the same time, slow convergence rate is also observed on the simplified model pushed in the FBneg direction once the buckling load is reached, and the analysis is terminated because the maximum number of increment has been reached. Since the flexural-torsional buckling load of the

front vertical post is smaller than the flexural-torsional buckling load of the back vertical post, the buckling load of the simplified cabinet model are reached first when the cabinet is pushed in the FB (+Z) direction than when the cabinet model is pushed in the FBneg (-Z) direction. The global buckling behavior may not reflect the overall behavior of the electrical switchboard cabinet because it has not been observed during reconnaissance surveys and experimental tests. Three possible reasons for this are: 1) the cabinet was not subjected to a load large enough to cause the vertical posts to buckle in flexural-torsional manner, 2) the possibility of local buckling of frame members was anticipated during the design-analysis process resulting in the addition of bracing to increase the capacity of the members, or 3) the elastic global buckling is not the weakest limit state.

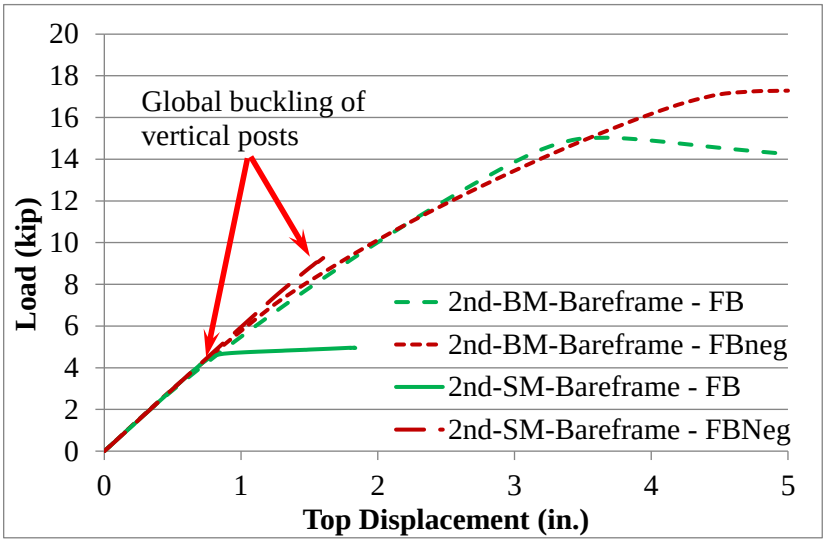

Figure 4.12 Second order pushover curves of the bare-frame cabinet in the front-back (FB) directions

Validation of the Full-cabinet Model

In the first order analyses, the pushover curves in the side-to-side (SS) and the front-back (FB) directions are characterized by bilinear curves (see Figure 4.13). The nonlinearity in the pushover curves is due to the failure of screw connection in shear. The simplified cabinet model is able to predict the pushover curves of the benchmark cabinet models for the SS and FB directions cases. It is noted that, in the full-cabinet

model, the warping constraints are only assigned in the left and right sides of the cabinet. Further investigations show that the simplified cabinet model without the warping constraint in the left and right sides of cabinets over-predicts the initial stiffness of the benchmark cabinet model by about 22%. This value is obtained based on the cabinet models pushed in the FB direction. This large overestimation may be caused by different relative displacement in the panel-frame connectors. This relative displacement is induced by different amount of warping deformation on the flanges of front and back vertical posts in the benchmark cabinet model. On the other hand, the simplified cabinet model pushed in the SS direction with or without the warping constraint in the front and back sides of the cabinet are almost the same.

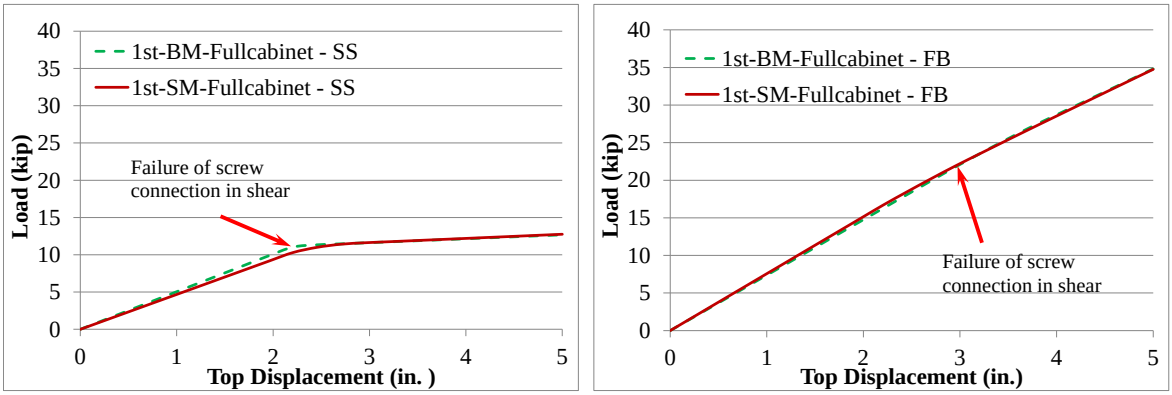

(a) Side-to-side (SS) direction (b) Front-back (FB) direction

Figure 4.13 First order pushover curves of the full-cabinet model

In the second order analyses, the pushover curves in the SS and FB directions are nonlinear. In the SS direction (see Figure 4.14), the nonlinearity is due to local deformation of the vertical posts, buckling of the panels and failure of screw connections in tensions. The local deformation occurred prior to buckling of panels, and, as in the bare-frame model, does not have significant effect on the overall behavior of the cabinet. The tensile failure of the screw connection is triggered by the significant eccentricity of the panel-frame connection and deformation of panels and framing members. This limit state corresponds to the limit states observed during experimental testing of the cabinet as shown in Figure 4.15. Note that the screw connection in the class I configuration fails in

shear rather than tension because the eccentricity of the panel-frame connection in the class I cabinet configuration is 80% smaller than the eccentricity of the panel-frame connection in the class II configuration.

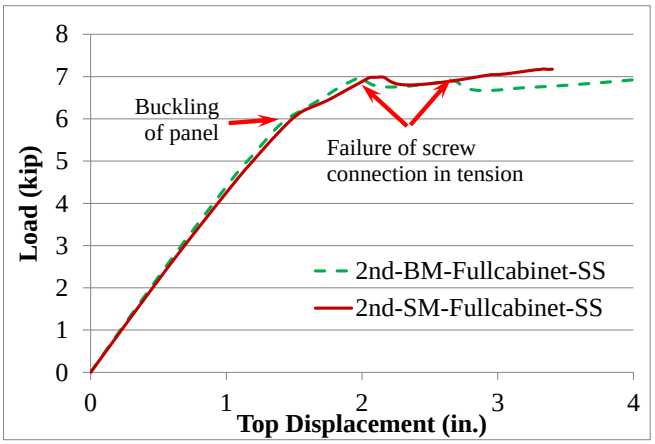

(a) Second order pushover curves

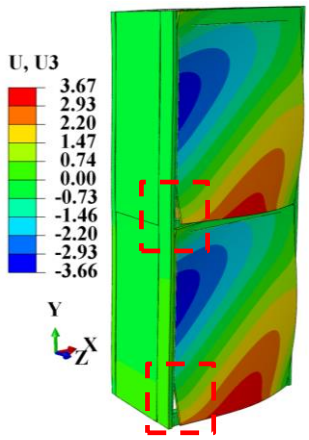

(b) Deformation in the Z direction showing buckling of panels

Figure 4.14 Pushover analysis of the full-cabinet model in the side-to-side (SS) direction

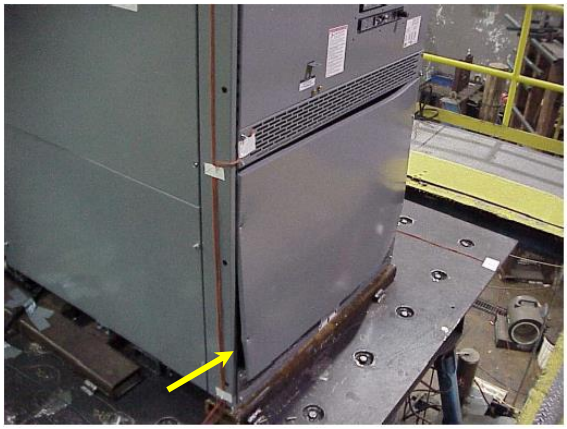

Figure 4.15 Buckling of panels and failure of screw connections in tension observed in experimental test (picture courtesy of: Wyle Laboratories. (2008))

In the front-back (FB (+Z) and FBneg (-Z)) directions, the nonlinearity in the pushover curves (see Figure 4.16.a) obtained from the benchmark cabinet model is a result of global buckling of the vertical posts, local deformation of the flanges of vertical posts and buckling of panels. Of these, the most critical limit state is the global buckling of the vertical posts. This global buckling mode is similar to the flexural-torsional buckling mode observed in the bare-frame model. The simplified model is able to capture

the initial stiffness of the cabinet model. However, it exhibits a similar convergence problem as the bare-frame model once the buckling load of the vertical posts is reached. The global buckling loads of the full-cabinet models are slightly smaller than the buckling loads of the bare-frame models because the attached panels increase the overall cabinet rigidity beyond that offered by the framing members. As a result, the framing members are subjected to higher moments that will eventually reduce the buckling load.

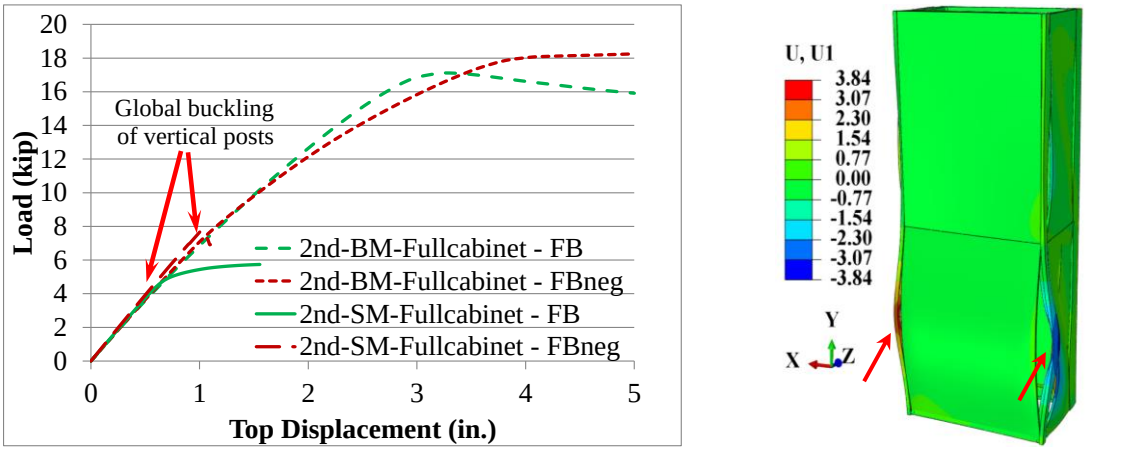

(a) Second order pushover curves

(b) Global buckling of the back vertical posts (FBneg)

Figure 4.16 Pushover analyses of the full-cabinet model in the FB (+Z) and FBneg (-Z) directions.

Overall, the simplified cabinet models are able to predict the behavior of benchmark cabinet models. One caveat related to the use of the simplified cabinet model for pushover analysis in the front-back direction is the post-global buckling behavior observed in the benchmark cabinet model. However, given the accuracy of the simplified models to predict the initial stiffness of that case and the irrelevancy of the limit state (global buckling) compared to the observations made during the reconnaissance surveys and experimental tests, the behavior of the simplified models in the front-back direction is acceptable.

4.4 Effects of the Interaction between Panels and Framing Members to the Behavior of Electrical Switchboard Cabinets

4.4.1 Effect of Edge Contact on the Behavior of Electrical Switchboard Cabinets

In this section, behavior of electrical switchboard cabinets with the class II configuration is further explored to study the effect of contact between the corners of the panels and the flanges of vertical posts on the overall behavior of the cabinet. Construction gaps of 0.1 - 0.2 in. usually exist along the vertical posts and panels. When these gaps are closed (at the corners) due to lateral load, the stiffness of the cabinet is expected to increase. To study this behavior, two CONNECTOR–STOP features are assigned to the corners of the panels and vertical posts as shown in Figure 4.17. This feature assigns “zero” stiffness springs when the deformation between the connecting points is less than the provided gap. However, it will assign “rigid” springs when the deformation between the connecting points exceeds the gap. This feature was applied to each corner point between the vertical posts and panels for both benchmark and simplified cabinet models of the class II configuration. Additional rigid beam constraints have to be defined in the simplified cabinet model between the centroidal axis of the vertical post and two points on the flanges of the vertical post in which the two connector features are connected to. Afterward, pushover analyses (without geometric nonlinear effect) in the side-to-side (SS) direction were conducted to study the effect of this interaction to the behavior of the cabinet.

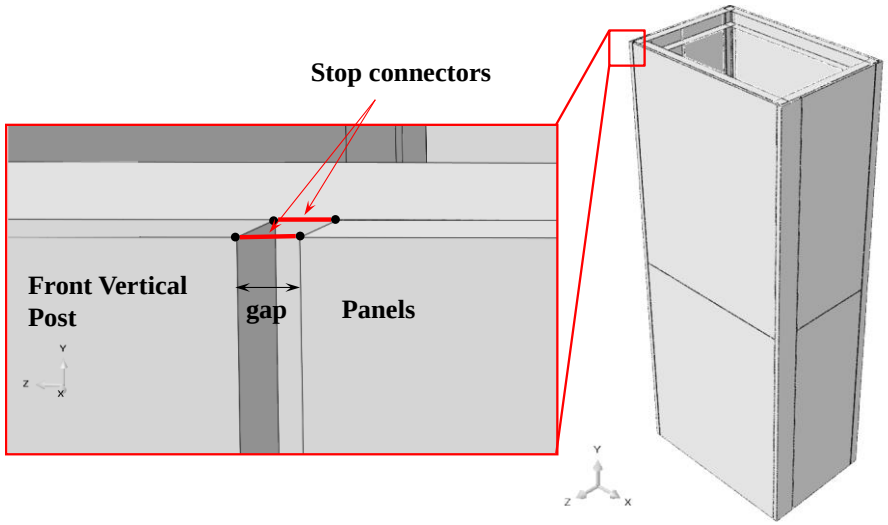

Figure 4.17 Stop connectors assigned to each corner of the electrical cabinet between the panels and the vertical posts.

Figure 4.18 shows the 1st-order pushover curves of the benchmark cabinet model with the connector-stop feature implemented in the SS direction (1st-BM-Fullcabinet-SS-WCon). A plot of the pushover curve without the connector-stop feature (1st-BM-Fullcabinet-SS-WoCon) is also included for comparison. At an applied top displacement of approximately 1 in., the deformation of some of the connectors exceeded the gap, and the stiffening behavior was observed in the pushover curves. This behavior also causes the failure of the screws at lower top displacement value with almost the same load level as the model without the connector-stop feature. The pushover curves (1st-SM-Fullcabinet-SS-WCon) obtained from the simplified cabinet model is able to show behavior similar to that observed in the benchmark cabinet model.

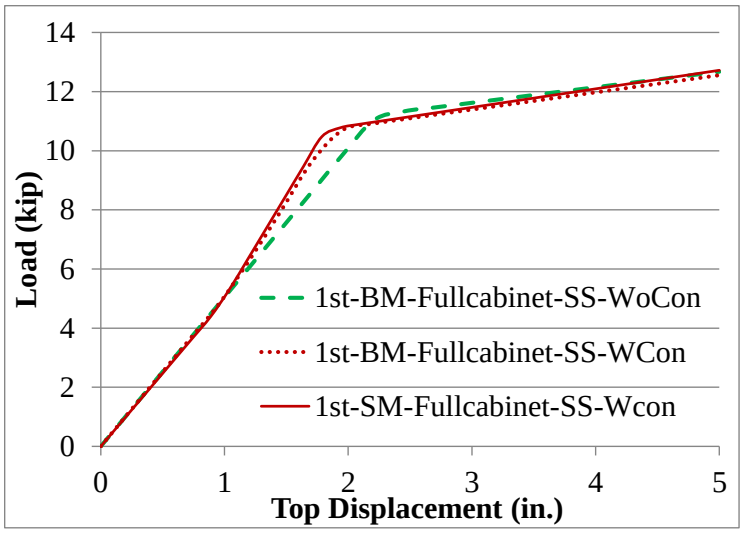

Figure 4.18 1st-order pushover curves of the cabinet with stop/lock features: side-to-side (SS) direction

Application of this feature in the modeling of the cabinet may have an impact on the overall rigidity of the cabinet depending on the following: 1) the gap distance, and 2) amount of deformation of the cabinet. Figure 4.19 shows the effect of gap distances on the stiffening behavior of the electrical cabinet. As the gap becomes larger, the stiffening behavior occurs at higher top displacement values; and as the gap gets smaller, the stiffening effect occurs at a lower top displacement value. This value can be as low as in the condition in which loading or displacement is just applied at the top of the cabinet. In this case, the initial stiffness of the cabinet model considering this connector-stop feature is about 40% greater than the initial stiffness of cabinet model without considering this feature. This stiffening effect is not included further in the analyses in Chapter 5 and 6 to limit the scope of observation. In other words, the gap between the panel and vertical posts is assumed to be large enough to accommodate the relative deformation between these two structural components.

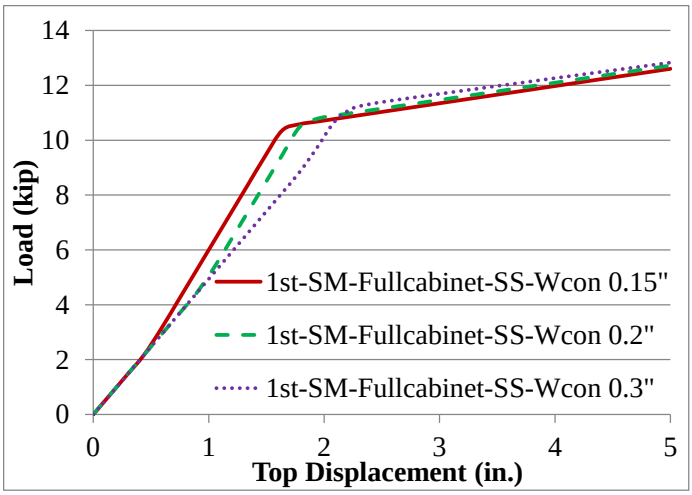

Figure 4.19 Effect of gap distance to the behavior of electrical cabinet

4.4.2 Effect of the Number of Fasteners between Panels and Framing Members on the Behavior of the Electrical Switchboard Cabinet

In this section, results are presented for a sensitivity study on the number of fasteners used and their impact on the behavior of an electrical cabinet. Only the benchmark cabinet models are used in this study so that all limit states of the cabinets can be captured. Three different screw layouts are taken as the independent variables as follows: 1) PL 1, 2) PL 2, and 3) PL 3 (see Figure 4.20). The PL 1 layout consists of four screws located at each of the four corners of each panel (see Figure 4.20.a). In the PL 2 layout, another pair of screws are located at the midspan of each vertical edge of each panel (Figure 4.20.b). Lastly in the PL 3 layout, two pairs of screws are placed on the vertical edges of panels between the top and bottom corner points to divide the edges into three equal-length sections (Figure 4.20.c). Pushover analyses in the side-to-side (SS) and the front-back (FB) directions were conducted for each configuration by excluding (1^{st} order) and including (2^{nd} order) the geometric nonlinear effect.

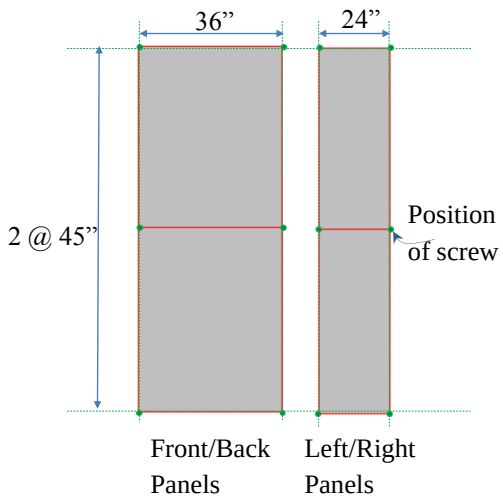

(a) PL 1

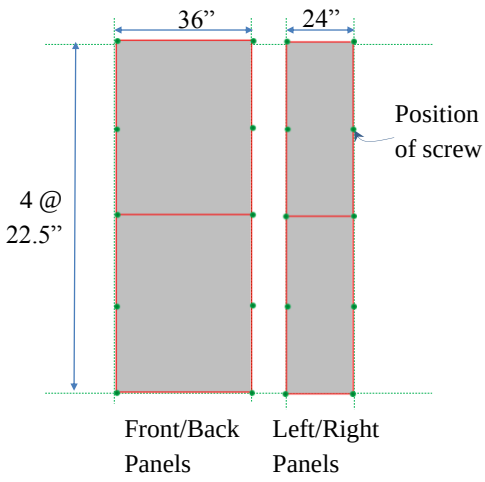

(b) PL 2

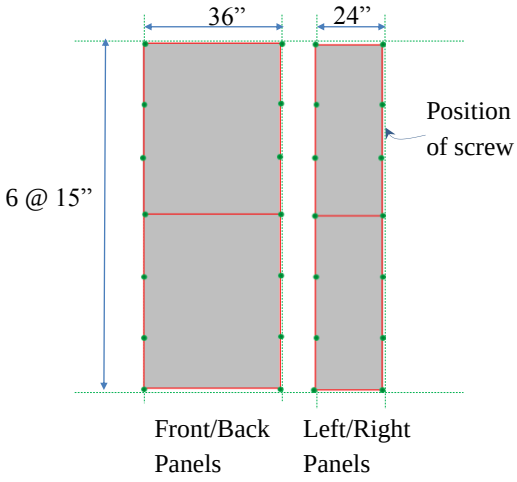

(c) PL 3

Figure 4.20 Three screw layouts considered in this study

The first order pushover curves in the SS and FB directions are shown in Figure 4.21. Overall, increasing the number of fastener along the vertical edges of the cabinets increases the stiffness and the capacity of the cabinets. In the SS direction, the limit state of the cabinet is the shear failure of the screw connections. At the same time, the behavior of the cabinet is linear in the FB direction.

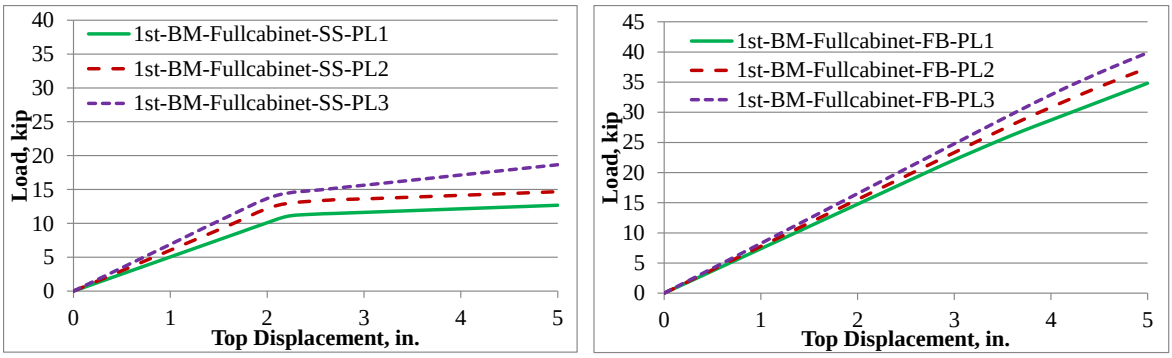

(a) Side-to-side (SS) direction (b) Front-back (FB) direction

Figure 4.21 First order pushover curves for the cabinet with different screw layout

In the second order analyses, as discussed in Section 4.3.2, the significant limit states of the cabinet model with the PL 1 layout pushed in the SS direction are associated with the buckling of the panel and the tension failure of the screw connection. Increasing the number of fasteners on the vertical edges of the cabinet leads to increased overall stiffness and capacity of the electrical cabinet without changing the limit states (see Figure 4.22.a). The cabinet panels will buckle before the screw connections fail due to tensile force. Although the screw connections still fail under the tensile force, it appears that force redistribution due to the additional screws prevents the stiffness drop of the cabinet observed in the PL 1 model. If the capacity of the cabinet is defined as the load level where the first screw connection fails, reducing the vertical distance between the screws increases the capacity (see Figure 4.22.b) of the cabinet. Adding one screw between the corners screws in the original configuration (PL 1) increases the capacity of the cabinet by 50%, and if two additional screws are added between the corners screws, the capacity of the cabinet increases by 66%.

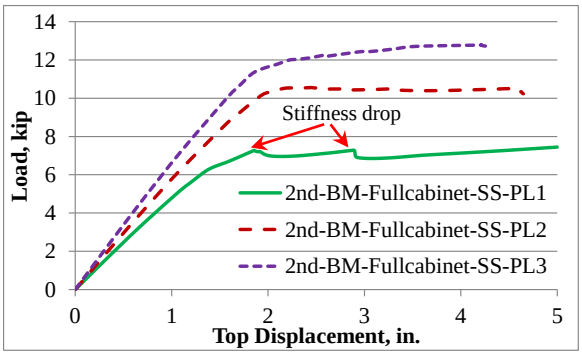

(a) 2nd order pushover curves of the cabinet

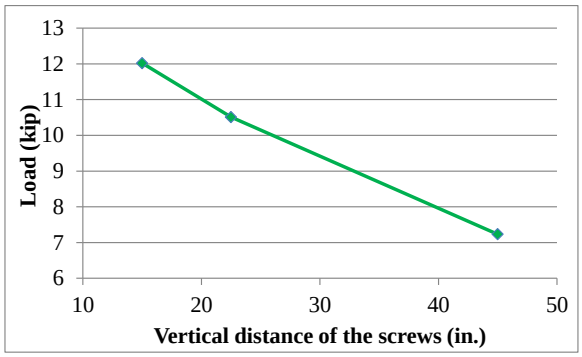

(b) Relation between the capacity of the cabinet and the vertical distance of the screws

Figure 4.22 Effect of different screw layout to the behavior of cabinet pushed in the SS direction

The 2nd order pushover curves of the cabinet in the negative and positive FB directions are shown in Figure 4.23. Overall, increasing the number of screws along the edges of the panels increases the stiffness of the cabinet. The limit states of the cabinet are associated with local buckling of the vertical posts, buckling of the side panels, and global buckling of the vertical posts. The additional screws provide added restraint to the vertical posts. Thus, the vertical posts buckle over a shorter buckling length (see Figure 4.24).

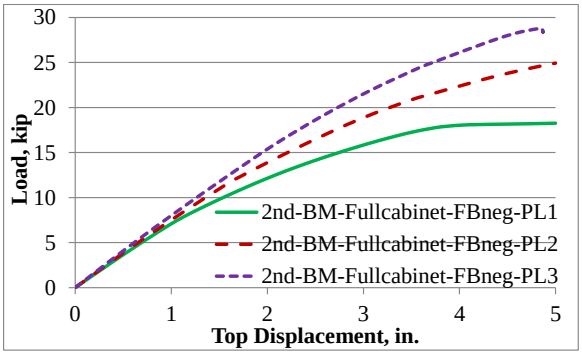

(a) Negative front-back (FBneg)direction

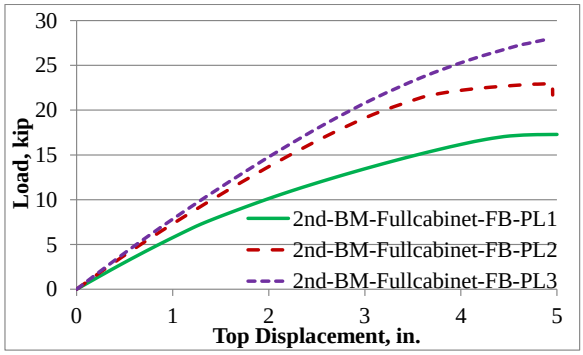

(b) Front-back (FB) direction

Figure 4.23 Second order pushover curves of the cabinet with different screw layout

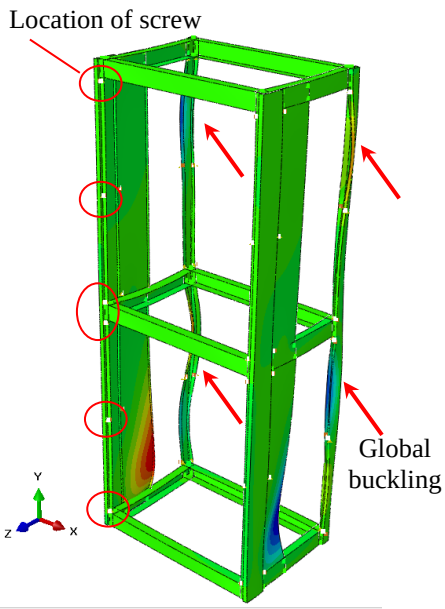

a) PL 2 pushed in the –Z (FBneg) direction

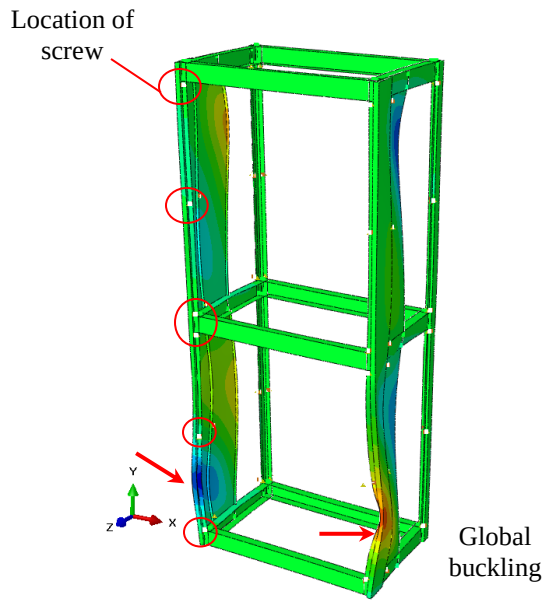

b) PL 2 pushed in the +Z (FB) direction

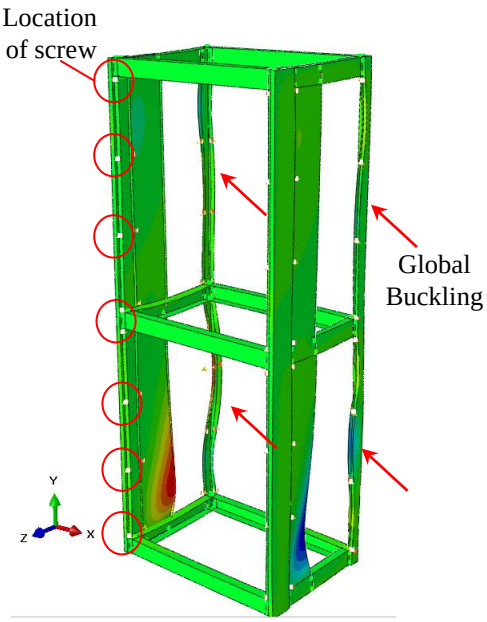

c) PL 3 pushed in the –Z (FBneg) direction

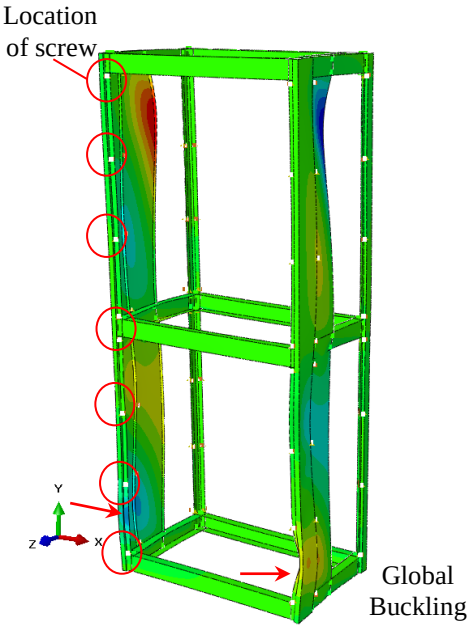

d) PL 3 pushed in the +Z (FB) direction.

Figure 4.24 Effect of the additional screws to the flexural torsional buckling of the vertical posts; contour showing the deformation of cabinet in the X direction.

4.4.3 Effect of Multiple Front Panels on the Behavior of the Electrical Switchboard Cabinet

In a more realistic case, the number of front panels in this class of electrical switchboard cabinet is usually greater than two. The results of an investigation of the

effect of multiple front panels on the behavior of electrical switchboard cabinet are presented in this section. In this study, two layouts (PL 4 and PL 6) are considered in addition to the PL 1 layout (see Figure 4.20.a). Four front panels having the same dimensions are used in the PL 4 layout (see Figure 4.25.a). Then, six front panels are used in the PL 6 layout as shown in Figure 4.25.b. Each panel is connected to the cabinet by four screws attached at its four corners. Static pushover analyses in the side-to-side (SS) direction were conducted to investigate cabinet behavior by excluding (1st order) and including (2nd order) the geometric nonlinear effect.

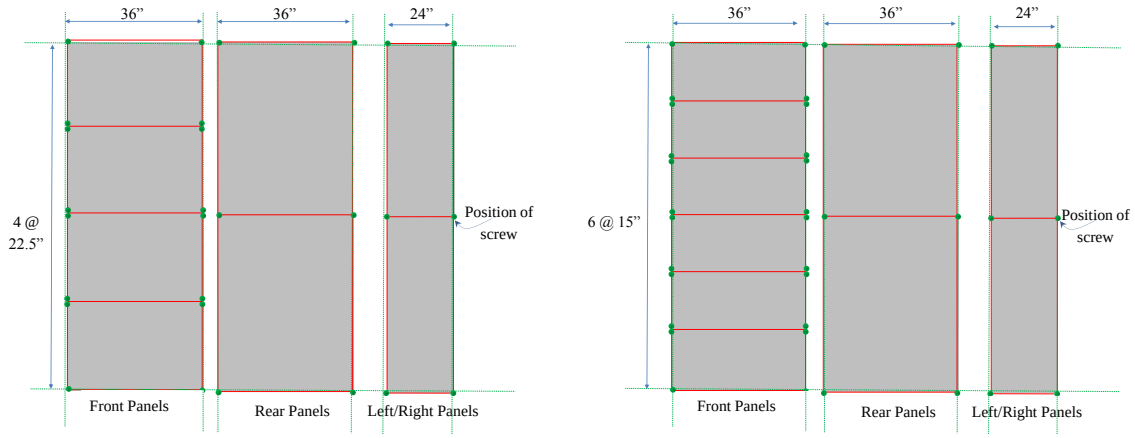

(a) PL 4 layout (b) PL 6 layout

Figure 4.25 Additional layouts of the front panels considered in this study

The pushover curves of the cabinet model with PL 1, PL 4, and PL 6 layouts under first order analyses are presented in Figure 4.26.a. In general, additional front panels reduce the stiffness of the cabinet. This finding contradicts the finding discussed above concerning the behavior of the cabinet with two front panels and multiple screws (PL 2 and PL 3). One explanation of this behavior is the increase of flexibility of the vertical posts due to the fact that more forces are transferred from the shear interaction of the front panels. This phenomena is also observed in the behavior of reinforced concrete framing system infilled with slit masonry walls (Jiang et al., 2015). The slit in the masonry walls produces lower rigidity but higher ductility for the overall system. For both PL 4 and PL 6 layouts, the first stiffness reduction is caused by the shear failure of

the screw at the back panel. Meanwhile, the second stiffness reduction is caused by the shear failure of the screw at the front panel. In the second order analyses, additional front panels tend to reduce both the initial stiffness of the cabinet and the panel buckling load of the cabinet. The first stiffness reduction is caused by buckling of back panels followed by tensile failure of back screw connections. Afterwards, the screws at the front panels of cabinet models with PL 4 and PL 6 layouts fail under tensile or shear force and the front panels eventually buckle. If the capacity of the cabinet is defined as the limit load of front screws, additional front panels tend to increase the capacity of the cabinet. However, if the capacity of the cabinet is defined as the buckling load of back panels, additional front panels tend to reduce capacity

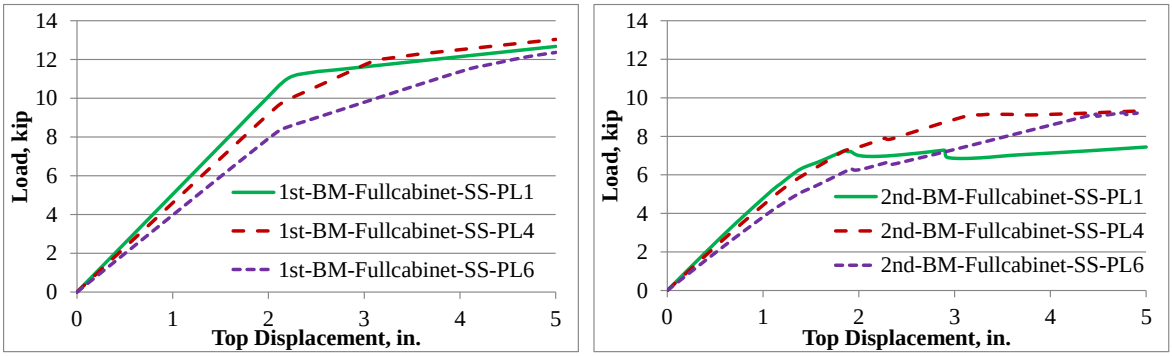

(a) First order analysis (b) Second order analysis

Figure 4.26 Effects of the multiple front panels to the pushover curves of the cabinet in the side-to-side direction

CHAPTER 5

APPLICATION OF THE SIMPLIFIED CABINET MODELS IN FREQUENCY RESPONSE ANALYSIS

In the two previous chapters a method to generate simplified finite element models for two configurations of electrical switchboard cabinets has been proposed and validated statically to the corresponding benchmark cabinet models. In practical application, dynamic characteristics and behaviors of electrical cabinets are often needed in their seismic evaluation process. To obtain this information two of the most common types of analyses are the frequency response analysis and time history analysis. Chapters 5 and 6 discuss how the simplified cabinet models can be used in the frequency response analysis and the time history analysis, respectively. Chapter 5 also presents: 1) methods proposed to incorporate the mass of electrical devices into the structural model and selection of the damping model for the analysis, and 2) results of sensitivity study on distribution of electrical devices (e.g. busbars, main circuit breaker, and meter devices) inside the cabinet using the frequency response analysis. These results provide useful information to determine the distribution of electrical devices hosted in a cabinet assembly analyzed in Chapter 6. It is noted that the simplified cabinet models are not validated to the corresponding benchmark cabinet models in these dynamic analyses. Therefore, future work to validate the results of the simplified cabinet models to the corresponding benchmark cabinet models or even experimental tests may be needed.

5.1 Description of the Electrical Cabinet Configurations

5.1.1 Structural Configurations

The class of the cabinet selected for this study is similar to the class II configuration discussed in Chapter 4. Therefore, all structural components of the cabinets

(framing members, unfolded panels, and connections) are constructed from the same cross sections and configurations shown in Figure 5.1.

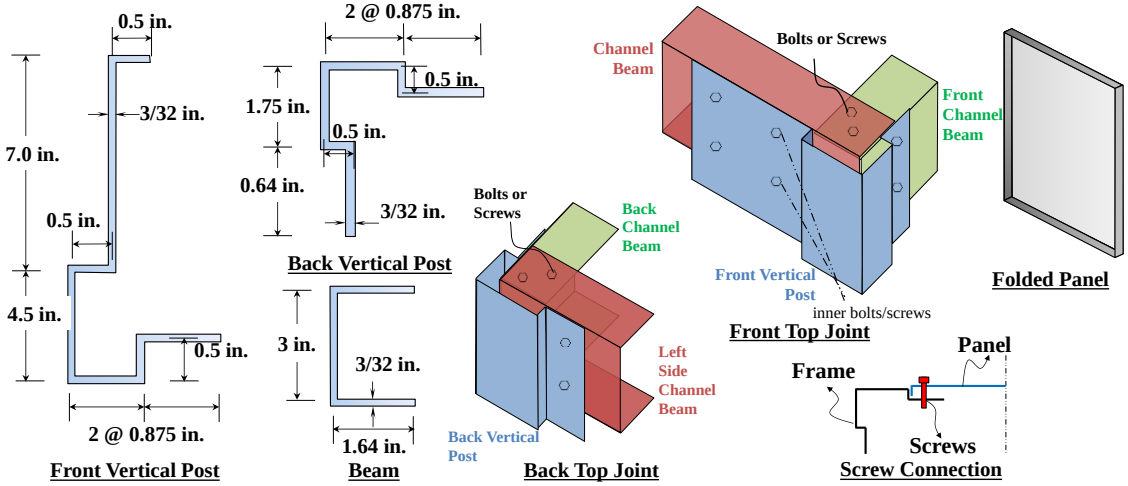

Figure 5.1 Cross sections and configurations of the structural components

Five main features, that differentiate the cabinet considered in this chapter and the cabinet discussed in the previous chapter, are:

- The width, depth and height of the current cabinet are 30 in., 36 in., and 90 in., respectively
- The cabinet is fixed at the four bottom corners of the cabinet and at the mid-span of the base channel beam along the depth of cabinet (see Figure 5.2.a)
- There is no horizontal channel beams at mid-height of the cabinet
- Vertical intermediate members (L-1.75 in. x 1.25 in. x 3/32in.) are located on the left and right sides of the cabinet, and they are connected to the base channel using 4 screws arranged symmetrically (see Figure 5.2.a)
- Electrical devices (busbars, main circuit breakers, and meter devices) are included in the computational model

Figure 5.2.b shows the overall configurations of the cabinet together with the busbars attached on the vertical intermediate posts of the cabinet.

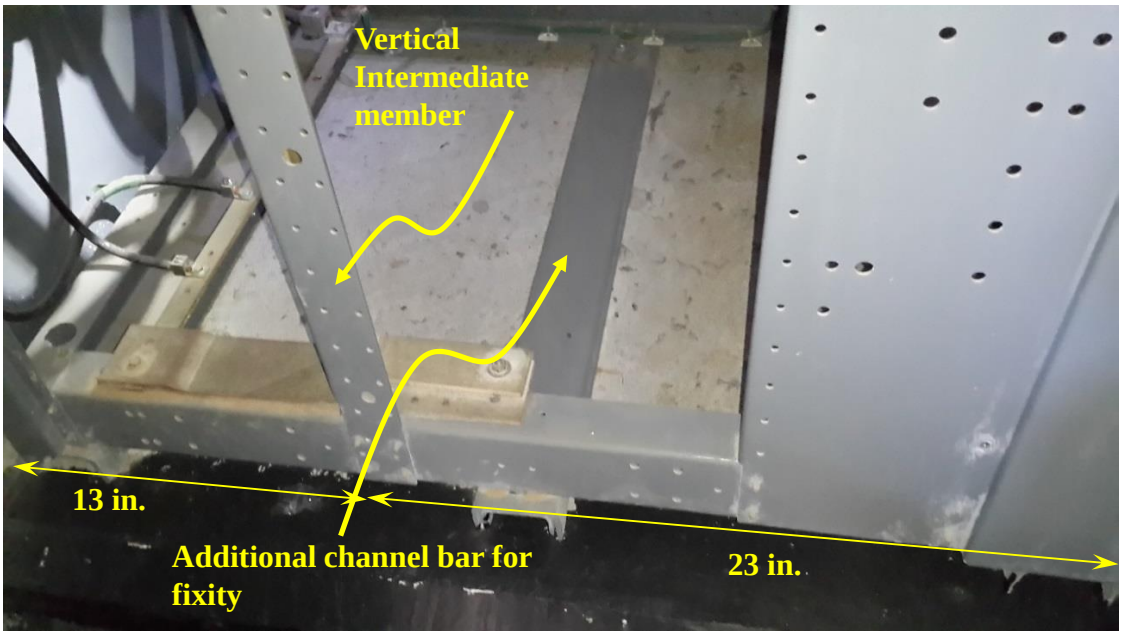

(a) Photo of cabinet showing additional fixity at the base, connections between intermediate post and base channel, and front vertical post.

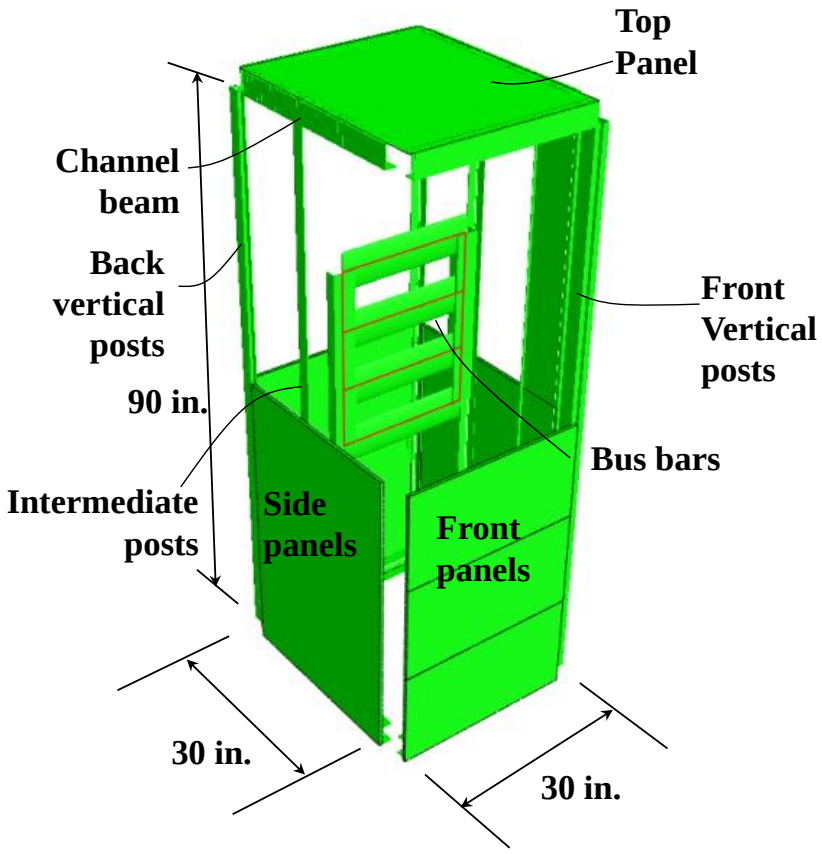

(b) Structural geometry of cabinet with busbars attached to vertical intermediate posts (top back, left, right, and several front panels are intentionally removed for clarity)

Figure 5.2 The geometric model of the cabinet and internal busbars.

5.1.2 Distribution of the Electrical Devices.

In practice the electrical devices mounted inside electrical cabinets are scattered and the type and size of the electrical devices such as busbars, main circuit breakers, meters, relays, and current transformers (CT) are highly varied. For this study, four busbars, a main circuit breaker and three meter devices are considered for this study because they are expected to have a significant effect on the dynamic behavior of the electrical cabinet due to their mass, distribution and location. This judgement is made based on specific electrical switchboard cabinets observed during site visits at the Sustainable Education Building at Georgia Tech. This should not be used to generalize the distribution or characteristics of the same devices in other classes of cabinets or even similar devices in any electrical cabinet.

Busbars are usually arranged horizontally or vertically in a group and are made of copper. For this study, only busbars running horizontally across the width of the cabinet are considered. Generally such busbars would be spliced to busbars in side-by-side cabinets and connections to circuit breakers within the cabinet might exist, but these are not included in this model. These horizontal busbars are usually attached to insulation bars which in turn are connected to the framing system. Four attachment points between the insulation bars and the framing system are provided through “rigid” steel brackets (Z shape) using a single bolt at each attachment point. These busbars are typically attached to the back or intermediate vertical posts, respectively. For this study, the busbar assembly is located at the mid-depth of the cabinet (see Figure 5.3)

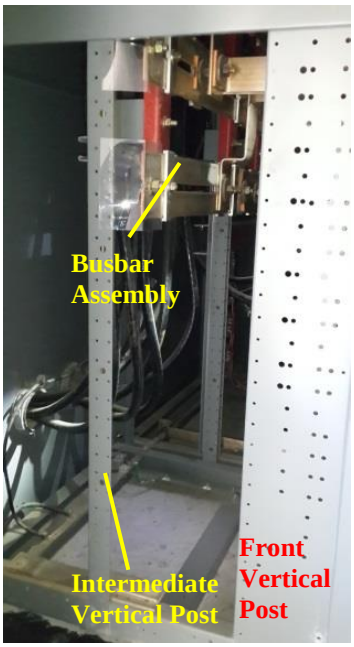

(a) Photo of the busbar assembly located at the mid-depth of the cabinet

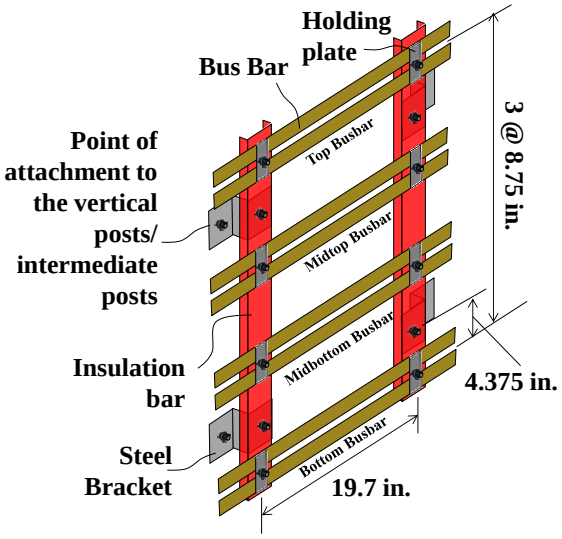

(b)3D sketch of the busbar assembly

Figure 5.3 Configurations of busbar assembly considered in this study

A single main circuit breaker is located at the front of the cabinet and attached to the front vertical posts through two channel beams and a folded steel plate using screws (see Figure 5.4). The assumed height, width, and depth of the breaker are 11.84 in., 7.48 in., and 6.75 in., respectively. In addition, the weight of the main circuit breaker considered in this study is 25 lb, and the location of the center of gravity is shown in Figure 5.4.d.

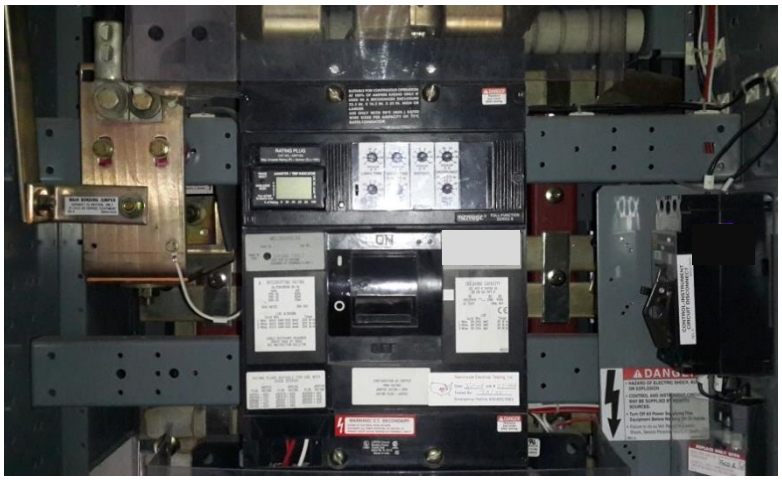

(a) Front view of the circuit breaker

(b) Side view

(c) Screw connection between the horizontal channel beams and the front vertical posts

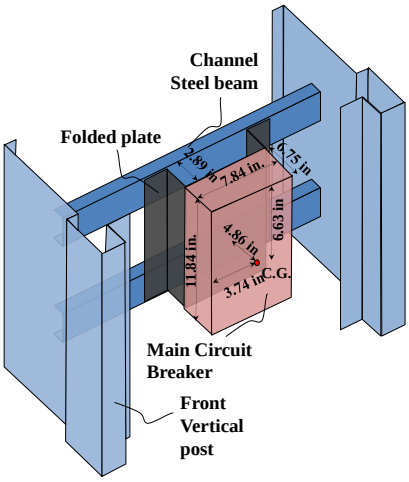

(d) 3D sketch of the main circuit breaker

Figure 5.4 Details of the geometric and structural configuration of the cabinet internal electrical devices.

Meter devices are usually distributed over the front panels of the cabinet in various patterns (see Figure 5.5.a). Figure 5.5.b. shows details of the attachment of a single meter device to a front panel. The meter mounts to side rails that are cantilevered from a bezel affixed to the front panel, and a screw on each side are used to retain the slide. The weight of the device is 3.97 lb, and the height, width, and the depth of the device are 3.8 in., 3.8 in., and 6.4 in., respectively. For this study, three meter devices symmetrically arranged in a row across a front panel are considered.

(a) Meter devices located on the front panels

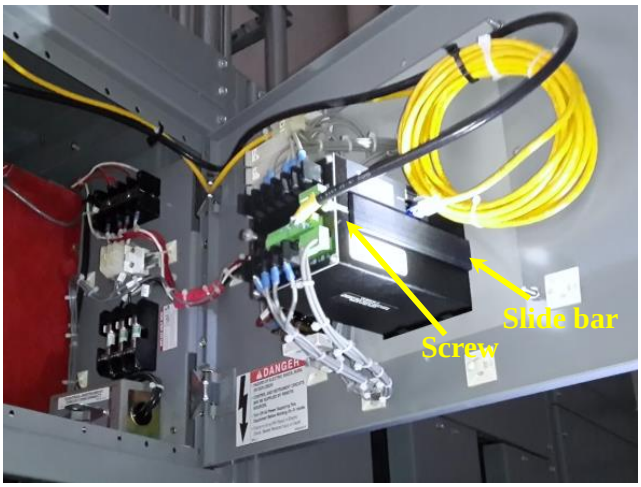

(b) Attachment details

Figure 5.5 Photos of typical meter devices mounted in front panels of an electrical switchboard.

5.2 Modeling and Analysis Strategies

5.2.1 Modeling Strategies

The structural components of the electrical cabinet are modeled using the proposed method to generate the simplified model of the cabinet. The framing members are modeled using Timoshenko beam elements and the panels are modeled using shell elements. At the same time, the connection between the framing members themselves and between the panels and framing members are modeled using combination of springs and constraint equations as described in Chapter 4. In addition, the intermediate vertical posts are modeled using Timoshenko beam elements and their connection to the base and top channel beams are assumed to be rigid. Finally, the cabinet base is fixed at six locations: four at the corners and two at the mid-span of the channel beam along the side edges (see cross signs in Figure 5.6).

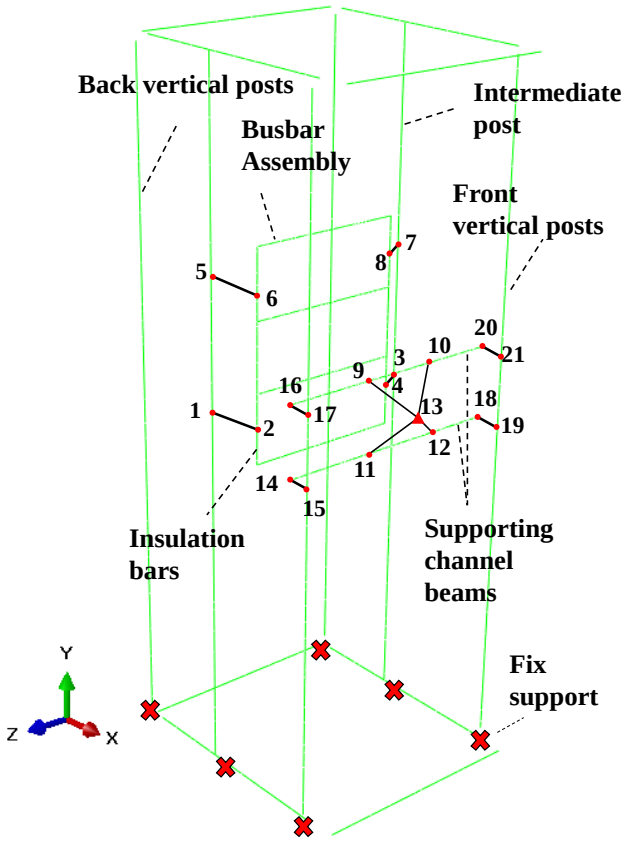

Figure 5.6 Detailed assignments of boundary conditions, attachments between busbars and intermediate posts, attachments between the center gravity of the main circuit breaker with the supporting channel beams, and attachments of the supporting channel beams to front vertical posts.

The busbars are modeled using Timoshenko beam elements with cross sectional properties and mass density (ρ_{copper} = 8.394 x 10^{-7} kip-s^2/in^2) directly inputted into ABAQUS. Similarly, the insulation bars are modeled using Timoshenko beam model with cross sectional properties and mass calculated automatically by ABAQUS from the input cross sectional dimensions and mass density ($\rho_{insulation}$ = 1.684 x 10^{-7} kip-s^2/in^2). The busbars are assumed to be pin-connected to the insulation bars. In addition, the whole busbar assembly (together with the insulation bars) is connected to the intermediate posts at four attachment points using CONNECTOR, BEAM feature in ABAQUS (see 1-2, 3-4, 5-6, and 7-8 in Figure 5.6). This feature rigidly constrains all DOFs of the connecting nodes. Releasing the rotational DOF constraints will introduce a

local singularity to the model due to a rigid body rotation of the assembly of busbars about the vertical axis of the cabinet.

The main circuit breaker is modeled as a lumped mass at its center of gravity (see joint 13 in Figure 5.6). Four rigid beam connectors (see 9-13, 10-13, 11-13, and 12-13 in Figure 5.6) are then used to connect the center of gravity to the two supporting channel beams. The supporting beams are modeled using Timoshenko beam elements and are attached to the centroid of the vertical posts using equations that provide rigid beam and warping kinematic constraints to the connecting nodes (see 14-15, 16-17, 18-19, 20-21 in Figure 5.6). These equations are written in the same way as the one describe for the panel-frame connection (see Section 3.4).

Figure 5.7 shows the location of meter devices in a front panel. The meter devices are represented as "rigid" shell elements (E_{meter} = 10 E_{steel}) that have density value obtained from the ratio of the mass of the device to the volume of the shell elements occupied by the device. This decision is made based on the assumption that the meter device is relatively rigid compared to the surrounding thin steel panels and thus has a stiffening effect to the panel. The fact that large portion of a meter device is located at the back of the front panels introduces an eccentricity between the center of mass and the front panels. This eccentricity introduces inertial forces and moments into the panel. Hence, a more realistic model is to represent the mass of the meter device as a lumped mass at its center of mass, and rigidly connect the nodes of the shell elements within the area of the meter device to the center of mass. Further investigations on this modeling technique are needed in the future contingent on the availability of more detailed geometrical and material data for these devices.

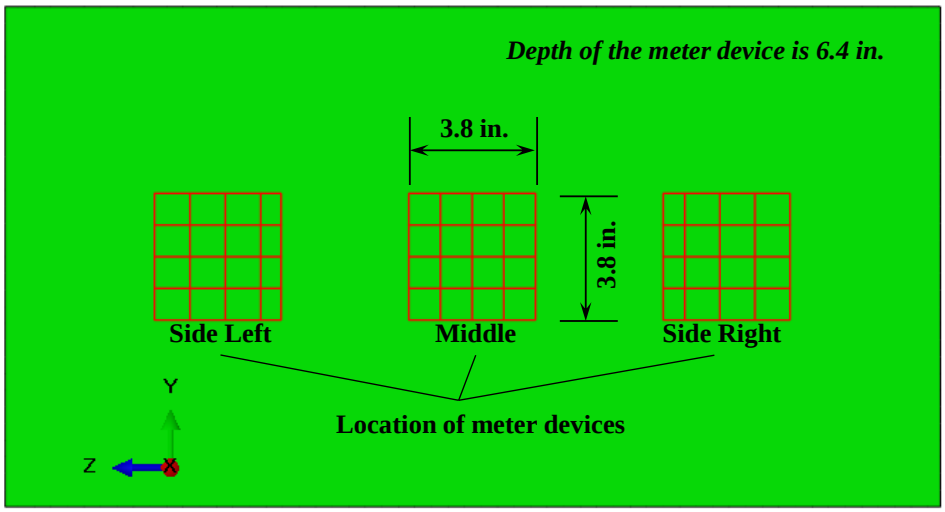

Figure 5.7 Location of meter devices in a front panel

5.2.2 Analysis Strategies

Frequency Response Analysis

There are many parameters including natural frequencies and response functions that can be used to identify the dynamic characteristics of a structure. Due to its simplicity eigen-frequency analysis is the most common method used to obtain the natural frequencies of a structure. In this method, the linear stiffness and mass matrices of the structural model are assembled to form a system of linear equations. The eigenvalues and eigenvectors of the system of equations are then calculated. The mode shapes and natural frequencies of the structure correspond to the eigenvectors and the square root of the eigenvalues, respectively. Damping is not included but can be assigned to each mode (i.e., modal damping).

Another method to obtain the natural frequencies of a structure is through computational frequency response analysis. This method requires the structure to be subjected to a constant low-magnitude sinusoidal ground excitation in a specific direction and with varying forcing frequency. This method provides information related to the natural frequencies and the response function of the structure. In addition, this method

enables incorporation of damping to the structure that can impact the magnitude of the response function and may slightly alter the natural frequencies of the structure. Unlike the eigen-frequency analysis that gives all natural frequencies of the linearized structure, the frequency response analysis will give only the natural frequencies for the mode shapes corresponding to the direction of the applied ground excitation. This method is very similar to the sine-sweep test employed in experimental structural dynamic studies, and such tests are sometimes conducted on an electrical switchboard cabinet to find its natural frequencies.

Due to its similarity to the experimental sine-sweep test, a computational frequency response analysis is applied in this study through the STEADY STATE DYNAMICS, DIRECT command in ABAQUS. The command performs a direct-solution steady state dynamic analysis procedure in ABAQUS. This analysis is used to calculate the steady-state dynamic linearized response of a system to harmonic excitation. The response is directly calculated in terms of the physical degree of freedom of the model represented by its stiffness, mass and damping matrix.

In this analysis, the cabinet models are subjected to a constant low magnitude (0.05 g) sinusoidal base acceleration with varying forcing frequencies (1- 70 Hz) in two orthogonal translational directions. This analysis provides information related to the natural frequencies and the response function of the cabinet. The natural frequencies of the cabinet are determined based on the receptance plot of the top story drift of the cabinet, and the response function (accelerance) plot is calculated based on the acceleration response of the electrical devices or their attachment points.

Theoretically, the response function plots will be unbounded if damping is not introduced to the model. Therefore, damping needs to be included in the numerical model to represent a more realistic behavior. There are many damping models (e.g. Rayleigh, rate-independent) that can be incorporated into the numerical analysis, and for this study, rate-independent (also called structural) damping is selected because it assigns the same

damping ratios to all forcing frequencies in steady state analysis. Hence, there is a fair comparison for the maximum accelerance. Djordjevic and O'Sullivan (Djordjevic and O'Sullivan, 1995) proposed several viscous damping ratio values (3% - 4%) as part of an EPRI guideline for the development of in-cabinet seismic demand for devices mounted in electrical cabinets. These damping ratio values were obtained based on in-situ modal testing data of 57 cabinets as well as engineering judgements. These values are categorized based on the fundamental frequency of the cabinet (4% for 9.5 – 13 Hz, 3.5% for 13 – 20 Hz, and 3% for 13 – 20 Hz). The low damping value that is associated with welded local plate modes is assigned to the higher fundamental frequency range because it has been observed in the testing that more local modes are observed in the cabinets with fundamental frequency located in those ranges.

A structural damping ratio of 3.5% is selected for the investigation presented in this chapter based on engineering judgement and preliminary observations of the fundamental frequencies and higher local modes of the simplified cabinet models without damping. This damping ratio corresponds to a loss factor of 7%. Ideally, the damping ratio of the cabinet should be found through experimental modal identification testing of the cabinet. One caveat to this type of test is that it cannot be used to qualify the electrical devices or the cabinet based on the AC 156 guideline (AC-156, 2010); instead, response of the cabinet to multi-frequency random excitation is required for that purpose.

Sensitivity Study of the Maximum Accelerance of Electrical Devices or their Attachment Points to the Vertical Distribution of the Devices Inside the Cabinet.

The frequency response analysis discussed in the previous section is utilized to provide information on how the electrical devices (busbars, main circuit breaker, and meter devices) should be distributed inside the electrical cabinet. This information is useful to determine the distribution of the electrical devices inside the cabinet assembly model discussed in Chapter 6. As it is discussed in Section 5.1.2, the distribution of

electrical devices is usually scattered although some devices (specifically the devices considered in this study) may have a pattern, such as: 1) busbars are located at the back or middle of the cabinet, 2) main circuit breaker are attached on the front vertical posts, and 3) meter devices are attached on the front panels. It should be noted that these patterns are found in specific electrical devices hosted in a class of electrical cabinets investigated during the site visits. Therefore, no generalization should be made on the distribution of the devices in other class of cabinets or even any similar devices in any class of cabinets. Further data inventories and judgments are needed to possibly identify some patterns for broader class and application of electrical devices.

Three mass arrangements are selected as the independent variables in this study based on the patterns discussed above:

1) Location of the busbars is varied along the height of the cabinet,
2) Location of the main circuit breaker is varied along the height of the cabinet while the busbars are held at the mid-height of the cabinet, and
3) Location of the meter devices is varied along the height of the cabinets while the busbars are held at the mid-height of the cabinet.

Busbars are included in the second and third variables cases because they have been observed in most single cabinets during site visits. The next section will present the results obtained for each independent variable.

5.3 Effect of the Busbars Locations

A single assembly of four horizontal copper busbars on 8.75 in. centers is considered in this study. Four height levels of the busbar assembly are considered in this study. The height of the bottom attachment joints (see 1-2 and 3-4 in Figure 5.6) is utilized to label these levels: 1) 145 for 14.5 in., 2) 290 for 29.0 in., 3) 435 for 43.5 in., and 4) 580 for 58.0 in. Figure 5.9.a. and b. show receptanace plots of the story drift in the front-back (FB) and side-to-side (SS) directions. The location of the busbar assembly

changes the magnitude of the receptance, especially in the higher natural frequencies in the FB direction. However, it does not significantly change the natural frequencies of the cabinet because the busbars are located at the intermediate posts that are not the main lateral load bearing components. Therefore, its contribution to the stiffness of the cabinet is negligible.

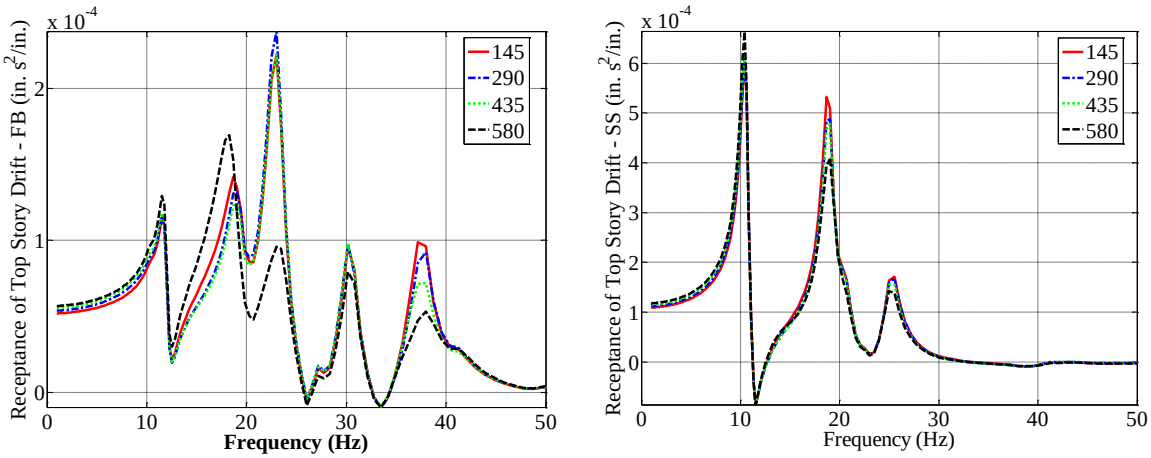

(a) Front-back (FB) direction (b) Side-to-side (SS) direction

Figure 5.8 Receptance of top story drift for different busbar locations

Accelerances are then calculated at the midpoint of each busbar in the busbar assembly for each different level. The maximum accelerance and the frequency at which it occurs are recorded. The plots of the maximum accelerance at the midspan of each busbar versus the height ratio of each busbar for the frequency response analysis in the front-back (FB) and the side-to-side (SS) directions are shown in Figure 5.9.a and b. The height ratio of each busbar is calculated by normalizing the distance between the base of cabinet and the midpoints of each busbar (measurement points) to the total height of cabinet. Each dot style in the plots represents a different position (top, midtop, midbottom, or bottom, see Figure 5.3) of the busbar within the busbar assembly. The level of each busbar assembly is identified using the labels 145, 290, 435 and 580 as described in the previous paragraph.

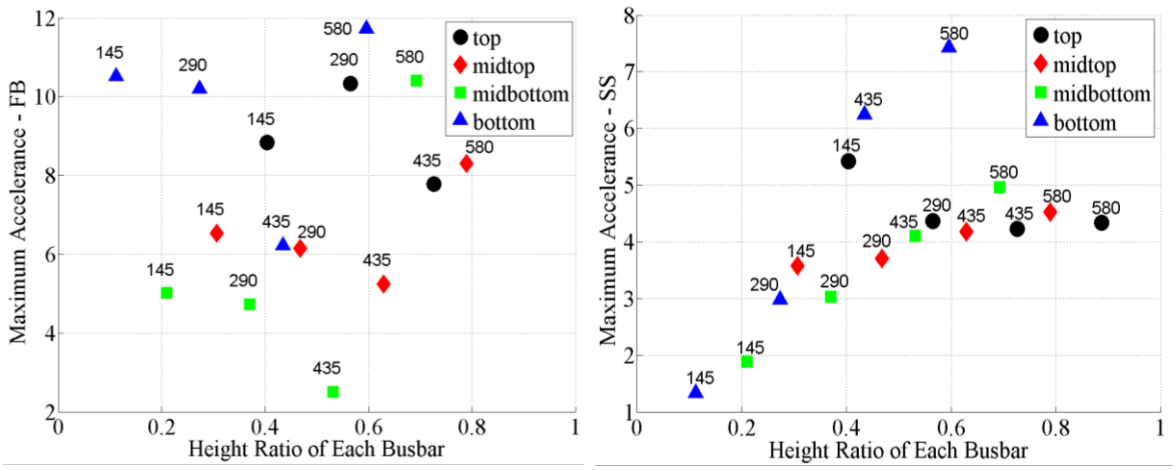

(a) Front-back (FB) direction (b) Side-to-side (SS) direction

Figure 5.9 Busbars - Plot of the maximum accelerance for steady-state analysis

In the FB direction, the plot of the maximum accelerance to the height ratio of each busbar is scattered due to different behavior of each busbar at different frequencies. If the busbars within each assembly are observed, the bottom and the top busbars have larger maximum accelerance than the midtop and midbottom busbars. If busbar in each position (top, midtop, midbottom, or bottom) is observed as the location of busbar assembly increases, the maximum accelerance will decrease up to level 435 then will increase at level 580. To further explain these results, the maximum accelerance plot of busbar assembly at level 145 is investigated (see Figure 5.10).

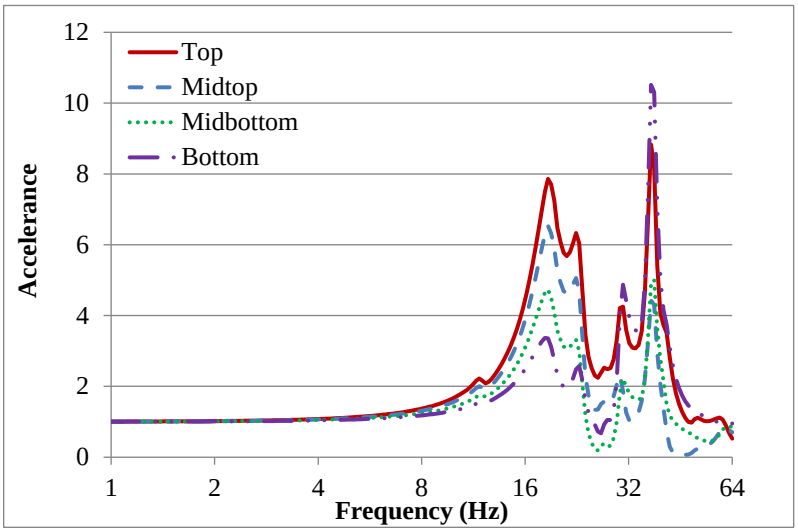

Figure 5.10 Accelerance plot of frequency response analysis in the FB direction with the busbars assembly at level 145

In this plot, two significant frequencies (18.65 Hz and 37.17Hz) exist in all busbar positions. In the first frequency (18.65 Hz), the accelerance of each busbar increases with its height in the assembly. This result seems reasonable since the accelerance usually increases with height in such a cantilevered structure. However at the second frequency (37.17 Hz), the top and bottom busbars have larger accelerances than the midtop and midbottom busbars, and further investigation of the cabinet model has shown that this behavior is caused by the local deformations of the top and bottom busbars that are significantly larger than the midtop and midbottom busbars (see Figure 5.11). These behaviors are also observed in the busbar assembly located at level 580. At the same time for the busbar assembly located at levels 290 and 435, two significant frequencies that are closely spaced (37.17 in. and 37.96 in.) characterize the accelerance plot of the busbar in each position, and the accelerance at the top and bottom busbars are higher than the midtop and midbottom busbars for both frequencies (similar to the second frequency in the busbar arrangements at levels 145 and 580).

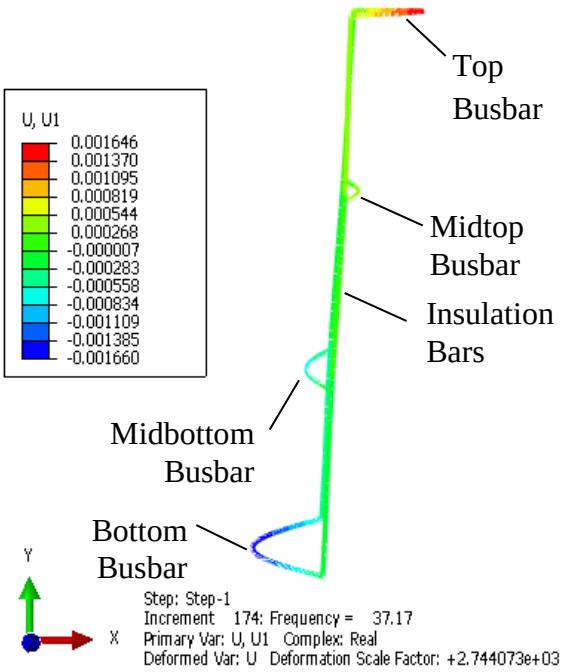

Figure 5.11 Local deformation of the busbars in the second significant frequency for busbar assembly located at level 145 (contour showing the deformation in the X direction, and all other framing members and panels are intentionally removed for clarity)

In the SS direction, the maximum accelerance tends to increase as the position of the busbars in the busbar assembly increases; except for the busbar assembly located at levels 435 and 580, the maximum accelerance tends to decrease as the position of a busbar in the assembly increases. These behaviors can be explained further by observing the accelerance plot of the busbar assembly located at levels 145 and 435 below.

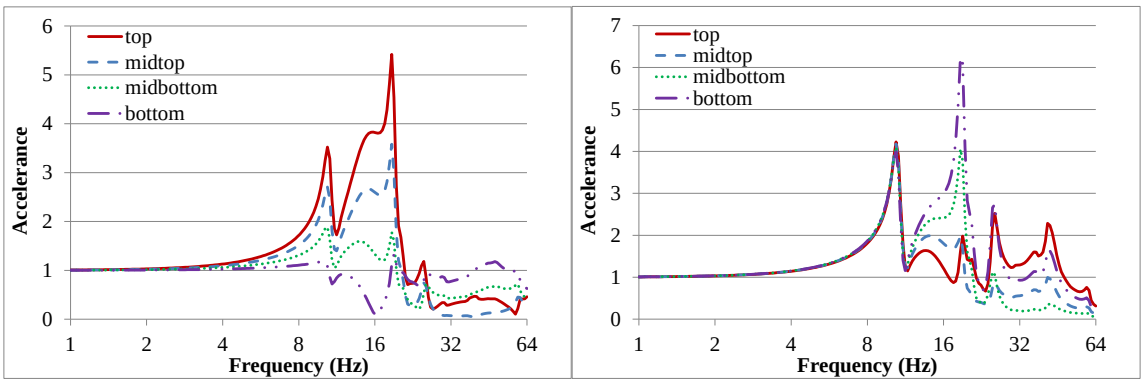

(a) Level 145 (b) Level 435

Figure 5.12 Accelerance plot of frequency response analysis in the SS direction for two different assembly heights

The accelerance of the busbar assembly located at level 145 is characterized by two significant frequencies (10.61Hz and 19.04 Hz). For both frequencies, the maximum accelerance tends to increase as the position of the busbar within the assembly increases. In most cases, the accelerance of the second frequency is larger than the first frequency; except for the midtop and midbottom busbars, the accelerance of the first frequency is slightly larger than the second frequency. Similar to the accelerance plot of the busbar assembly located at level 145, the accelerance of the busbar assembly located at level 435 can be characterized by two significant frequencies (10.61 Hz and 18.65 Hz) as well. The accelerance of the first frequency is larger than the second frequency; except for the bottom busbar, the accelerance of the second frequency is larger. Local flexural deformation of the busbar at the measured location may explain why the accelerance at one frequency is larger than the other one.

Figure 5.13 shows the frequencies at which the maximum accelerance occurred. In the FB direction, the maximum accelerance is distributed at the second and the fifth natural frequencies of the cabinets. At the same time in the SS direction, the maximum accelerance is distributed at the first and the second natural frequencies. Based on these results, higher order modes of the cabinet are important in analyses related to the busbars in the cabinet.

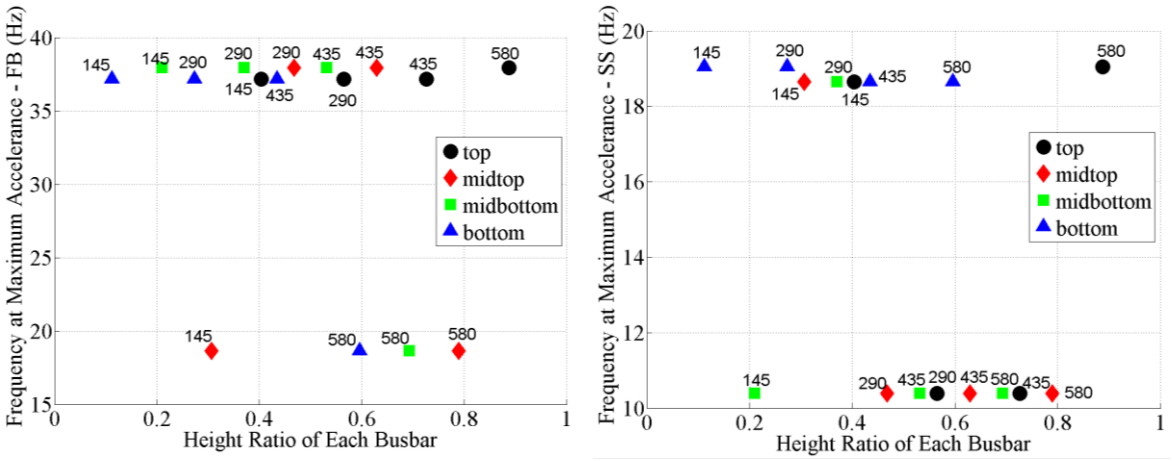

(a) Front-back (FB) direction (b) Side-to-side (SS) direction

Figure 5.13 Busbars - Plot of the frequency at which the maximum accelerance occurs for steady-state analysis.

5.4 Effect of Main Circuit Breaker Location

Four height variations of the main circuit breaker are also considered in this study. These height variations correspond to the height of the bottom attachment point between the bottom supporting channel beam and the front vertical posts (see 14-15 and 18-19 in Figure 5.6), and these heights are labeled as levels 145, 295, 425 and 595 to indicate their location at 14.5 in., 29.5 in., 42.5 in. and 59.5 in., respectively.

The variation in location of the main circuit breaker along the height of the cabinet slightly alters the higher natural frequencies of the cabinet as shown in Figure 5.14.a and b. At the same time, the fundamental frequency is relatively insensitive to the variation in the location of main circuit breaker. Although the supporting channel beams

for the circuit breaker are attached to the front vertical posts, their overall contribution to the rigidity of the cabinet is small.

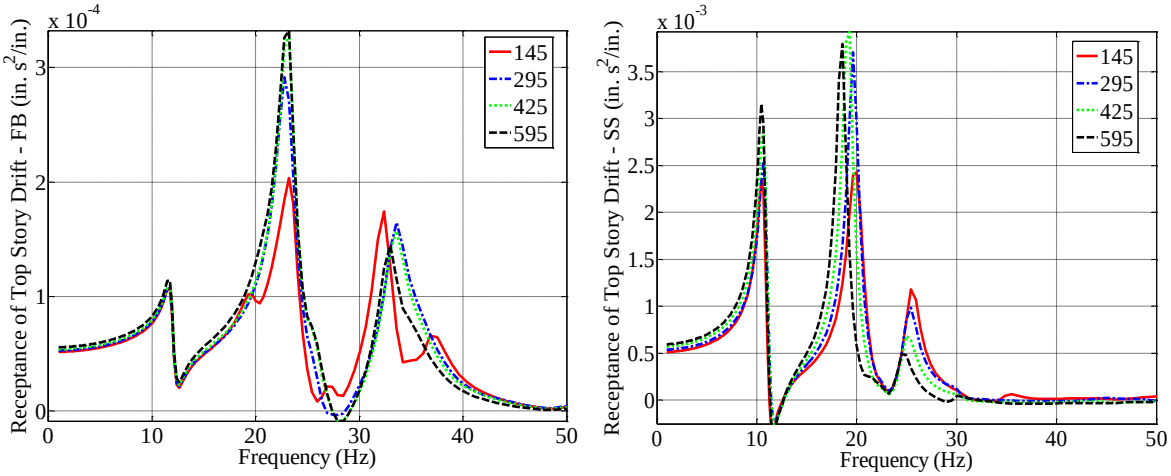

(a) Front-back (FB) direction (b) Side-to-side (SS) direction

Figure 5.14 Top story drift receptance as a function of main circuit breaker location

The acceleration at the points of attachment (see joints 9, 10, 11, and 12 in Figure 5.6) between the center of gravity of the circuit breaker and the supporting channel beams is measured. These joints are selected because they are critical in maintaining the integrity of the circuit breaker with the cabinet. Another possible point of measurement is at the center of mass of the circuit breaker. This point may be useful if the vibration sensitivity of electrical component inside the circuit breaker is of interest in future investigations. These measurement points (9, 10, 11 and 12) are respectively labeled as the top left, top right, bottom left and bottom right in the plots of the maximum accelerance of the attachment points against the height ratio of each attachment point as shown in Figure 5.15. The height ratio of each attachment point is defined as the height of each attachment point over the total height of the cabinet. In both FB and SS directions, the maximum accelerance tends to increase as the level of the circuit breaker increases. This behavior is similar to the behavior of a building structure in which the floor acceleration typically increases as the height of the floor increases.

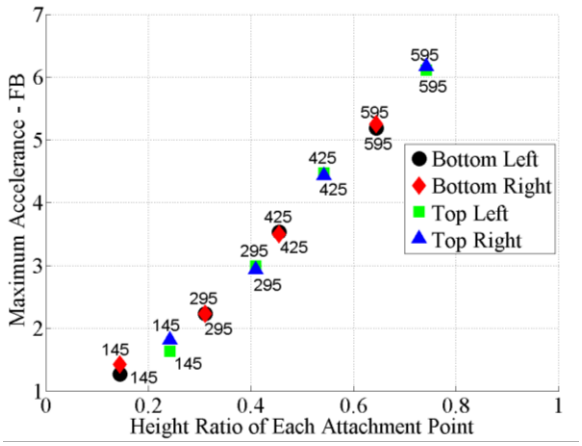

(a) Front-back (FB) direction

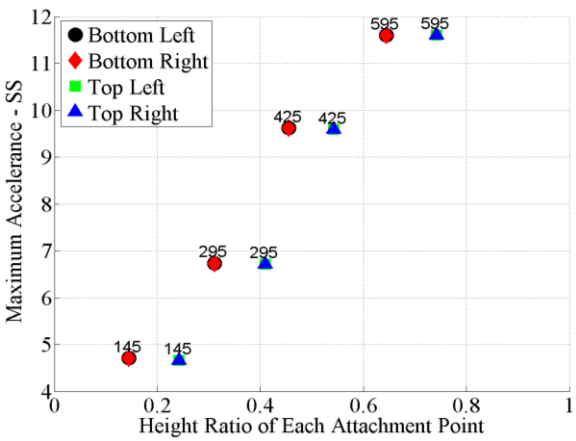

(b) Side-to-side (SS) direction

Figure 5.15 Main Circuit Breaker - plot of the maximum accelerance for steady-state analysis

Figure 5.16 shows the plot of the frequency at which the maximum accelerance occurs against the height ratio of each attachment point. In the FB direction, the maximum accelerance occurs approximately at the second or third natural frequency in that direction. At the same time in the SS direction, the maximum accelerance occurs approximately at the second natural frequency, except for the circuit breaker located at lowest level 145, the maximum accelerance occurs at higher natural frequencies.

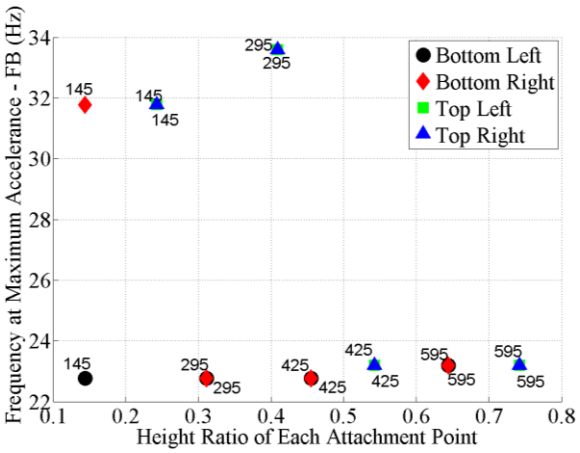

(a) Front-back (FB) direction

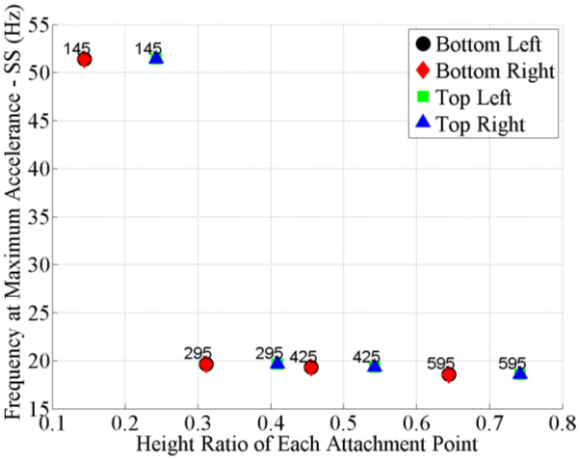

(b) Side-to-side (SS) direction

Figure 5.16 Main Circuit Breaker - plot of the frequency at which the maximum accelerance occurs for steady-state analysis

5.5 Effect of the Distribution of Electrical Devices Attached to the Front Panels

A set of three meter devices arranged symmetrically on a front panel is investigated in this study. Six height variations for the meter devices are considered in this study based on the location of their front panel. These height variations are labeled as Level 1, Level 2, Level 3, Level 4, Level 5, and Level 6 to indicate the height of the center point of the lowest to the highest front panels, respectively. Figure 5.17.a and b show the receptance plots of the top story drift in the FB and SS directions, respectively. The variations of the location of meter devices slightly alter the higher natural frequencies in the FB direction. However, the fundamental frequency in the FB direction and the natural frequencies in the SS direction are relatively insensitive to the location of the meter devices.

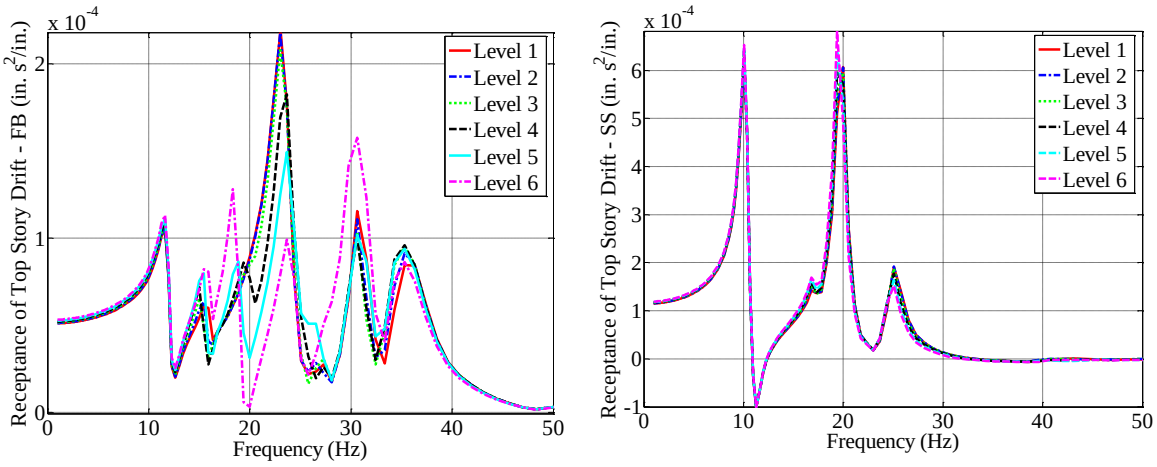

(a) Front-back (FB) direction (b) Side-to-side (SS) direction

Figure 5.17 Meter devices - plot of the receptance of the top story drift

Accelerations at the middle point of each meter device are measured and the results are labeled with side left, middle and side right to indicate the left, middle and right meter devices respectively. The maximum accelerance for each meter device is then recorded and plotted against the height ratio of the middle point of each meter device (see Figure 5.18.a and b.). This ratio is calculated by normalizing the height of the middle points of each meter device to the height of cabinet. In general, the maximum accelerance

of the meter devices in the FB and SS directions tends to increase as the positions of the meter devices increase except for the Level 1 case in the FB direction where the maximum accelerance of that case is higher than the Level 2 case. This behavior is caused by the greater deformation of the first panel in the Level 1 case than the second panel in the Level 2 case as shown in Figure 5.19. In addition, for the FB and SS directions the maximum accelerance of the middle meter device in the FB direction is always larger than the maximum accelerance of meter devices on either side of it. At the same time, the maximum accelerance is always larger in the FB direction than in the SS direction if the maximum accelerance in both directions are compared for each level. This behavior is consistent with the observations made by Merz and Ibanez (Merz and Ibanez, 1990) that the response (e.g. accelerance) of the devices attached on an enclosure panel is more dominant for input loads in a direction perpendicular to the panel surface.

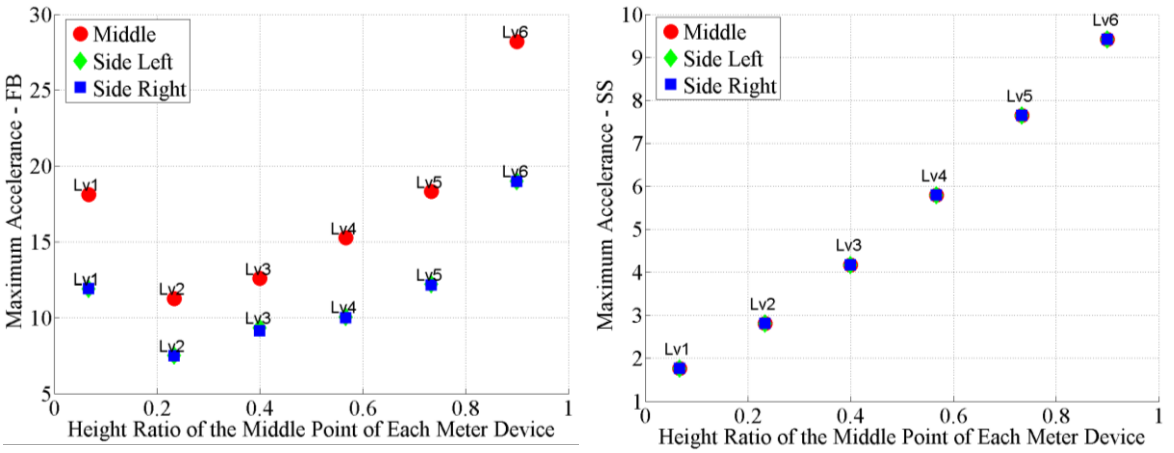

(a) Front-back (FB) direction (b) Side-to-side (SS) direction

Figure 5.18 Meter devices - plot of the maximum accelerance for steady-state analysis

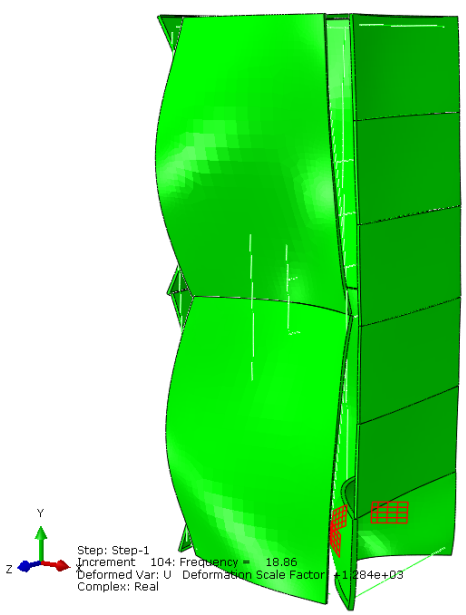

(a) Deformation of first panel in Level 1 case

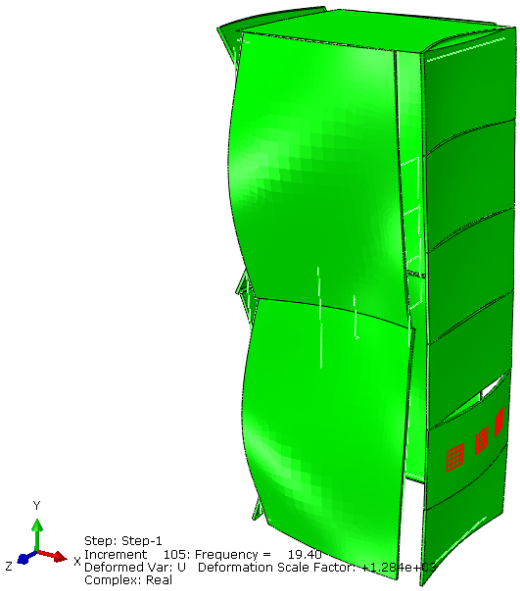

(b) Deformation of second panel in Level 2 case

Figure 5.19 Deformation of the front panels at the maximum accelerance of the frequency response analysis in FB direction.

Figure 5.20 shows the plot of the frequencies at which the maximum accelerance occurs against the height ratio of the middle point of each meter device. In the FB direction, most of the maximum accelerance occurs at the third natural frequency. Only for the Level 3 case does the maximum accelerance occur at the second natural frequency (see Figure 5.20.a). In the SS direction, all of the maximum accelerance occurs at the second modes as shown in Figure 5.20.b. In producing this plot, some of the data corresponding to higher frequencies (> 45 Hz) is omitted because it may obscure the important dynamic characteristics of the cabinet within a more reasonable range of frequency (1- 33Hz).

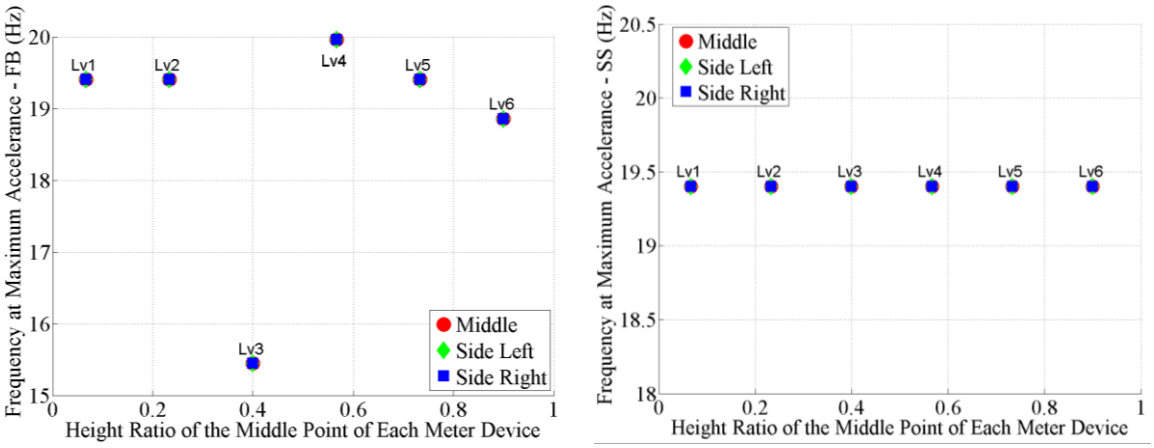

(a) Front-back (FB) direction (b) Side-to-side (SS) direction

Figure 5.20 Meter devices - plot of the frequency at which the maximum accelerance occurs for steady-state analysis

5.6 Summary

This chapter discusses how the simplified cabinet model can be used in a frequency response analysis to find the natural frequencies of a cabinet. In addition, possible ways to incorporate the mass of electrical devices into the simplified cabinet model are also presented. The simplified cabinet model provides more convenient and efficient ways to investigate the behavior of an electrical cabinet than a high fidelity model of the cabinet. The reason is that in the high fidelity model there are many more unique measuring points that could be selected to represent the behavior of the components that are being analyzed. For example, in a simplified model a measuring point at the center of mass of a busbar or circuit breaker may be used to represent the general behavior of the device. This simplicity may not be found in a high fidelity model of the cabinet in which the busbar and circuit breaker are represented using shell elements and brick elements, respectively. In such a model, more measuring points may be needed, and this requirement can complicate the post-processing analysis.

In addition to its simplicity, the simplified cabinet model has also shown a similar capability to capture important behaviors of electrical cabinet that have been observed by

other researchers using experimental tests or high fidelity models, such as the importance of local modes of electrical devices in the dynamic behavior of cabinet.

Despite all of the benefits, it should be noted that the simplified cabinet model developed using the proposed method described in Chapter 3, 4 and 5 has not been validated dynamically to the corresponding benchmark cabinet model or experimental test results. Future works to validate this methodology may be needed especially related to the assumption made to the mass and damping models.

This chapter has also presented the results of a sensitivity study of the maximum accelerance of electrical devices or their attachment points to the vertical distribution of the devices inside the cabinet. In general, the maximum accelerance tends to increase as the location of electrical devices increases, although in some notable cases, the local modes of the devices may alter this observation.

Based on this information, most of these electrical devices are distributed in the upper-half of the cabinet assembly model considered for time history analysis in Chapter 6, except for a set of meter devices which is located at the second lowest front panel. The selection of this location is influenced by the observations made during the site visits at the Sustainable Education Building at Georgia Tech.

Finally, similar sensitivity studies on representative cabinet configurations may be useful for future work related to vulnerability studies of electrical cabinets. In addition, the results of such sensitivity studies can provide information on how selected electrical devices hosted inside the cabinets should be distributed to minimize their service vibration environment.

CHAPTER 6

APPLICATION OF THE SIMPLIFIED CABINET ASSEMBLY MODEL IN TIME HISTORY ANALYSIS

This chapter describes the development of a simplified finite element model for a cabinet assembly based on the methodology proposed in Chapter 3 and 4 for the structural model and Chapter 5 for the mass model. In addition, this chapter also discusses the damping and the inter-cabinet connection models incorporated in the simplified cabinet assembly model. This model is then utilized to investigate the effect of geometric nonlinearity and extreme input ground motions on the dynamic behavior of the cabinet assembly with proper support conditions using time history analysis. Then, the simplified cabinet assembly model is combined with a simplified boundary condition model proposed by Hur (Hur, 2012) to predict the dynamic behavior of the cabinet assembly with poor support conditions. The structural configurations of the cabinet assembly are selected based on the observation of actual cabinets at the Sustainable Education Building in Georgia Tech. On the other hand, the distribution of the electrical devices within the cabinet was defined on the basis of the results of the sensitivity study described in Chapter 5 and additional observations made during the site visit.

6.1 Description of the Structural Configurations and Electrical Devices

6.1.1 Description of the Structural Configurations

The cabinet assembly consists of two cabinets with identical structural configuration as described in Chapter 5. Each cabinet is constructed using two front, back and intermediate vertical posts. These vertical posts are tied together at the top and bottom of the cabinet using plain channel beams. The cross sections of the front, back, and intermediate vertical posts, and the beams are shown in Figure 6.1.a. In addition, the

front and back vertical posts are connected to the channel beams using screws or bolts as shown in Figure 6.1.b, and the intermediate vertical posts are connected to the channel beams using four screws arranged symmetrically. Two folded panels are used to fill each opening in the back, left and right sides of the cabinet assembly, and six folded panels are used to close the front opening of each cabinet. These panels are connected to the framing members using a screw at each corner of the panels as shown in Figure 6.1.c. An unfolded panel is finally used to cover the top opening of each cabinet. These panels are also connected using screw connections at the four corners of each panel.

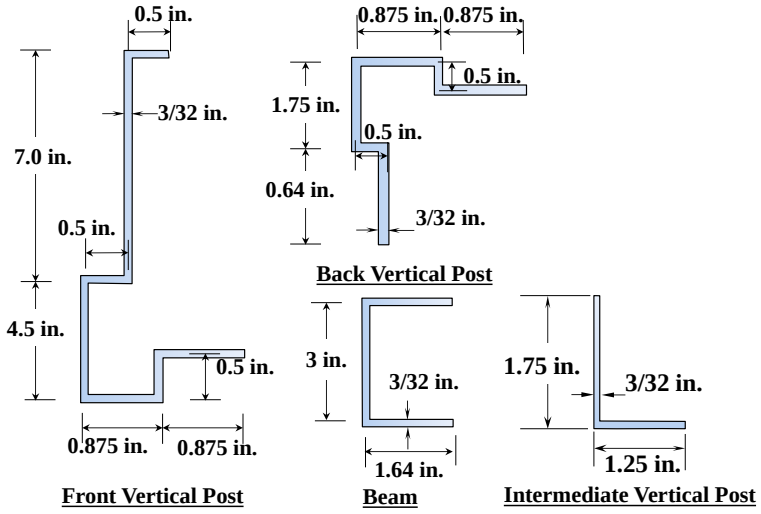

(a) Cross section of framing members

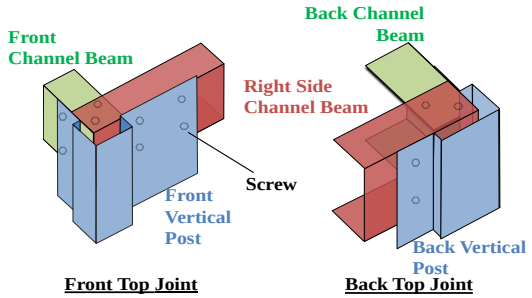

(b) Configurations of connection between framing members

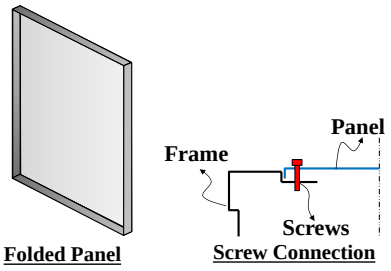

(c) Configurations of the folded panels and their connection to the framing members

Figure 6.1 Cross sections and configurations of the structural components

Two types of inter-cabinet connections are provided between the two cabinets: 1) bolted connection along the coincident front and back vertical posts of the cabinet

assembly, and 2) lap-splice connection between the busbars. A single bolt is used to connect the front and back vertical posts at the top, middle and bottom of the adjacent cabinets (a total of six bolts). The configuration of the bolted connection is shown in Figure 6.2.a. Figure 6.2.b. shows a configuration of the lap-splice connection for the busbars. A single hook-style plate is used to connect the busbars between cabinets using a single bolt. It should be noted that these connection types are specific to the cabinet assembly observed during the site visit. Hence, no generalization should be made to another class of cabinet and even to the same class of cabinet since the types of inter-cabinet connection may be different (e. g., a flat plate may be used to connect the busbars instead of a hook-style plate).

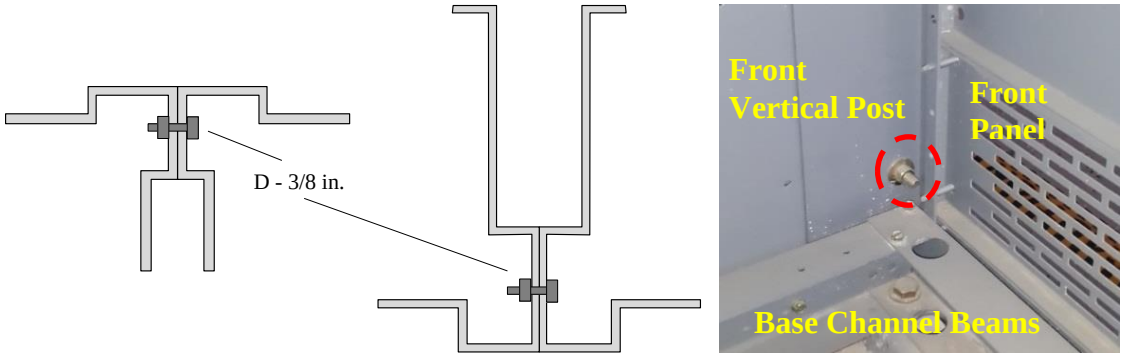

(a) Bolted connections along vertical posts

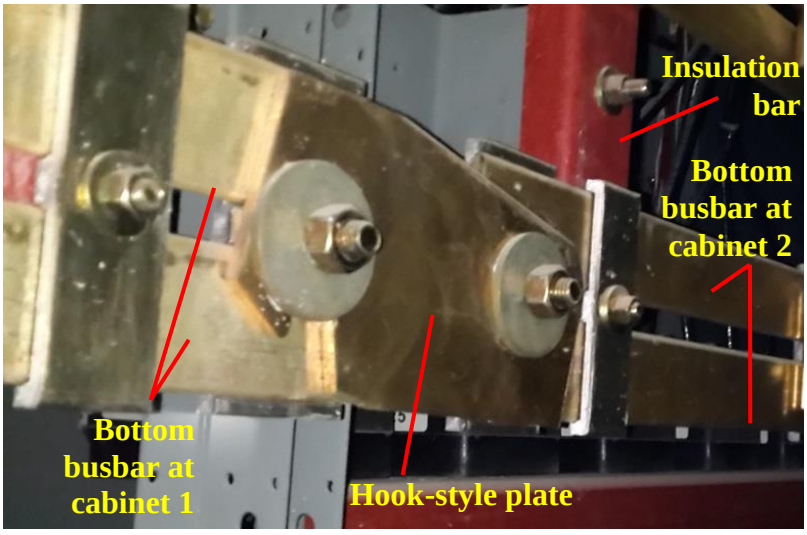

(b) Lap-splice connection between busbars

Figure 6.2 Types of inter-cabinet connections

6.1.2 Description of the Electrical Devices

Three types of electrical devices (busbars, main circuit breaker, and meter devices) as described in Chapter 5 are considered in this study. These devices are mostly distributed in the upper-half of the cabinet assembly, except for a set of meter devices (see Figure 6.3). This distribution is selected based on the results of the sensitivity study presented in Chapter 5 and the observations made during the site visit. In both cabinets, the busbars are connected to the intermediate vertical posts at 43.5 in. above the ground. This value indicates the height of the bottom attachment point of the busbar assembly to the intermediate vertical posts. In addition, a main circuit breaker is located at 42.5 in. above the ground in one cabinet. This value indicates the height of the bottom supporting bar in the cabinet. Furthermore, meter devices symmetrically arranged on panels 2, 4 and 5 are located at the other cabinet (see Figure 6.3). All of these electrical devices are attached inside each individual cabinet in the same way as described in Section 5.2.1

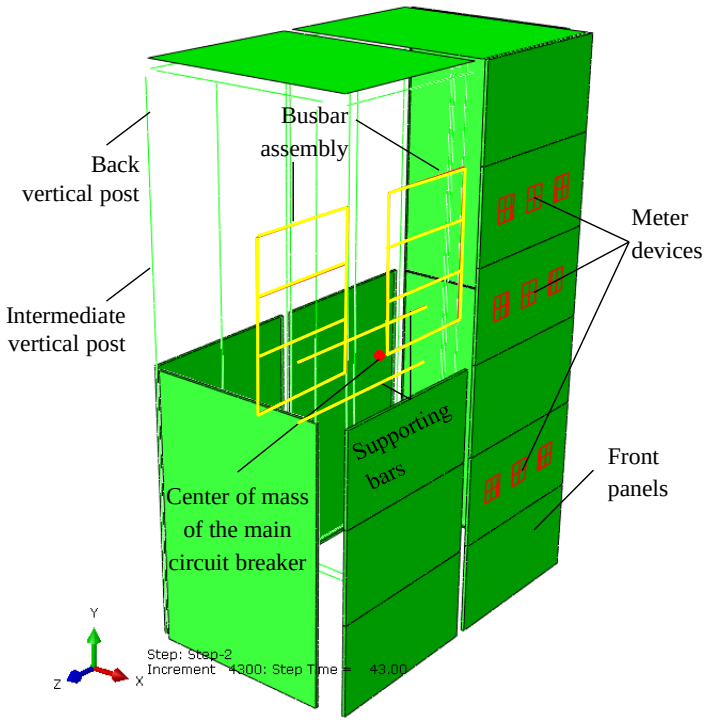

Figure 6.3 Location of electrical devices in the cabinet assembly (some components are intentionally removed for clarity)

6.2 Modeling and Analysis Strategies

6.2.1 Modeling Strategies

The structural components and the electrical devices are modeled using the same methodology described in Chapters 3, 4 and 5. Additional CONNECTOR features with BEAM (see 1-2 in Figure 6.4) and JOIN (see 3-4, 5-6, 7-8, 9-10 in Figure 6.4) properties are included in the simplified cabinet assembly model to handle the bolted and the lap-splice inter-cabinet connections, respectively. The connector with BEAM property rigidly constrains two nodes in the inner front and back vertical posts at the top, middle and bottom of the cabinet to represent the bolted inter-cabinet connection. The connector with JOIN property constrains the translational DOFs of the inner end-nodes (see points 3, 5, 7, and 9 in Figure 6.4) in a busbar assembly to the opposite inner end-nodes (see points 4, 6, 8, and 10 in Figure 6.4) in the other busbar assembly to represent the lap-splice connection. This property is selected based on the assumption that the lap-splice connection will fully transfer only the translational forces but does not have the capability to transfer moments.

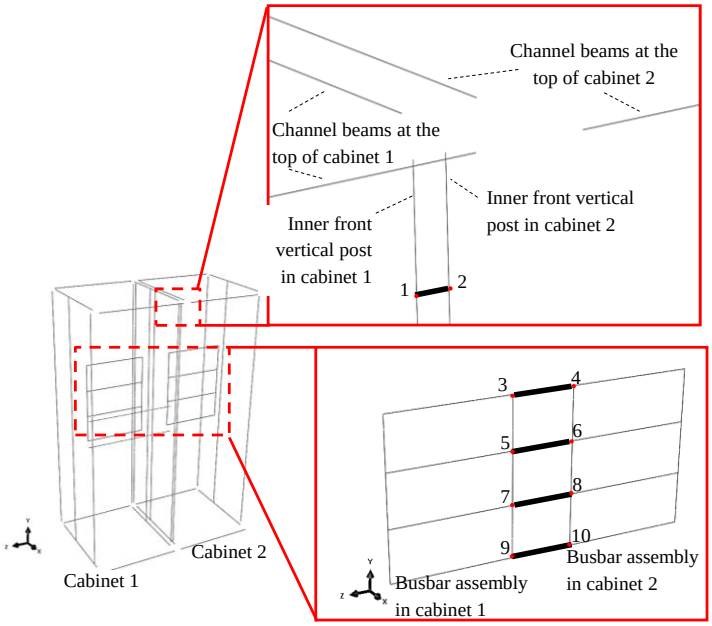

Figure 6.4 Location of the additional connector features for the inter-cabinet connections

6.2.2 Input Ground Motion

There are many input ground motions that can be applied to the cabinet assembly, and the decision on which to use is made based on the purpose of the analysis. In this study, a ground motion that satisfies appropriate seismic qualification guidelines is selected. Two guidelines that are typically used for the seismic qualification of electrical components are AC156 and IEEE 693. AC156 is more general in terms of its application to a general class of nonstructural components. However, the IEEE693 guideline is more relevant to the electrical equipment located in a typical electrical substation. Both guidelines require a set of nonstationary broadband random excitations that meets the specified required response spectra (RRS) in three orthogonal directions. The RRS of both guidelines are almost the same. However, the AC156 guideline has a lesser (-10%) tolerance on how much the calculated response spectra (CRS) can be under the RRS compared to IEEE 693 guideline that has a tolerance of -15%.

The generation of the input ground motion for AC156 typically is delegated to the testing laboratory, and it usually involves third party software. On the other hand, Takhirov et al. (Takhirov et al., 2005) have proposed a set of input ground motion (labeled as TestQke) that meets the requirement of IEEE 693. The comparison between the CRS of the ground motion and the IEEE 693 RRS with 2% damping and 1.0 g PGA (labeled as IEEE 2% PL) in the X and Y directions are shown in Figure 6.5.a. and b. In addition, the comparisons of the CRS and the IEEE RRS with 5% damping (labeled as IEEE 5% PL) are shown in Figure 6.5.c. and d. Based on those plots, the proposed ground motions are suitable for the RRS specified in the IEEE 693 guideline (within the tolerance). However, the proposed ground motion is not suitable for AC156 guideline that requires the CRS to be calculated with 5% damping value. The reason is because there are many valley-points of the CRS that are under-predicted below the tolerance limit of the AC156 guideline. Despite this under estimation, the overall shape of the CRS

is still reasonable in general. The ground motions proposed by Takhirov et al. are selected for this study because the main purpose of this study is to investigate the behavior of the cabinet assembly under a reasonable input motion, and not to seismically qualify a particular class of cabinet.

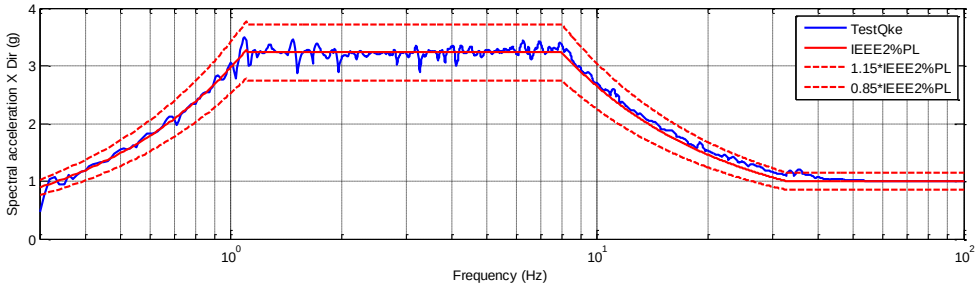

(a) X direction 2% damping

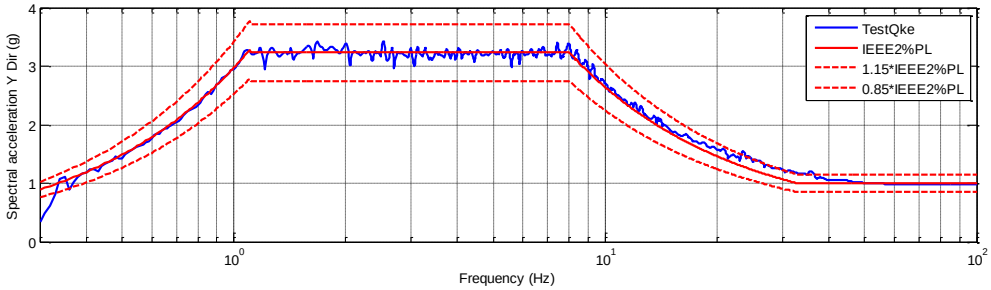

(b) Y direction 2% damping

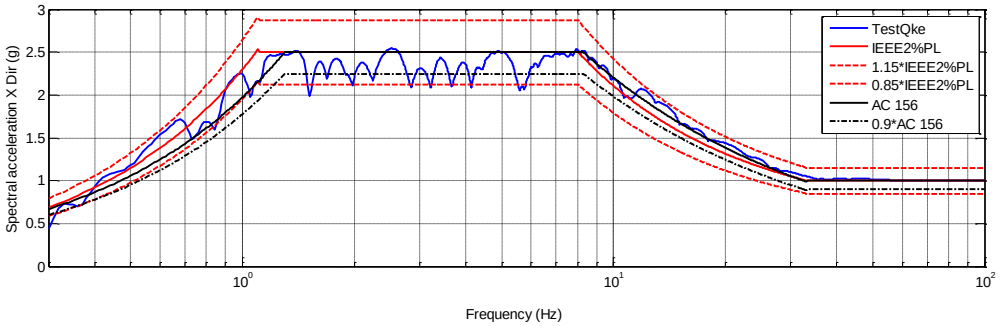

(c) X direction 5% damping

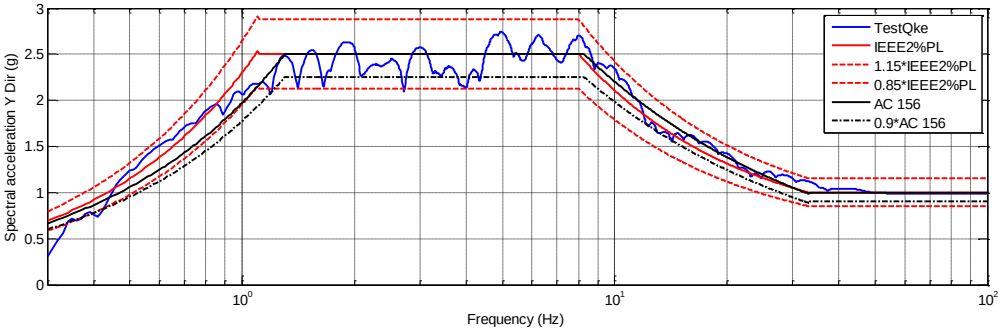

(d) Y direction 5% damping

Figure 6.5 Comparison of the calculated response spectra (CRS) and the required response spectra (RRS)

6.2.3 Analysis Strategies

The simplified cabinet assembly model described in Section 6.2.1 was utilized to investigate the effect of geometric nonlinearity, high peak ground acceleration (PGA), and partial fixity on the dynamic behavior of the cabinet assembly using the results of nonlinear time history analysis of the following five cases:

1. Properly anchored cabinet assembly – geometric linear – PGA = 1.0 g
2. Properly anchored cabinet assembly – geometric nonlinear – PGA = 1.0 g
3. Properly anchored cabinet assembly – geometric linear – PGA = 2.5 g
4. Partially anchored cabinet assembly (inner supports removed) – geometric linear – PGA = 1.0 g
5. Partially anchored cabinet assembly (outer supports removed) – geometric linear – PGA = 1.0 g

In the first case, the base of the electrical cabinets are fixed at 12 points (three points at the outer left and right sides, and 6 points at the inner sides) as shown in Figure 6.6.a. This case represents an ideal construction condition for the cabinet assembly, and its behavior will be used as a reference to the response of the cabinet assembly in the other cases. The second and third cases are similar to the first case. However in the second case, the geometric nonlinear effect is included in the analyses to investigate its effect on the behavior of the cabinet assembly (e.g. buckling of panels). In addition in the third case, the peak ground acceleration (PGA) of the input ground motion is scaled from 1.0 g to 2.5 g to investigate the effect of high PGA to the behavior of the cabinet. This scale factor is considerably high knowing that the maximum possible scale factor if the cabinet is located on the top of a building is 3.0 (ASCE, 2010). In the fourth and fifth cases, the inner and the outer corner supports are removed as shown in Figure 6.6.b and c, respectively. These cases may represent poor construction practices that may exist in the field. At the location of the removed supports, a boundary condition that simulates

rocking behavior of a rigid body system is implemented as shown in Figure 6.7 (Hur, 2012). This boundary condition has a "rigid" compressive stiffness but "zero" tensile stiffness in the vertical direction. In addition, the horizontal direction of the supports at the pivot points in rocking behavior is fixed. Meanwhile, the horizontal direction of the supports opposite to the pivot points is free. No sliding behavior is included in this boundary condition model because it is assumed that it is prevented by the retained supports.

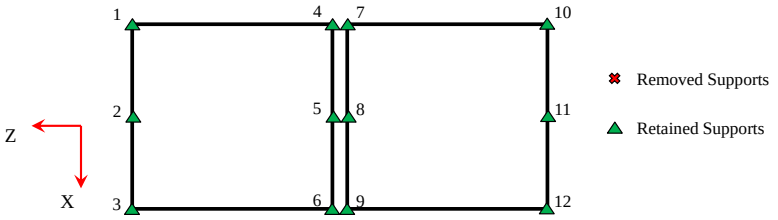

(a) Boundary condition in Cases 1, 2 and 3

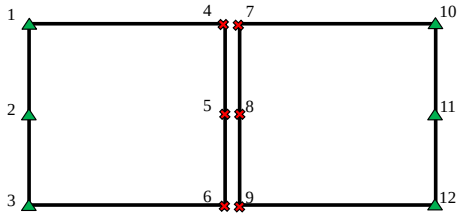

(b) Boundary condition in Case 4: inner supports removed

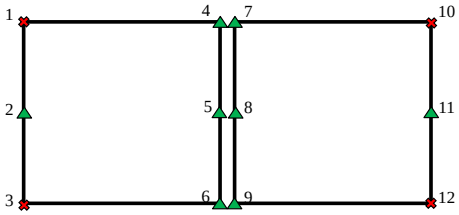

(c) Boundary condition in Case 5: outer supports removed

Figure 6.6 Plan view of cabinet boundary conditions

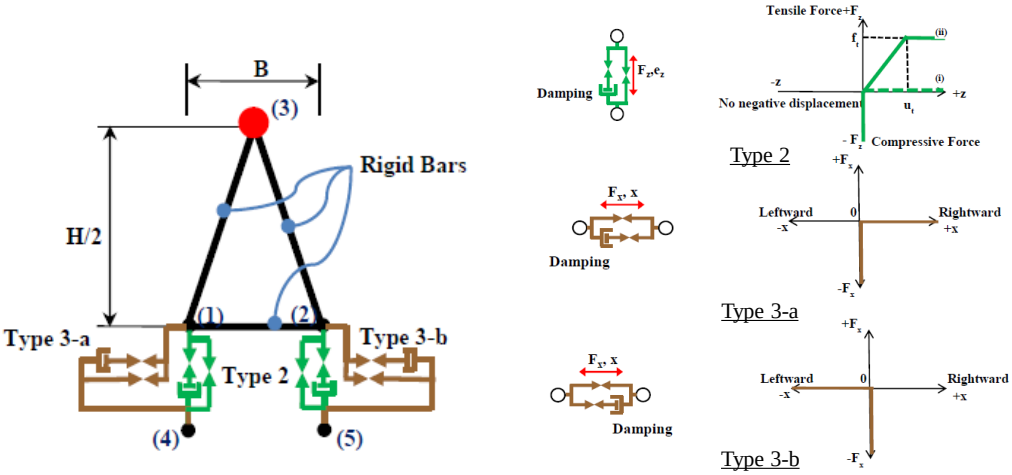

Figure 6.7 Boundary condition model used to capture rocking behavior (figures courtesy: Hur (2012))

The cabinet assembly is initially subjected to gravity load in all cases. Next, non-linear time history analyses were performed on the cabinets in the two orthogonal horizontal directions using the implicit solver (Hilber, Hughes and Taylor) embedded in ABAQUS. This solver is a generalization of the Newmark average acceleration method. Thus, it is numerically stable for any time increment. In all cases except the second one, the analyses are conducted without considering the geometric nonlinear effect. Therefore, the only nonlinearity included in the simplified cabinet assembly model is contributed from the springs that define the failure of the panel-frame connection.

For the damping model of the cabinet assembly, the three viscous damping ratios discussed in Section 5.2.2 are adapted into the Rayleigh damping model. These damping ratios are divided into the fundamental frequency bins based on the investigation of the experimental tests of electrical cabinets (Djordjevic and O'Sullivan, 1995): 1) Bin 1 (9.5 Hz-13 Hz) – 4% damping, 2) Bin 2 (13Hz-20Hz) – 3.5% damping, and 3) Bin 3 (> 20Hz) – 3% damping. These damping values are then used to determine the Rayleigh damping coefficients ($\alpha = 5.06$, $\beta = 0.000177$) that are assigned to all numerical models of the cabinet assembly considered in this chapter. These coefficients are determined by trial and error such that the calculated damping ratio is close enough to the damping values within the frequency bins as shown in Figure 6.8. The calculated maximum mean difference and its standard deviation are 0.00296 and 0.00297, respectively (in Bin 1, based on an assumption that the angular frequency is uniformly distributed). Rayleigh damping is selected because it is very convenient to use and is available in most of the commercial FE software.

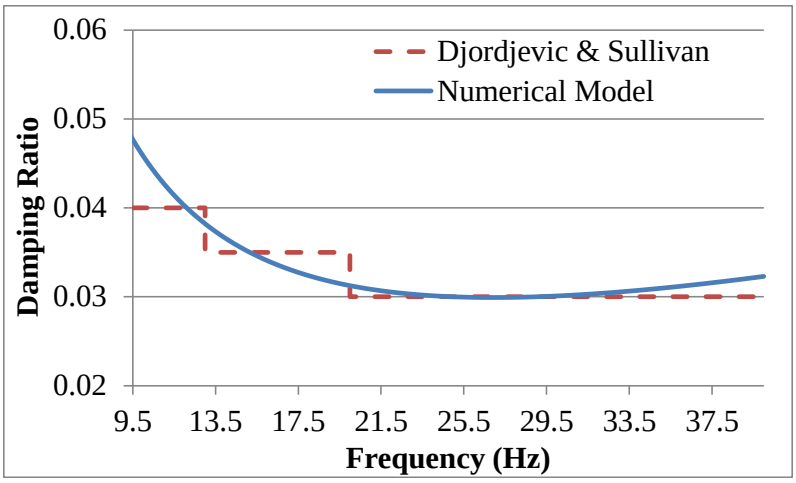

Figure 6.8 Comparison of the viscous damping ratio assigned to the numerical model and the damping values specified by Djordjevic and Sullivan.

6.3 Effect of Geometric Nonlinearity on the Behavior of the Cabinet Assembly

The acceleration of the electrical devices and their attachment points in the simplified cabinet assembly models are measured. For busbars, the acceleration is measured at the midspan of the top busbar in each busbar assembly and at the attachment points of the busbar assemblies to the intermediate vertical posts. At the same time, the acceleration for the main circuit breaker is measured at the attachment points of the circuit breaker to the supporting bars and at the attachment points between the supporting bars and the front vertical posts. In addition, the acceleration for the meter device is measured at the midpoint of the middle device. Afterward, the amplification factors are calculated by taking the ratio of the maximum acceleration at each measuring point to the PGA of the input ground motion. For each type of attachment points, a maximum amplification factor is then selected from the amplification factors corresponding to the particular type of attachment points (e.g. attachment points of the busbar assemblies to the intermediate vertical posts). The second and the third columns of Table 6.1 show the amplification factor (labeled as Amp.) of the case 1 cabinet assembly for input ground motions in both translational directions (X – FB direction and Z - SS direction). The amplification factors of the busbar and the meter devices are larger in the FB direction

than in the SS direction. On the other hand, the amplifications of the attachment points between busbars and intermediate posts, the attachment points between the circuit breaker and the supporting bars, and the attachment points between the supporting bars and the vertical posts are slightly larger in the SS direction than in the FB direction. The third and fourth columns in Table 6.1 shows the amplification factors for the case 2 cabinet assembly in which the geometric nonlinear effect is included in the time history analysis. In general, including the geometric nonlinear effect does not lead to a significant change in the amplification factor for the electrical devices and their attachment points to the cabinet, except for the attachment point of the busbars to the intermediate posts.

Table 6.1 Comparison of the amplification factor for the electrical devices and their attachment points to the cabinet for Cases 1 (properly anchored – geometric linear) and 2 (properly anchored – geometric nonlinear)

Devices	Case 1		Case 2	
	Amp. FB	Amp. SS	Amp. FB	Amp. SS
Top busbar 1	2.19	1.35	2.21	1.32
Top busbar 2	2.20	1.35	2.27	1.35
Attachment point between busbar assembly and intermediate post	1.46	1.82	1.64	2.72
Attachment point between circuit breaker and supporting bars	1.04	1.24	1.04	1.23
Attachment point between supporting bars and vertical posts	1.05	1.24	1.05	1.23
Meter devices(at Level 2)	1.68	1.08	1.68	1.06
Meter devices (at Level 4)	1.81	1.24	1.83	1.23
Meter devices (at Level 5)	2.05	1.29	2.09	1.27

Further investigations of the cabinet assemblies have shown that the maximum top story drifts of the case 1 cabinet assembly are 0.053% in the SS direction and 0.047% in the FB direction. At the same time, the maximum top story drifts of the case 2 cabinet assembly are 0.054% (in the SS direction) and 0.048%. (in the FB direction). These

values are very close to the top story drifts of the case 1 cabinet assembly. In addition, the changes of the shearing and tensile reactions forces are also relatively small. Only one shearing (at node 2 in Figure 6.6.a) and two tensile (at node 5 and 11 in Figure 6.6.a) reaction forces of the case 2 cabinet assembly are about 18% and 45% larger than the corresponding reaction forces in the case 1 cabinet assembly.

6.4 Effect of Extreme PGA to the Behavior of the Cabinet Assembly

If the PGA of the input ground motion is increased from 1.0 g to 2.5 g, the acceleration responses of the electrical devices and their connections are also increased. However, this increase does not occur in their acceleration amplification factors which are nearly the same (see Table 6.2).

Table 6.2 Comparison of the amplification factor for the electrical devices and their attachment points to the cabinet between the Cases 1 (properly anchored – 1.0 g) and 3 (properly anchored – 2.5 g)

Devices	Case 1		Case 3	
	Amp. FB	Amp. SS	Amp. FB	Amp. SS
Top busbar 1	2.19	1.35	2.28	1.35
Top busbar 2	2.20	1.35	2.36	1.35
Attachment point between busbar assembly and intermediate post	1.46	1.82	1.44	1.83
Attachment point between circuit breaker and supporting bars	1.04	1.24	1.04	1.24
Attachment point between supporting bars and vertical posts	1.05	1.24	1.05	1.24
Meter devices(at Level 2)	1.68	1.08	1.57	1.08
Meter devices (at Level 4)	1.81	1.24	1.69	1.25
Meter devices (at Level 5)	2.05	1.29	2.11	1.30

The increment of the PGA also increases the maximum top story drifts of the cabinet (0.202% in the FB direction and 0.187% in the SS direction). Even though the maximum top story drifts are increased, the behavior of the cabinets is still likely rigid

and remains in a linear elastic state. In addition, almost all of the supports in the case 3 cabinet assembly have shear reaction forces that are about 3.5 times larger than the reaction forces of the case 1 cabinet assembly. At two supports (node 6 and 9 in Figure 6.6.a), the reaction forces of the case 3 cabinet assembly are 25 times larger than the reaction forces of the case 1 cabinet assembly. It is important to note that a significant increase in the tensile reaction forces also occurs in almost all supports, and the maximum tensile reaction force (at node 8 in Figure 6.6.a) is approximately 13 times the corresponding reaction force of the case 1 cabinet assembly.

6.5 Effect of Partial Fixity to the Behavior of the Cabinet Assembly

The amplification factors for the electrical devices and their attachment points for the cases 4 and 5 cabinet assemblies in which the inner and outer supports are removed are shown in Table 6.3. The changes in the support boundary conditions do not lead to a significant change in the amplification factor for the electrical devices and their attachment points.

Table 6.3 Comparison of the amplification factor of the electrical devices and their attachment points to the cabinet between Cases 1 (properly anchored), 4 (inner support removed), and 5 (outer support removed)

Devices	Case 1		Case 4		Case 5	
	Amp. FB	Amp. SS	Amp. FB	Amp. SS	Amp. FB	Amp. SS
Top busbar 1	2.19	1.35	2.18	1.35	2.17	1.35
Top busbar 2	2.20	1.35	2.20	1.35	2.20	1.35
Attachment point between busbar assembly and intermediate post	1.46	1.82	1.46	1.88	1.42	1.83
Attachment point between circuit breaker and supporting bars	1.04	1.24	1.04	1.26	1.05	1.23
Attachment point between supporting bars and vertical posts	1.05	1.24	1.05	1.26	1.06	1.23
Meter devices (at Level 2)	1.68	1.08	1.69	1.13	1.68	1.08
Meter devices (at Level 4)	1.81	1.24	1.81	1.27	1.80	1.23
Meter devices (at Level 5)	2.05	1.29	2.05	1.31	2.04	1.29

In addition, the maximum top story drift of the case 4 cabinet assembly in both directions are 0.049% (FB) and 0.047% (SS), and the maximum top story drift of the case 5 cabinet assembly are 0.047% (FB) and 0.057% (SS). These results show that there is also no significant change in the top story drift of the cabinet assembly (compared to the case 1 cabinet assembly) if the inner or outer supports are removed, and with such small drift, the cabinet appears to behave like a rigid box. Further investigations have shown that the shear reaction forces of the case 4 cabinet assembly can increase up to 2.0 times at node 3 and 10 in Figure 6.6.b and 2.7 times at node 12 in Figure 6.6.b of the corresponding reaction forces in the case 1 cabinet assembly. These reaction forces correspond to the input ground motion in the SS (Z) direction. On the other hand, the tensile reaction forces are slightly increased by about 10% at node 1, 10 and 12 (see Figure 6.6.b) for input ground motion in the SS (Z) direction. For the case 5 cabinet assembly, the shear and tensile reaction forces can increase up to 15 times (node 2 and 11 in Figure 6.6.c – input ground motion in the FB (X) direction) and 3.8 times (node 2 in Figure 6.6.c – input ground motion in the SS (Z) direction) of the corresponding reaction forces of case 1 cabinet assembly, respectively. These amplifications on the reaction forces (except the tensile reaction force in case 4) will most likely cause failure to the anchor bolts, and eventually will cause the cabinet to slide or overturn.

6.6 Summary

In addition to its straight forward property as described in Section 5.6, this study has demonstrated the adaptable property of the simplified cabinet model, generated using the proposed method, since it can be combined with an existing simplified boundary conditions model (finite-element-base model) to predict the behavior of a partially anchored cabinet assembly. This study has also shown that:

- In general, the selected cabinet assembly model is insensitive to the geometric nonlinear effect.

- The selected cabinet assembly model is relatively rigid even if the magnitude of the input ground motion has been increased from 1.0 g to 2.5 g.
- The effect of partial fixity on the amplification factor on the electrical devices and their attachment points to the cabinet assembly is insignificant. However, it has significant effect to the amplification of the reaction forces of the partially anchored cabinet assembly.

Future work is needed to investigate the nonlinear capability of the simplified cabinet assembly model in more detail. Some parameters that can be modified are: 1) dimensions of the cabinet assembly, 2) number and distribution of electrical devices, and 3) input ground motion. This investigation may also include improvement of the definition of the nonlinear modeling features to handle effects of dynamic load such as cyclic behavior and reduction on the buckling load. In addition, validation of the simplified cabinet assembly model using the corresponding benchmark cabinet assembly model or experimental test results may be needed.

CHAPTER 7

CONCLUSIONS AND FUTURE WORK

7.1 Conclusions

The major contribution of this research is related to the development of the method to generate simplified finite element models of properly anchored electrical switchboard cabinets. The simplified cabinet model generated using the proposed method is generic, straightforward and adaptable. The model is generic because it is developed solely based on an engineering mechanics approach. Hence, it is applicable to a wide range of electrical cabinets. In this research, two configurations are selected to represent both simpler cabinet and a more complex electrical cabinet. The simplified cabinet models are then statically validated using the corresponding benchmark cabinet models. The results of the validation show that the simplified cabinet models are able to predict nonlinear behaviors of properly anchored electrical cabinets, such as failure of the screw connection between panel and framing member, buckling of panels, and elastic local buckling near the ends of thin-walled section framing members.

The simplified cabinet model is straightforward to use because the results obtained from the model are easier to understand than the results from a high fidelity model of the corresponding cabinet. In the simplified cabinet model, there are more unique measuring points that can be selected to represent the behavior of the cabinet or the electrical devices. This may not be found in the high fidelity model of the electrical cabinet in which a structural analyst is faced with many measuring points for a single component or device, and this may complicate the post-processing analysis of the cabinet model.

The simplified cabinet model is adaptable because it can be integrated with other finite-element-based boundary condition models proposed by other researchers. These

models typically have the capability to predict the behavior of poorly or partially anchored rigid cabinets. The simplified cabinet model is developed based on an assumption that the cabinet is fixed at the base, but failure of the anchorages of electrical cabinets has been found in past reconnaissance surveys. Incorporation of the simplified cabinet model and a boundary condition model could broaden the scope of application of the simplified cabinet model to predict the behavior of inadequately or partially anchored cabinets.

Another contribution of this research is related to the hybrid Timoshenko beam model that can be used to capture elastic local buckling behavior of thin-walled open-section beam members subjected to double curvature bending. The hybrid beam model consists of the Timoshenko beam elements and a nonlinear spring at each end of the framing members. The properties of the nonlinear springs can be generated using two methods: 1) shell element method, and 2) effective-width prediction method. In the shell element method, the spring properties are generated based on the behavior of the members predicted using shell element models of the members. On the other hand in the effective-width prediction method, the spring properties are generated based on the prediction of the behavior of the members using an effective-width approach.

7.2 Future Work

There are a number of areas in which this research could be expanded to consider additional key aspects of switchboard cabinet behavior:

1. Beam Element Model

A hybrid Timoshenko beam element model was developed during the course of this research. The beam model can handle elastic local buckling behavior of cold-formed steel members under double curvature bending. The beam element model uses rotational springs in which one of the methods to generate their properties is the effective-width prediction method. However, the application of this method in more complex conditions

(e.g. unusual configurations, inelastic conditions, inclusion of local geometric imperfections, effect of dynamic load) is still unclear, and improvement on the effective-width prediction is needed so that it is more applicable to a wide-range of problems. In addition, it may be possible to develop a finite element beam model that can handle the localized buckling behavior automatically and in a simpler manner than the existing models proposed by other researchers.

2. Electrical Cabinet Model

Properly anchored cabinet model: Although the simplified cabinet model has been statically validated to the corresponding benchmark cabinet models, there are still two important questions that remain: 1) how accurate is the benchmark cabinet model in predicting behavior observed in an experimental test, and 2) how accurate is the simplified cabinet model in predicting the dynamic characteristic and behavior of the cabinet. Validations of the simplified cabinet models using experimental test results may be necessary to improve the confidence level in the application of the proposed method in static and dynamic analyses.

Inadequately anchored cabinet model: This research has introduced a simple boundary condition model developed by Hur (Hur, 2012), and combined this model to the simplified cabinet assembly model. Considering the importance of the boundary condition model and various types of supports incorporated to the cabinet, there is still a need to improve the capability of the existing boundary condition model. One possible improvement is to include the interaction between the anchor bolts and the beam members at the base of the cabinet which may be critical for certain types of supports.

3. Fragility Functions

Some of the challenges in producing fragility functions for the electrical cabinet are related to the variability of the configuration of the cabinets and types of electrical devices contained within the cabinet. The variability of the cabinets highly depends on the manufacturer and the demand of the consumer. Each manufacturer usually has their

own specific configurations for the electrical cabinet and can depend on the demand of the consumer and the location of the cabinets. In addition, there is still no clear information on: 1) which types of electrical devices are attached to a cabinet and 2) how the electrical devices are distributed within a cabinet. Therefore, there is a need to select some common configurations of electrical cabinets for the study. Subsequently, the distribution of electrical devices inside those cabinets that will give the highest reasonable responses can be searched, and the simplified cabinet model may be useful for this purpose. Afterward, the demand and the damage state of the cabinets have to be clearly defined prior to the development of the fragility function, and this clearly requires extensive analysis. The simplified cabinet model may also be useful in these studies.

APPENDIX A

PREDICTION OF THE BEHAVIOR OF PLAIN CHANNEL MEMBER SUBJECTED TO DOUBLE CURVATURE BENDING

In this appendix, detail calculations of the behavior of cold-formed steel member subjected to double curvature bending are presented using an example of plain channel section. All of the calculation steps are referred to the discussions in Section 3.2.

Problem:

A plain channel member having length of 36 in. is subjected to double curvature bending. All DOFs at the end of the member are fixed, except for the in-plane bending direction. Calculate the end-rotation of the member as the end-moments are applied to the ends of the member incrementally. The dimensions of the cross section are shown in Figure A.1. Assume that the material is linear elastic with modulus of elasticity, E = 29,500 ksi and Poisson's ratio, ν = 0.3.

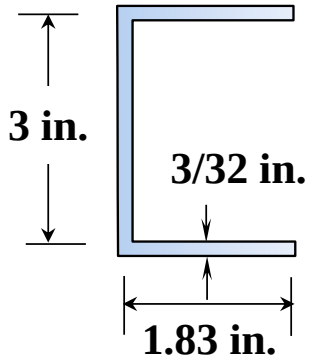

Figure A.1 Dimensions of the plain channel section

Solution:

1. Geometrical and material information

$h = 3in.$ $t = 3/32in.$ $b_f = 1.83in.$ $L = 36in.$ $E = 29{,}500ksi$ $\nu = 0.3$

$$G = \frac{E}{2(1+\nu)} = 11{,}350ksi$$

2. Calculation of the buckling stress of the plate model

The buckling stress is calculated based on the following plate model and shape function using the Rayleigh-Ritz approach.

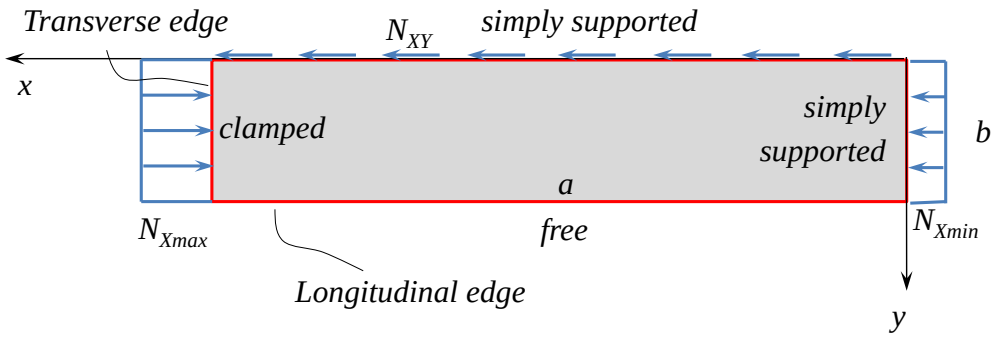

Figure A.2 Plate model used to calculate the buckling stress

$$u(x,y) = C_1\left(2\sin\left(\frac{\pi x}{a}\right)+\sin\left(\frac{2\pi x}{a}\right)\right)\left(\sin\left(\frac{\pi y}{2b}\right)+\sinh\left(\frac{\pi y}{2b}\right)\right) \quad \text{Eqn A.1}$$

In the Rayleigh-Ritz approach, the variation of the total energy (*Π*) acting on the member is set to zero to solve for the buckling stress/load of the system. Two types of energy are considered in the system: Strain Energy (*U*) and Work (*W*).

$$\Pi = U + W \quad \text{Eqn A.2}$$

$$\delta\Pi = \delta U + \delta W = 0 \quad \text{Eqn A.3}$$

The strain energy is calculated using the following function which is formulated based on the bending and twisting deformation of a differential plate element.

$$U = \frac{1}{2}D\iint\left[\left(\frac{\partial^2 u}{\partial x^2}\right)^2+\left(\frac{\partial^2 u}{\partial y^2}\right)^2+2\nu\left(\frac{\partial^2 u}{\partial x^2}\right)\left(\frac{\partial^2 u}{\partial y^2}\right)+2(1-\nu)\left(\frac{\partial^2 u}{\partial x\partial y}\right)^2\right]dxdy \quad \text{Eqn A.4}$$

, where $D = \dfrac{Et^3}{12(1-\nu)^2}$

Meanwhile, the work consider in the energy of the system is based on the forces acting on the mid-plane of the plate: N_x and N_{xy}.

$$W = \frac{-1}{2}\iint\left[N_x\left(\frac{\partial u}{\partial x}\right)^2 + 2N_{xy}\left(\frac{\partial u}{\partial x}\right)\left(\frac{\partial u}{\partial y}\right)\right]dxdy \qquad \text{Eqn A.5}$$

Since N_x is linearly varying along the length of the plate, it is simplified into one variable N_{Xmax} using statical equilibrium equation of the beam member as follow

$$N_x = N_{X\max}\left(1 - \frac{2a}{L} + \frac{2x}{L}\right) \qquad \text{Eqn A.6}$$

Similarly, N_{xy} also can be expressed in terms of N_{Xmax} using the static equilibrium of the plate as follow

$$N_{xy} = N_{X\max}\left(\frac{2b}{L}\right) \qquad \text{Eqn A.7}$$

Afterward, the strain energy (U) and the work (W) are evaluated and inserted to the expression of total energy (Π). The variation of the total energy can be expressed as

$$\delta\Pi = \frac{\partial\Pi}{\partial C_1}\delta C_1 = 0 \qquad \text{Eqn A.8}$$

, where C_1 is the magnitude of the deformation of the plate

As the variation of magnitude of the deformation is not zero (If it is zero, the solution is trivial), thus the term $\frac{\partial\Pi}{\partial C_1} = 0$. This expression can be calculated by taking the derivative of the total energy with respect to C_1. Setting this differentiation to zero and inserting the

geometrical and mechanical information, the critical maximum distributed force N_{XmaxCR} can be written as

$$N_{X\max CR} = \frac{-0.00441933L(8569.08 + 464.802a^2 + a^4)}{a^2(-0.689505L + a)} \qquad \text{Eqn A.9}$$

, and the buckling stress is obtained by taking the ratio of N_{XmaxCR} to the thickness of the plate, *t*.

$$\sigma_{X\max CR} = \frac{-0.00441933L(8569.08 + 464.802a^2 + a^4)}{a^2(-0.689505L + a)t} \qquad \text{Eqn A.10}$$

3. Calculation of the buckling moment

The buckling moment equation of the framing member can be written from the buckling stress of the plate as follow

$$M_{CR}(a) = \frac{\sigma_{X\max CR} I_{xx}}{h/2} \qquad \text{Eqn A.11}$$

This equation is a function of the cut-off length of the member (*a*) used to derive the buckling stress of the plate model. Furthermore, the minimum length required (a_{min}) to initiate the buckling of the member is calculated by setting the derivative of the buckling moment equation with respect to the cut-off length (*a*) to zero and solving for *a*. Thus, the buckling moment of the member can be obtained by back-substituting the minimum length to the buckling moment equation.

$$M_{CRMember} = M_{CR}(a_{\min}) \qquad \text{Eqn A.12}$$

For this example, the minimum length required (a_{min}) to initiate buckling of the member is 6.89 in. and the buckling moment of the member is 42.91 kip-in. This minimum length is about 4 times the width of the flange.

4. Calculation of the cross-sectional moment curvature data.

Prior to buckling of the member, the rigidity of the beam member is calculated using the gross cross sectional properties of the channel section for each incremental moment. Afterward, the curvature is calculated by dividing the moment to the beam rigidity (*EI*)

$$\phi = \frac{M}{EI} \qquad \text{Eqn A.13}$$

On the other hand, the rigidity of the beam is calculated using the effective cross section if the moment value is above the buckling moment of the member. The effective cross section of the beam is obtained by reducing the width of the flange using an effective width approach. The effective width of the compressed flange is calculated using

$$b_e = \sqrt{\frac{k_c \pi^2 D}{\sigma_{\max} t}} \qquad \text{Eqn A.14}$$

, where $k_c = \frac{\sigma_{X\max CR} t b_f^{\,2}}{D\pi^2}$ and σ_{max} is the stress on the flange due to moment M

The cross sectional curvature can then be calculated by taking the ratio of the moment to the effective beam rigidity (EI_{eff}).

$$\phi = \frac{M}{EI_{eff}} \qquad \text{Eqn A.15}$$

The moment-curvature plot calculated using the given geometrical and material information is shown in the figure below. The moment-curvature curve is characterized by the beam rigidity prior to and after buckling, and the buckling moment of the member

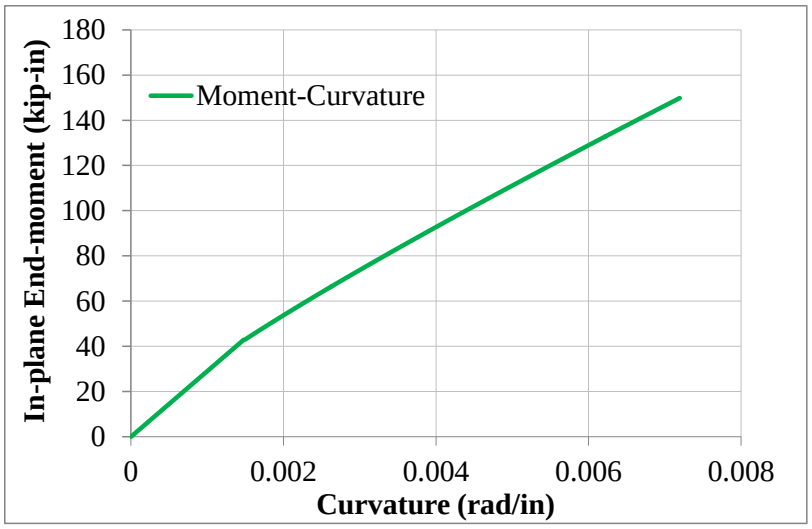

Figure A.3 Moment-curvature data of the plain channel section under local buckling on the flanges.

5. Calculation of the end rotation of the beam member.

After obtaining the moment-curvature data, the end-rotation of the member is calculated for a given incremental end-moment applied to the beam member. The end-rotation is obtained by numerically calculating the following integrations

$$\theta_{tot} = \int_0^L \phi(x)m(x)dx + \int_0^L \frac{f_s V(x)v(x)}{GA_w}dx \qquad \text{Eqn A.16}$$

, where:

$\phi(x)$ = curvature of the beam member caused by double curvature bending

$m(x)$= moment of the beam member caused by unit moment applied at one end of the beam member

f_s = shear shape factor (taken as 1.0)

$V(x)$ = shear of the beam member caused by double curvature bending

$v(x)$ = shear of the beam member caused by unit moment applied at one end of the beam member

G = shear modulus

A_w = shear area (area of web)

The first and second terms in the expression are the end-rotation of the member contributed by the bending moment and the shear deformation of the member, respectively. Following figure shows the comparison of the end-moment and end-rotation of the beam member obtained from this calculation (Effective-width Prediction) and finite element model of the beam member (2^{nd} Order Benchmark). The result of the prediction match the result of the finite element method.

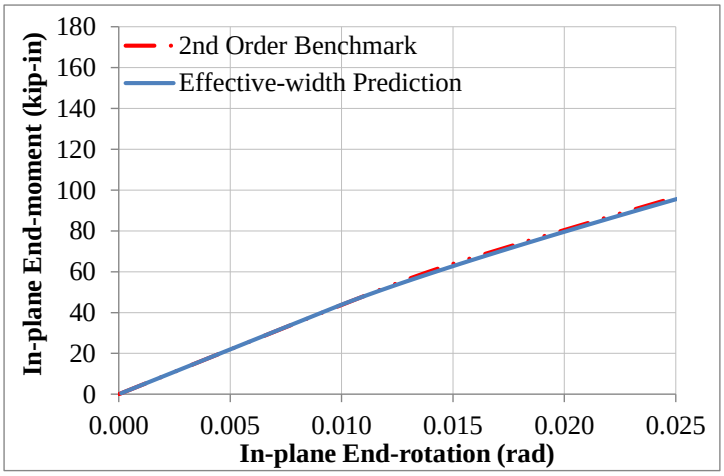

Figure A.4 Comparison of the in-plane end-moment and end-rotation of the beam member obtained using the effective-width calculation and the finite element method

APPENDIX B

CALCULATION OF WARPING DEFORMATION OF COLD-FORMED STEEL MEMBERS

The back vertical post of the Class II cabinet configuration is selected as the example used to show how the warping constraint between the points of attachment of screw connection on the flanges/webs of the vertical post and the centroid of the post at the same longitudinal coordinate. Two assumptions are made in this example:

1. The ends of the member is assumed to be free to warp, and partially fixed in the torsional direction with spring constant β.
2. The warping deformation is calculated based on the shear center of the cross section

Problem:

Calculate the warping deformation of a point at the back vertical post of the Class II cabinet configuration. The point is located at x = 0.5 in. from the end of the member and y = 1.229 in. The length of the vertical post is 45 in.

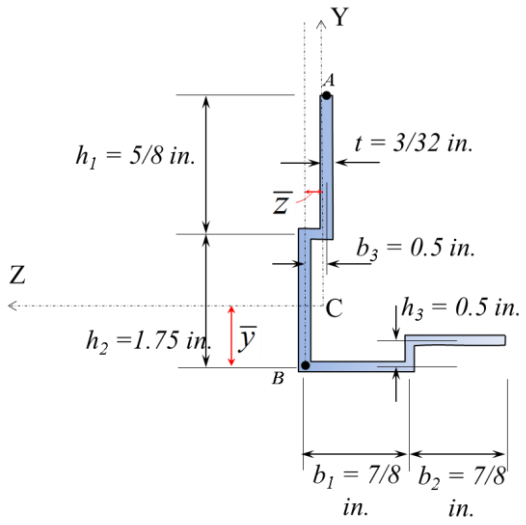

Figure B.1 Cross section of the back vertical post of the Class II cabinet configuration

Solution:

1. Calculate the cross sectional properties of the cross section

Centroid:

The centroid of the cross section is calculated using the first area moment of the cross section, and it is located at $\bar{z} = 0.47\,in.$ and $\bar{y} = 0.831\,in.$

Moment of Inertia:

The second area moments of the cross section about the *Z* and *Y* axes are calculated using the parallel axes theorem of each individual area assembling the cross section.

$I_z = 0.255\,in^4$

$I_y = 0.116\,in^4$

$I_{zy} = 0.042\,in^4$

2. Calculate the shear center of the cross section

Before the shear center is calculated, the shear flow on each element of the cross section is defined separately for shear force acting in the *Z* and *Y* axes using the following formula

$$\pi t = \frac{-V_y}{I_z I_y - I_{zy}}\left[I_y \int_0^s ytds - I_{zy} \int_0^s ztds \right] \qquad \text{Eqn B.1}$$

$$\pi t_y = \frac{V_z}{I_z I_y - I_{zy}}\left[I_{zy} \int_0^s ytds - I_z \int_0^s ztds \right] \qquad \text{Eqn B.2}$$

ds is the differential length along the midline of the cross section located at distance *s* from the free edge of the cross section.

The shear center can be calculated by taking the moment of the forces acting on the cross section about the centroid.

$$z_o = \frac{1}{V_y} \int_0^m \pi t\, r\, ds = 0.779 in. \qquad \text{Eqn B.3}$$

$$y_o = \frac{1}{V_z}\int_0^m \pi t\, r\, ds = -0.887 in. \qquad \text{Eqn B.4}$$

Note that z_o and y_o are measured with respect to the centroid of the cross section, and r is the distance from the tangent at any point of the midline to the centroid, and m is the total length of the midline.

3. Calculate the torsional and warping constant

The torsional constant of open-section can be calculated using

$$C = \frac{1}{3}\sum mt^3 \times G = 16.018\, kip - in^2 \qquad \text{Eqn B.5}$$

Before calculating the warping constant, the double sectorial area (ω_s) of the cross section has to be first defined.

$$\omega_s = \int_0^s r ds \qquad \text{Eqn B.6}$$

Now, r is measured with respect to the shear center of the cross section. Afterward, the warping function of the cross section can be calculated using

$$w = D - \omega_s \qquad \text{Eqn B.7}$$

, where $D = \frac{1}{m}\int_0^m ds \int_0^s r ds$, is a constant depending on geometrical dimensions of the cross section.

Finally, the warping constant can be calculated using

$$C_1 = Et\int_0^s (D - \omega_s)^2 ds \qquad \text{Eqn B.8}$$

4. Derive the formula for the angle of twist based on the assumed boundary condition of the member

The angle of twist of the member can be calculated by solving the second order differential equation below.

$$T = C\varphi` - C_1\varphi```$$ Eqn B.9

The torsional force T is distributed linearly based on equation

$T = T_o + t_o x$, where T_o is the torsional moment at the end of the member and t_o is the torsional load acting on the member.

The solution of this differential equation is shown in Eqn 3.15 and it is presented again below in the context of this discussion.

$$\varphi(x) = \frac{T_o x}{k^2 C_1} + \frac{t_o x^2}{2k^2 C_1} + \frac{A_1}{k}\sinh(kx) + \frac{A_2}{k}\cosh(kx) + A_3$$ Eqn B.10

, where $k = \sqrt{\frac{C}{C_1}}$

The four unknowns (T_o, A_1, A_2 *and* A_3) are calculated based on the assumed boundary conditions at the ends of the member ($\varphi(0) = \varphi(L) = T_o/\beta$, $\varphi``(0) = \varphi``(L) = 0$). Solving the unknowns and substituting back the unknowns to Eqn B.10, the angle of twist of the member can be expressed as

$$\varphi(x) = -\frac{2\beta t_o[\sinh(kL - kx) - \sinh(kL) + \sinh(kx)])}{2C_1 k^4 \beta \sinh(kL)} \ldots\ldots$$ Eqn B.11

$$\ldots\ldots + \frac{k^2 \beta t_o[x^2 \sinh(kL) - Lx\sinh(kL)] - C_1 L k^4 t_o x \sinh(kL)}{2C_1 k^4 \beta \sinh(kL)}$$

, where β is the stiffness of torsional spring at the ends of the member.

5. Calculate the warping deformation at the longitudinal position where the panels are attached to the framing member.

The warping of a point on the flanges of the cross section at certain longitudinal distance can be calculated by scaling the warping function with the rate of twist as follow

$$w_a(x,s) = \varphi'(x)[D - \omega_s(s)] \qquad \text{Eqn B.12}$$

The warping deformation of a point located at x = 0.5 in. from the end of the member and y = 1.229 in. is -0.225 in. This warping deformation corresponds to the angle of twist of 0.421 rad. This point is located at the position where the side panel is attached to the back vertical post.

For the vertical posts in the Class II cabinet, the warping deformation and angle of twist are calculated based on a reference axis located at the shear center of the post. Trial calculations shown that the amount of warping deformations at the FB and SS attachment points are more reasonable if it is calculated based on this reference axis (The amount of warping deformations in the FB attachment points is smaller than the amount of warping deformation in the SS attachment points). On the other hand, the warping deformation of the vertical posts in the Class I cabinet is calculated based on a reference axis located at the centroid because trial calculations shown that the results are more reasonable. The warping deformations and the angle of twist of the front vertical post of the Class II cabinet configuration and the vertical post of the Class I cabinet configuration are also calculated using the same method and the results are tabulated in the following table.

Table B.1 Warping deformation and angle of twist of the front vertical post of the Class II cabinet configuration and the vertical post of the Class I cabinet configuration

	w - front	w - side	φ - front	φ - side
Front Vertical Posts – Class II	N/A	0.122 in.	N/A	0.027 rad
Vertical Posts – Class I	-0.154 in.	-0.154 in.	0.075 rad	0.075 rad

Note:

1. Front or side label indicates the front or left/right side of the cabinet, respectively.
2. The warping deformation and the angle of twist of the vertical post in the Class I cabinet configuration are calculated at x = 0.1 in. based on the location of the screw connection between the panel and framing member on the Class I cabinet configuration.
3. The warping constraint is not assigned to the attachment points located at the front and back sides of cabinet in the Class II cabinet configuration

APPENDIX C

ABAQUS INPUT COMMANDS FOR MODELING FEATURES

Table C.1 ABAQUS input commands for modeling features assigned in the simplified cabinet model

Structural Components	ABAQUS Command	Notes
Framing Member	B31	Timoshenko beam element
	CONN3D2 – JOIN, REVOLUTE[1]	Rotational Spring in the in-plane bending direction and rigid constraints for the rest of DOFs
Panels	S4R	Shell elements with reduced integration
Connection between Framing Members	CONN3D2 – JOIN, ROTATION	Rotational springs in each orthogonal direction and rigid constraints for all translational DOFs.
	CONN3D2 – BEAM	Rigid beam constraints
Connection between Panels and Framing Member	CONN3D2 – CARTESIAN, ALIGN[1]	Translational springs in each orthogonal direction and rigid constraints for all rotational DOFs.
	CONN3D2 – CARTESIAN, ROTATION[2]	Translational and rotational springs in each orthogonal direction
	CONN3D2 – BEAM	Rigid beam constraints
	EQUATION	Rigid beam and warping constraints

[1] Only in Class I configuration

[2] Only in Class II configuration

Table C.2 ABAQUS input commands for modeling features assigned in the benchmark cabinet model

Structural Components	ABAQUS Command	Notes
Framing Member	S4R	Shell elements with reduced integration
Panels	S4R	Shell elements with reduced integration
Connection between Framing Members	FASTENER - BEAM	Rigid beam constraints between connecting nodes of framing members at the location of the screws
Connection between Panels and Framing Member	CONN3D2 – CARTESIAN, ALIGN	Translational springs in each orthogonal direction and rigid constraints for all rotational DOFs.

Table C.3 ABAQUS input commands for modeling features assigned in the model of connections between framing members

Structural Components	ABAQUS Command	Notes
Framing Member	S4R	Shell elements with reduced integration
Connection between Framing Members	FASTENER - BEAM	Rigid beam constraint between connecting nodes of framing members at the location of the screws
End Constraint	MPC – BEAM	Rigid beam multi-point constraints between the nodes at the outer end of a member to the centroid of that end.
	COUPLING – DISTRIBUTING[1]	Free warping constraint between the nodes at the outer end of a member to the centroid of that end.

[1] Only in translational and torsional directions

REFERENCES

AC-156, I.-E. (2010). Acceptance Criteria for Seismic Certification by Shake-Table Testing of Nonstructural Components, International Code Council. **ICC-ES AC 156**.

AISI (2007). North American Standard for Cold-formed Steel Framing-General Provisions. S100-07. USA, American Iron and Steel Institute.

ASCE (2010). Minimum design loads for buildings and other structures. Reston, Va., American Society of Civil Engineers : Structural Engineering Institute.

Ayhan, D. and B. Schafer (2012). Moment-Rotation Characterization of Cold-Formed Steel Beams Depending on Cross-Section Slenderness. Proceedings of the 15th World Conference on Earthquake Engineering.

Bauchau, O. A. and J. I. Craig (2009). Structural analysis: with applications to aerospace structures, Springer Science & Business Media.

Boresi, A. P. and R. J. Schmidt (2003). Advanced mechanics of materials. New York, John Wiley & Sons.

Bradford, M. A. and M. Azhari (1995). "Buckling of plates with different end conditions using the finite strip method." Computers & structures **56**(1): 75-83.

Bridget, F., C. Jerome and A. Vosseller (1934). "Some New Experiments on Buckling of Thin Wall Construction." Transactions of the ASME **56**(8): 569-578.

Bulson, P. S. (1969). The stability of flat plates. Great Brittain, Elsevier Publishing Company.

Cho, S. G., D. Kim and S. Chaudhary (2011). "A simplified model for nonlinear seismic response analysis of equipment cabinets in nuclear power plants." Nuclear Engineering and Design **241**(8): 2750-2757.

Chopra, A. K. (2007). Dynamics of structures. New Jersey, Pearson Prentice Hall.

Cook, R. D., D. S. Malkus, M. E. Plesha and R. J. Witt (2004). Concepts and applications of finite element analysis. New Delhi, John Wiley & Sons.

Dassault Systemes. (2012). Abaqus 6.12 documentation. RI, USA, Dassault Systemes Simulia Corp.

Davies, J., P. Leach and D. Heinz (1994). "Second-order generalised beam theory." Journal of Constructional Steel Research **31**(2): 221-241.

Djordjevic, W. and J. J. O'Sullivan (1995). Guideline for Development of In-cabinet Seismic Demand for Devices Mounted in Electrical Cabinets. NP-7146-SL R1. California, US, Electrical Power Research Institute.

ECCS (1984). The Design and Testing of Connections in Steel Sheeting and Sections. England, Constrado.

EQE Engineering. (1991). Summary of the Seismic Adequacy of Twenty Classes of Equipment Required for the Safe Shutdown of Nuclear Plants. San Francisco, California, EPRI.

Fulop, L. A. and D. Dubina (2004). "Performance of wall-stud cold-formed shear panels under monotonic and cyclic loading Part I: Experimental research." Thin-Walled Structures **42**(2): 321-338.

Gatscher, J. A., G. L. McGavin, P. J. Caldwell and American Society of Civil Engineers. (2012). Earthquake protection of building equipment and systems : bridging the implementation gap. Reston, Va., American Society of Civil Engineers.

Gere, J. M. and B. J. Goodno (2013). Mechanics of materials. Stamford, CT, Cengage Learning.

Goodno, B. J., N. C. Gould, P. Caldwell and P. L. Gould (2011). "Effects of the January 2010 Haitian Earthquake on Selected Electrical Equipment." Earthquake Spectra **27**(S 1): S 251-S 276.

Gupta, A., S. K. Rustogi and A. K. Gupta (1999). "Ritz vector approach for evaluating incabinet response spectra." Nuclear Engineering and Design **190**(3): 255-272.

Gupta, A. and J. F. Yang (2002). "Modified Ritz vector approach for dynamic properties of electrical cabinets and control panels." Nuclear Engineering and Design **217**(1-2): 49-62.

Hur, J. (2012). Seismic performance evaluation of switchboard cabinets using nonlinear numerical models. Atlanta, Ga., Georgia Institute of Technology.

IEEE Power Engineering Society. (2006). IEEE Recommended Practice for Seismic Design of Substations: IEEE Std 693-2005, The Institute of Electrical and Electronics Engineers, Inc.

Jiang, H., X. Liu and J. Mao (2015). "Full-scale experimental study on masonry infilled RC moment-resisting frames under cyclic loads." Engineering Structures **91**: 70-84.

Kulak, G. L. and E. Y. Wu (1997). "Shear lag in bolted angle tension members." Journal of Structural Engineering **123**(9): 1144-1152.

Libove, C., S. Ferdman and J. J. Reusch (1949). "Elastic buckling of a simply supported plate under a compressive stress that varies linearly in the direction of loading."

McGuire, W., R. H. Gallagher and R. D. Ziemian (2000). Matrix structural analysis. United States of America, John Wiley & Sons.

Merz, K. and P. Ibanez (1990). "Guidelines for estimation of cabinet dynamic amplification." Nuclear engineering and design **123**(2): 247-255.

Notohardjono, B. D., S. Canfield and J. A. Cooke (2009). Sesimic Evaluation of Large Server Computer Structure. The ASME 2009 Pressure Vessels and Piping Division Conference, Praguem Czech Republic, ASME.

Pham, H. S. and C. D. Moen (2015). Stiffness and Strength of Single Shear Cold-Formed Steel Screw-Fastened Connections. Blacksburg, VA, Virginia Tech.

Popovic, D., G. J. Hancock and K. J. R. Rasmussen (1999). "Axial compression tests of cold-formed angles." Journal of Structural Engineering **125**(5): 515-523.

Powers, D. L. (2009). Boundary value problems: and partial differential equations, Academic Press.

Schafer, B. and T. Peköz (1998). "Computational modeling of cold-formed steel: characterizing geometric imperfections and residual stresses." Journal of Constructional Steel Research **47**(3): 193-210.

Silvestre, N. and D. Camotim (2003). "Nonlinear generalized beam theory for cold-formed steel members." International Journal of Structural Stability and Dynamics **3**(04): 461-490.

Takhirov, S. M., G. L. Fenves, E. Fujisaki and D. Clyde (2005). Ground Motions for Earthquake Simulator Qualification of Electrical Substation Equipment. Berkeley, Pacific Earthquake Engineering Research Center.

Timoshenko, S. and J. M. Gere (2009). Theory of elastic stability. Mineola, N.Y., Dover Publications.

Timoshenko, S. P. (1945). "Theory of bending, torsion and buckling of thin-walled members of open cross section." Journal of the Franklin Institute **239**(3): 201-219.

Timoshenko, S. P. (1945). "Theory of bending, torsion and buckling of thin-walled members of open cross section." Journal of the Franklin Institute **239**(4): 249-268.

Von Karman, T., E. E. Sechler and L. Donnell (1932). "The strength of thin plates in compression." Trans. ASME **54**(2): 53-57.

Wang, S. and S. Errera (1971). Behavior of cold rolled stainless steel members. International Specialty Conference on Cold-Formed Steel Structures.

Winter, G. (1947). "Strength of thin steel compression flanges." Transactions of the American Society of Civil Engineers **112**(1): 527-554.

Wyle Laboratories. (2008). Seismic Testing on QED-2 & SPEED-D Switchboard Configurations. Huntsville, AL, Wyle Laboratories.

Young, B. (2004). "Tests and design of fixed-ended cold-formed steel plain angle columns." Journal of structural engineering **130**(12): 1931-1940.

Yu, C. and B. W. Schafer (2007). "Simulation of cold-formed steel beams in local and distortional buckling with applications to the direct strength method." Journal of Constructional Steel Research **63**(5): 581-590.

Yu, W.-W. and R. A. LaBoube (2010). Cold-formed steel design. Hoboken, New Jersey, John Wiley & Sons.

Zeinoddini, V. and B. Schafer (2012). "Simulation of geometric imperfections in cold-formed steel members using spectral representation approach." Thin-Walled Structures **60**: 105-117.